Negative microfilm 64–6705
received from university

KULWICKI, Bernard Michael, 1935–
THE PHASE EQUILIBRIA OF SOME COMPOUND SEMICONDUCTORS BY DTA CALORIMETRY.

The University of Michigan, Ph.D., 1963
Engineering, chemical

University Microfilms, Inc., Ann Arbor, Michigan

THE PHASE EQUILIBRIA OF SOME COMPOUND SEMICONDUCTORS BY DTA CALORIMETRY

By

Bernard Michael Kulwicki

A dissertation submitted in partial fulfillment
of the requirements for the degree of
Doctor of Philosophy in the
University of Michigan
1963

Doctoral Committee:

Professor Donald R. Mason, Chairman
Professor Lee O. Case
Professor Ernst Katz
Professor Joseph J. Martin
Professor Giuseppe Parravano

ACKNOWLEDGMENTS

The author would like to express his sincere gratitude to Professor Donald R. Mason for his guidance and assistance which were given throughout the course of this work.

The assistance in the form of fellowships from American Cyanamid Corporation and Union Carbide Corporation is likewise appreciated. Special thanks is due to Texas Instruments, Inc., whose financial support was particularly welcome. Acknowledgment is also due to the Department of Chemical and Metallurgical Engineering for their partial support of this research.

The author also wishes to thank Dr. Raymond C. Sangster of Texas Instruments and Dr. Alan J. Strauss of Lincoln Laboratories for the samples which they provided, and the Computing Center of the University of Michigan for the computer time which was donated.

The following students also deserve credit for their assistance: Messrs. R. G. Grammens and E. K. Parrott who helped with the DTA measurements, Messrs. N. Delgass and R. J. Bassett who performed the chores of glass-blowing and sample preparation, Mr. S. J. Lewis who carried out many of the fusion operations, and last but not least Mr. A. N. Currim whose expert assistance in solving the boundary value problems associated with heat conduction in the system is greatly appreciated.

THE PHASE EQUILIBRIA OF SOME COMPOUND SEMICONDUCTORS BY DTA CALORIMETRY

Bernard Michael Kulwicki

ABSTRACT

This work may be divided into three parts: 1) a theoretical study of heat transfer in the differential thermal analysis (DTA) equipment with subsequent development of two methods for the measurement of latent heats of fusion and transition; 2) the determination of the heats of fusion and transition of twenty compound semiconductors and the study of the nature of these transformations; and 3) the study of solid-liquid equilibria in the systems cadmium-tellurium, zinc-tellurium and indium-selenium.

The theoretical analysis showed that the thermal conductance of the system could be well approximated by its steady state value, and a theoretical expression for the time constant for exponential decay of the DTA curve was derived. The first method for the determination of the thermal conductance of the system is based on its theoretical calculation from the steady state formulae. Two variations of this method for indirectly measuring the thickness of the gas film between the silica sample tube and the nickel sample holder (a quantity which can be directly measured only imprecisely) are presented. The first is based on a comparison of the theoretically calculated time constant with its experimental counterpart. This method was tested with data on a number of standards, and good agreement was found between theory and experiment. The second variation, which could not be adequately evaluated, is based on the calculation of the film thickness from two measurements of the area under the DTA curve when gases of widely different thermal conductivity fill the system.

The second method for finding the thermal conductance depends on its calculation from the experimentally measured time constant and the estimated thermal capacity of the system. This method requires calibration of the equipment.

These methods are employed to measure the heats of fusion and transition of the following compounds whose melting points range from 800° to 1560°K: $Ag_2In_8Se_{13}$, Ag_2Se, Ag_2Te, Bi_2Se_3, Bi_2Te_3, CdSe, CdTe, GaAs, GaSb, InAs, InSb, In_2Se_3, InTe, In_2Te_3, PbSe, PbTe, Sb_2Se_3, Sb_2Te_3, SnTe and ZnTe. The entropies of fusion plus transition are found to vary from 2.2 cal/g atom °K for $Ag_2In_8Se_{13}$ to 9.6 cal/g atom °K for GaAs. The experimental precision is about ± 15% on the average.

Finally, phase equilibria in the systems Cd-Te, Zn-Te and In-Se were studied. Thermodynamic calculations suggest that CdTe and ZnTe molecules are stable in the melt, and it was established that the systems Cd-CdTe and Zn-ZnTe exhibit positive deviations from Raoult's law whereas the systems CdTe-Te and ZnTe-Te exhibit negative deviations. A two parameter correlation of the liquidus curves of these two systems is postulated.

The In-Se system contains five compounds two of which melt congruently, InSe (614°C) and In_2Se_3 (885°C) and three of which decompose peritectically, $In_{54}Se_{46}$ (553°C), $In_{47}Se_{53}$ (660°C) and $In_{20}Se_{80}$ (?) (745°C). Two monotectic reactions, at 520°C (indium-rich) and at 760°C (selenium-rich), were observed, as well as polymorphic transformations in In_2Se_3 (201°C) and $In_{20}Se_{80}$ (?) (650°C).

TABLE OF CONTENTS

	Page
ACKNOWLEDGMENTS	ii
ABSTRACT	iii
LIST OF TABLES	viii
LIST OF FIGURES	ix
LIST OF APPENDICES	xi
I. INTRODUCTION	1
A. State of the Art	1
B. Statement of the Problem	6
1. Direct Calculation of the Thermal Conductance	6
2. The Calculation of the Thermal Conductance from the Time Constant	8
II. HEAT TRANSFER IN THE DTA SYSTEM	10
A. Heat Conduction Model	10
B. Heat Conduction Prior to Melting -- Regime A	13
C. Heat Conduction During Melting -- Regime B	17
D. Heat Conduction Following Melting -- Regime C	23
E. The Thermal Conductance	28
F. Radiation in the DTA System	30
III. APPLICATION OF THE THEORY	34
A. Calculation of the Thermal Conductance Using the Theoretical Time Constant to Find the Gas Film Resistance	34

TABLE OF CONTENTS (Cont'd)

Page

B. Calculation of the Thermal Conductance Using Two Measurements of the Area Under the DTA Curve to Find the Gas Film Resistance. 38

C. Calculation of the Thermal Conductance from the Time Constant and the Thermal Capacity. 42

IV. HEATS OF FUSION AND TRANSFORMATION BY DTA CALORIMETRY. 45

A. Experimental Data. 45

B. Experimental Results. 48

C. $Ag_2In_8Se_{13}$. 51

D. Ag_2Se. 53

E. Ag_2Te. 53

F. Bi_2Se_3, Bi_2Te_3, Sb_2Se_3 and Sb_2Te_3. 54

G. GaAs, GaSb, InAs and InSb. 55

H. CdSe, CdTe and ZnTe. 55

I. In_2Se_3. 56

J. InTe and In_2Te_3. 57

K. PbSe, PbTe and SnTe. 58

L. Experimental Precision. 59

M. Discussion. 60

V. SOLID-LIQUID EQUILIBRIUM STUDIES. 63

A. The System Cadmium-Tellurium. 63

B. The System Zinc-Tellurium. 71

TABLE OF CONTENTS (Cont'd)

Page

C. The Indium-Selenium Phase Diagram. 75

D. Discussion. 79

VI. CONCLUSION. 83

A. Summary. 83

B. Advantages and Disadvantages of the Methods Used to Measure Latent Heats. 84

C. Recommendations. 85

APPENDICES. 86

BIBLIOGRAPHY. 175

LIST OF TABLES

Table		Page
3.1	Results of Computer Program DTA-19 for Standards	37
3.2	The Correlation Factor Z = C/C'	43
4.1	Heats of Fusion of Compound Semiconductors	49
4.2	Heats of Transition of Compound Semiconductors	50
4.3	Comparison of the Sum of the Entropies of Transition and Fusion with the Theoretical Prediction	52
4.4	Entropies of Transition and Fusion of Compound Semiconductors	61
5.1	Experimental Data for the Cd-Te Phase Diagram	64
5.2	Experimental Data for the Zn-Te Phase Diagram	72
5.3	Experimental Data for the In-Se Phase Diagram	76
A-III-1	Elements Used in the Preparation of Compounds	99
A-III-2	List of DTA Samples	103
A-IV-1	Specific Heats of Elements and Compounds at the Melting Point	113
A-IV-2	Specific Heats of Compounds at the Transition Point	114
A-IV-3	Thermal Conductivities of the Solid Near the Melting Point	116
A-IV-4	Emissivities of Elements and Compounds	118

LIST OF FIGURES

Figure		Page
2.1	Model for the Investigation of Heat Conduction in DTA.	11
2.2	Relationship between the Differential Temperature, θ, and the Thermal Conductance, G, during DTA. .	29
3.1	Analogous Electrical Circuit for Calculation of the Overall Thermal Conductance.	39
4.1	Some Typical DTA Curves Showing Differential Temperature versus Time and Selected Sample Temperatures.	46
4.2	Some Typical Semilogarithmic Plots for Finding the Time Constant for Exponential Decay of the DTA Curve.	47
5.1	The Phase Diagram for the Cadmium-Tellurium System.	65
5.2	The Integrand of the Excess Free Energy Function versus Composition for the Cadmium-Tellurium System.	68
5.3	The Liquidus Curves for the Cadmium-Tellurium System Plotted as $\log 4 N_{Cd} N_{Te}$ versus Reciprocal Reduced Temperature.	70
5.4	The Phase Diagram for the Zinc-Tellurium System. .	73

LIST OF FIGURES (Cont'd)

Figure		Page
5.5	The Liquidus Curves for the Zinc-Tellurium System Plotted as $\log 4 N_{Zn} N_{Te}$ versus Reciprocal Reduced Temperature.	77
5.6	The Proposed Phase Diagram for the Indium-Selenium System.	78
5.7	Semilogarithmic Plot of the Average Cluster Size, n , versus Reciprocal Reduced Temperature.	82
A-I-1	The DTA Samples inside the Nickel Block for Sample Arrangement B.	87
A-I-2	Block Diagram Showing Operation of the DTA Equipment.	89
A-II-1	Plot of Equation A-2.9 showing Relationships between Furnace Temperature and Autotransformer Setting for Heating and Cooling at Rates of 2.5 ^{o}C/min and Steady State Conditions.	96
A-V-1	Contour in the Complex Plane for Inversion of the Laplace Transforms, Equations A-5.29 and A-5.30. .	125

LIST OF APPENDICES

	Page
I. DTA EQUIPMENT AND PROCEDURE	86
II. DYNAMICS OF THE DTA FURNACE	93
A. Determination of the Time Constant	93
B. Operating Conditions and Procedures	94
C. Discussion	95
III. SAMPLE PREPARATION	98
A. Materials	98
B. Preparation of Alloys	101
C. Preparation of DTA Samples	101
IV. PHYSICAL PROPERTIES AND THEIR ESTIMATION	110
A. Heats of Fusion and Transformation	110
B. Densities	111
C. Heat Capacities	111
D. Thermal Conductivity	112
E. Emissivities	115
V. CONDUCTION OF HEAT IN THE SYSTEM DURING MELTING	119
VI. COMPUTER PROGRAMS AND EXPERIMENTAL DATA	133
A. Program Number DTA-19 for Direct Calculation of the Thermal Conductance	133
1. List of Variables	133
2. MAD Listing of Program	135
3. Data Card Format	140
4. Tabulation of Data Cards	141

LIST OF APPENDICES (Cont'd)

Page

B. Program Number DTA-16 for Direct Calculation of the Thermal Conductance. 145

1. List of Variables. 145

2. MAD Listing of the Program. 147

C. Program Number DTA-17 for Analysis of DTA Data. . . 152

1. List of Variables. 152

2. MAD Listing of Program. 153

3. Data Card Format. 155

4. Tabulation of Data Cards. 156

VII. NOMENCLATURE. 170

CHAPTER I

INTRODUCTION

Differential thermal analysis (DTA) is one method of recording time-temperature information for the purpose of studying thermal transformations, and consists in measuring the temperature difference between a sample and a reference as a function of time and/or temperature. Other methods have been described as well (3), but DTA remains as one of the oldest (50, 51) and most useful. DTA has met with widespread acceptance in many areas wherein a change in the rate of heat transfer to a sample generates a temperature difference. Many examples may be cited.*

The principal objective here is to determine the latent heats of fusion and transition of some twenty semiconducting compounds whose melting points range from 800°K to 1560°K by means of DTA calorimetry. The compounds are: $Ag_2In_8Se_{13}$, Ag_2Se, Ag_2Te, Bi_2Se_3, Bi_2Te_3, CdSe, CdTe, GaAs, GaSb, InAs, InSb, In_2Se_3, InTe, In_2Te_3, PbSe, PbTe, Sb_2Se_3, Sb_2Te_3, SnTe, and ZnTe. A second objective is the investigation of solid-liquid equilibria in the systems Cd-Te, Zn-Te, and In-Se.

State of the Art

DTA has long been recognized as being a powerful tool in the investigation of phase equilibria. Transition temperatures may be accurately pinpointed. Furthermore, the technique is amenable to the use of very small samples, making possible the study of rare materials. A typical example of this type of study is the work of O'Kane (66) who investigated solid-liquid equilibria in pseudobinary systems such as CdSe-In_2Se_3, ZnTe-In_2Te_3, etc. Solid-vapor equilibria may also be readily investigated as has been done by Markowitz and Boryta (56) who studied the behavior of NH_4Cl in a controlled pressure DTA unit.

---

* The purpose here is to cite illustrative references, rather than to compile a bibliography, which has been done by Smothers and Chiang (78). Over 1500 references are given.

DTA has also been used to investigate reactions in the solid state (26, 38, 78) thereby making possible the accurate definition of reaction temperatures and relative speed under a variety of experimental conditions. The study of thermal transitions in clays by DTA was first undertaken by Norton (64), and similar studies have been carried out by numerous workers.* Locke and Rase (53) have indicated the utility of a controlled pressure unit in the screening of catalysts so as to provide rapid, qualitative information on the chemical and physical changes which affect catalytic activity. Even such small heat effects as those due to specific heat changes accompanying the glass transition temperature of polymers may be readily investigated by DTA (41) and Steiner and Johnston (80) have discussed the application of DTA to the quantitative determination of specific heats.

In principle, DTA is also a calorimetric technique in which the heat absorbed or evolved during a thermal transition or chemical reaction may be determined by comparing the area under the DTA curve with that produced by a standard whose latent heat or heat of reaction is well known. In practice, however, its usefulness has been limited because of difficulties associated with accurately predicting the appropriate thermal conductance or apparatus constant of the system, particularly where a wide range of temperature is of interest.

Among the first to recognize the possibility of obtaining a quantitative measure of changes in heat content from cooling curves was Plato (69) who estimated the heats of fusion of a number of inorganic salts from the time of freezing on the cooling curves. His formulae as well as those of other investigators up to about 1925 were strictly empirical in nature and are thus of little interest here. Among the first to derive the relationship of proportionality between the heat of reaction and the area under the DTA curve were Steiner and Johnston (80) whose thorough article provides an excellent review of the art through 1928 as well as a comprehensive discussion of the merits and limitations of the technique as a

---

* Cf. reference (78) for bibliography.

quantative tool. This relationship has been derived by many other authors including Berg and Anosov (6) who measured the heats of dissociation of dolomite and related substances; Speil (79) who studied the thermal transitions in clays and related minerals; Vold (87) who measured the heats of fusion of stearic and benzoic acids, and Borchardt and Daniels (12) who were interested in determining the kinetic parameters of homogeneous, liquid phase chemical reactions.

At this point, the quantitative theory of DTA will be reviewed briefly. The equations presented first are essentially the same as those given by Vold (87), but using different symbols. The model for the DTA system comprises a sample and a reference material having substantially identical properties and physical geometries. They are placed inside a furnace and heated together under essentially identical conditions. Assuming that the sample temperature is uniform and that heat losses are negligible, a differential energy balance may be written for the sample as follows:

$$C\,dT = dE + K(T_s - T)\,dt \qquad 1.1$$

where C is the total heat capacity (cal/^{o}K), E is the energy evolved during thermal transition (cal), and K is the thermal conductance (cal/^{o}K-sec.). Similarly for the reference

$$C_r\,dT_r = K_r(T_s - T_r)\,dt \qquad 1.2$$

where no energy is evolved and hence the dE term does not appear.

In the above equations, the subscript s refers to the surroundings and the subscript r to the reference. Defining θ as the temperature difference between sample and reference $(T - T_r)$, and γ as the constant heating rate $(dT_r = \gamma\,dt)$, the following relation is obtained:

$$C\,d\theta = dE + C\gamma(\phi - 1)\,dt - K\theta\,dt \qquad 1.3$$

where $\phi = KC_r/K_rC$ and is dimensionless. Choosing the initial condition

$\theta = 0$ at $t = 0$, Equation 1.3 may be integrated for the condition $dE = 0$ to yield:

$$\theta = \gamma(\phi - 1)(C/K)(1 - e^{-Kt/C}) \qquad 1.4$$

whence the steady state value of θ is obtained:

$$\theta_{ss} = \gamma(\phi - 1)C/K \qquad 1.5$$

Thus Equation 1.3 becomes:

$$dE = K(\theta - \theta_{ss})\,dt + C\,d\theta \qquad 1.6$$

or

$$\Delta E = K \int_{t_1}^{t_2} (\theta - \theta_{ss})\,dt \qquad 1.7$$

Equation 1.7 is strictly valid only if θ_{ss} does not vary during the transition, i.e., the baseline remains constant. Even if the baseline does shift due to a change in the specific heat of the sample as a result of phase transformation, however, Steiner and Johnston (80) have shown that Equation 1.7 may still be used provided that the area is measured with respect to the extension of the final baseline.

Boersma (7) as well as Kronig and Snoodijk (46) have obtained this relation in a somewhat more elegant manner, and have shown that the assumption of uniform sample temperature is unnecessary provided that θ is the temperature difference between the center of the sample and the center of a matched reference. In addition, both authors have derived expressions for the thermal conductance in terms of thermal conductivity of the sample, that of the holder, and the geometry. Boersma has also derived correction terms which take into account the transfer of heat along the thermocouple wires.

In addition to the possibility of computing K from the geometry and thermal properties of the system, several other techniques are available. The first, due to Berg and Anosov (6) and also applied by Kornilov and Matveeva (45), consists in the admixture of a standard, whose transition heat is known, with the sample. The second possibility, proposed by Vold (87) consists in calculating K from the exponential decay of θ after the transition has been completed. A third method, recently proposed by Sturm (82) consists in computing the effective conductance from data taken by controlling the heating rates so as to obtain a constant thermal gradient. A fourth possibility consists in measuring the area under the curve produced by standards whose transition heats are known. This method is perhaps the least satisfactory particularly where a wide range of temperature is of interest, since at high temperatures radiation is an important contributor to the heat transfer mechanism. This method is quite useful, however, over short temperature intervals particularly where a large thermal resistance intervenes between the heat source and the sample. This fact has been pointed out by Boersma (7) as well as by Smith (76).

Further ingenious variations have been proposed by Eyraud (23), Wittig (91) and Lueck, Beste and Hall (55). The first two authors proposed methods in which the need to determine a numerical value for K is eliminated. Eyraud proposed using a temperature controller to regulate the temperature difference between the heat source and the sample while measuring the power input to the furnace as a function of time, with the area under the power-time curve being equal to the heat of transformation. Wittig suggested using an auxiliary heater within the sample. When varying quantities of electrical energy were injected via this heater, differing values of the area under the DTA curve were obtained, extrapolation to zero area yielding the heat of transformation. Lueck et al., who were interested in studying the kinetics of liquid phase chemical reactions, have developed a technique whereby nearly isothermal conditions may be maintained in the reaction cell, sensitive thermistors being used to measure the differential temperature (0.1 $^{\circ}$K at most). The thermal conductance was

determined from the exponential decay of the DTA curve to baseline after a drop of warm water was added to the reaction solution.

Statement of the Problem

The particular properties of the compounds studied in this work required modifications and refinements to the existing techniques.

The volatility and reactivity of our samples required their being sealed under vacuum in silica glass tubes.* Because of the fact that the dimensions of the silica tubing, and therefore the thermal conductance, varied from sample to sample, a simple calibration of the apparatus would not suffice. The method of Berg and Anosov could not be used because of the unavailability of suitable standards. In Sturm's method, as he himself admits, the heating rates resulting in a constant thermal gradient may be found only with difficulty. And the methods of Eyraud and Wittig not only do not appear to be any more direct or reliable than the two remaining methods which were used in this work; viz. direct calculation of the thermal conductance and measurement of the time constant, but also would require extensive modification of our equipment. The application of these two methods to our particular system is now considered.

Direct Calculation of the Thermal Conductance

Instead of using the aforementioned definition of the thermal conductance, viz.

$$K = \frac{\text{heat flux across system x area}}{\text{temperature difference}}$$

$$= \text{cal/sec}^{\circ}\text{K} \qquad 1.8$$

a slightly different definition will be used

$$G = \frac{K}{L} = \frac{\text{heat flux across system x area}}{\text{temperature difference x sample height}} \qquad 1.9$$

---

* Cf. Appendix III for description of the samples and their preparation.

$$G = \text{cal/sec-cm-}^{\circ}\text{K}$$

in which the conductance is normalized to a unit height of sample.

At steady state, it may be readily shown (22) that the conductance for thermal conduction across a cylindrical annulus is given by:

$$G_i = \frac{2\pi k_i}{\ln \eta_i} \qquad 1.10$$

where k_i is the thermal conductivity of the material in the annulus and η_i is the ratio of the outer radius to the inner radius.

For thermal radiation, a parallel heat transfer mechanism, the conductance is given by:

$$G_i = 8\pi R_l F_i \sigma T^3 \qquad 1.11$$

where R_l = the larger radius

F_i = shape factor which depends on the emissivities of the two surfaces and the geometry.

σ = the Stefan-Boltzmann constant

T = absolute temperature.

Now it is also true at steady state that the heat flux x area/sample height is constant, so that the individual conductances can be combined as follows.

$$G = \sum_i G_i \qquad \text{(conductances in parallel)} \qquad 1.12$$

$$\frac{1}{G} = \sum_i \frac{1}{G_i} \qquad \text{(conductances in series)} \qquad 1.13$$

Now if the last four equations plus Equation 1.7 are obeyed in the system it is clear that it will be possible to determine heat quantities by DTA. The information required to do this includes, 1) knowledge of the thermal properties of all components of the system; 2) their geometry;

and 3) an experimental measurement of the area under the DTA curve.

The DTA system consists in samples which are sealed under vacuum in silica sample tubes, each of which contains a concentric thermocouple well in the bottom. The samples are placed in a nickel block in which holes have been drilled in order to accommodate them. A gas film thus separates the silica tube from the wall of the nickel block.

The primary contributions to the overall conductance come from the gas film and the sample tube. Secondary contributions are due to the sample itself and, at high temperatures, thermal radiation. It is clear then, that a precise measurement of the physical dimensions of the gas film is required. This measurement is difficult to achieve directly because the gas film is very thin, so that its thickness is a small difference of large numbers. This complication may be resolved, however, if an independent method of evaluating the thickness of the gas film is available.

Two such methods are proposed in the following. In the first method, two measurements of the area under the DTA curve are obtained using different gaseous atmospheres having widely different thermal conductances, such as nitrogen and helium. The thickness of the gas film can then be computed from the two areas and the known thermal conductivities of nitrogen and helium respectively. In the second method, the thickness of the gas film can be found by comparing the experimental time constant for exponential decay (see Equation 1.4).

$$\tau_{exp} = - \left[\frac{d \ln | \theta - \theta_{ss} |}{d t} \right]^{-1} \qquad 1.14$$

of the DTA curve after completion of melting with the theoretical value found from a consideration of the differential equations governing heat conduction in the system. The precise formulation of these methods will be given in Chapters II and III.

The Calculation of the Thermal Conductance from the Time Constant

Inspection of Equations 1.4 and 1.14 leads to the following expression for the thermal conductance:

$$K = C/\tau_{exp} \qquad 1.15$$

where C is the thermal capacity of the system. A number of authors have used this formula including Vold (87) and Lueck, et al. (55). It is evident that the thermal conductance can be estimated provided that the thermal capacity of the system can be estimated.

In this regard several questions arise: Exactly what constitutes the thermal capacity of the system? Should C include the heat capacity of the sample plus that of the container, or that of the sample alone? If the container is included, should the entire container, or just that portion of it which is in thermal contact with the sample be included? Vold, who studied fusions of organic materials in a nickel sample container, found that her data were best explained by including the heat capacities of the sample and the entire container in the estimation of C. In the particular equipment used in this work, the heat flux is, for all practical purposes, radial, and the container is constructed from fused silica, a material of relatively low thermal conductivity. It is therefore unlikely that changes in the temperature of the container a few centimeters away from the sample would appreciably affect the heat flux to the sample. This would seem to imply that only a portion of the heat capacity of the container would, in this case, contribute to the thermal capacity of the system.

In succeeding chapters the theory of heat conduction and radiation in this system will be examined, the methods sketched here will be more fully developed and subsequently applied to experimental data, and the results will be critically examined in the light of present knowledge and theory.

CHAPTER II

HEAT TRANSFER IN THE DTA SYSTEM

In this section, the differential equations governing the flow of heat in the DTA system are considered together with appropriate boundary conditions which approximate the experimental system. Three regimes may be discerned: A) heat conduction in the system immediately prior to melting (or transformation); B) during melting; and C) immediately following melting of the sample. The equations describing the first regime are amenable to direct analytical solution in cylindrical coordinates. Those describing the second regime cannot be readily solved in cylindrical coordinates but the analogous problem in cartesian coordinates may be solved. The long time approximation in the cylindrical case may then be deduced by analogy. In the third regime, owing to the tediousness of the mathematical manipulations which are required, an expression for the temperature profile as a function of space and time cannot be easily obtained, but a great deal of useful information including a theoretical expression for the time constant of exponential decay can nevertheless be extracted. With these solutions, procedures for measuring latent heat effects can be formulated.

Heat Conduction Model

The model used in attacking this problem is depicted in Figure 2.1. The figure shows the DTA tube inside the nickel block as a series of concentric annular volumes. The central core is reserved for the thermocouple and hence is vacant free space. The first concentric annular volume (region 5) is the inner wall of the thermocouple well, the next (region 4) is the sample material, the next (region 3) is the outer wall of the sample tube, the next (region 2) is the gas film between the sample tube and the nickel block, (region 1).

During the operation of the DTA equipment, three different sets of boundary conditions may exist, establishing three distinct regimes of operation.

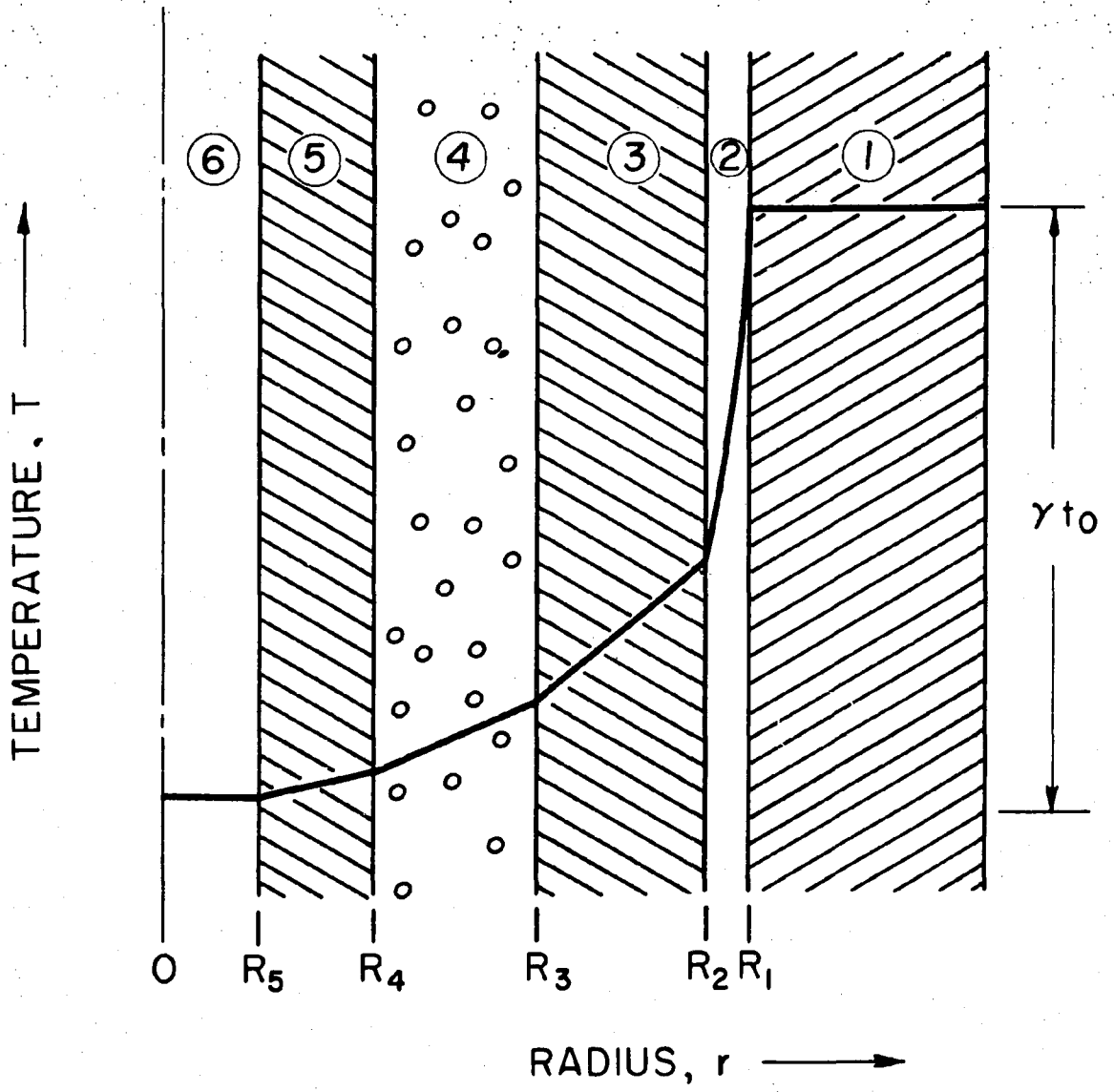


Figure 2.1. Model for the Investigation of Heat Conduction in DTA (Not to Scale).

Regime A defines the system under constant heating conditions wherein the temperatures at all points in the system are increasing linearly with time. Regime B defines the system during the time that the sample is melting, and Regime C defines the system as it is returning to the constant heating condition (Regime A) after the sample has melted. In all three regimes of operation it is assumed that, owing to its massiveness, the nickel block acts as a source for heat, and owing to its high thermal conductivity, its temperature is uniform, and also increases linearly with time, i.e.,

$$T_2(R_1, t) = \gamma(t + t_o) \qquad 2.1$$

where γ = heating rate, ^{o}K/unit time.

The differential equation governing the flow of heat in each contiguous region may be written in cylindrical coordinates as follows:

$$\frac{\delta^2 T}{\delta r^2} + \frac{1}{r}\frac{\delta T}{\delta r} = \frac{\rho c_p}{k}\frac{\delta T}{\delta t} \qquad 2.2$$

where
- T = temperature
- r = radius
- ρ = density
- c_p = specific heat
- k = thermal conductivity
- t = time

Internal sources and sinks are assumed to be absent. In terms of the normalized variables and parameters for region 4, Equation 2.2 becomes

$$\frac{\delta^2 v}{\delta \zeta^2} + \frac{1}{\zeta}\frac{\delta v}{\delta \zeta} = \tau\frac{\delta v}{\delta t} \qquad 2.3$$

where $v(\zeta, t) = T_4(r, t) - T_o$

$\zeta = r/R_4$

$\tau = R_4^2(\rho c_p)_4/k_4$

T_o = reference temperature

For region (3)

$$\frac{\delta^2 y}{\delta \zeta'^2} + \frac{1}{\zeta'} \frac{\delta y}{\delta \zeta'} = \tau' \frac{\delta y}{\delta t} \qquad 2.4$$

where $y(\zeta', t) = T_3(r, t) - T_o$

$\zeta' = r/R_3$

$\tau' = R_3^2(\rho c_p)_3/k_3$

For region (2)

$$\frac{\delta^2 z}{\delta \zeta''^2} + \frac{1}{\zeta''} \frac{\delta z}{\delta \zeta''} = \tau'' \frac{\delta z}{\delta t} \qquad 2.5$$

where $z(\zeta'', t) = T_2(r, t) - T_o$

$\zeta'' = r/R_2$

$\tau'' = R_2^2(\rho c_p)_2/k_2$

After determining the boundary conditions which satisfactorily approximate the physical system, a solution of the simultaneous differential equations, Equations 2.3 through 2.5 may be sought. This problem will be considered next, for regimes A, B, and C, each in turn.

Heat Conduction Prior to Melting - Regime A

Assuming that the heating rate is constant and equal to $\gamma^{\circ}K$/unit time, Equations 2.3 through 2.5 become:

$$\frac{d^2 v}{d\zeta^2} + \frac{1}{\zeta}\frac{dv}{d\zeta} = \gamma\tau$$

$$\frac{d^2 y}{d\zeta'^2} + \frac{1}{\zeta'}\frac{dy}{d\zeta'} = \gamma\tau' \qquad 2.6$$

$$\frac{d^2 z}{d\zeta''^2} + \frac{1}{\zeta''}\frac{dz}{d\zeta''} = 0$$

It has been assumed that the rate of accumulation of heat in the gas film is negligible compared to the rate at which heat is transferred across the film, or, in other words that the thermal diffusivity of the gas film is very large. For the particular system being considered here this approximation seems to be excellent although in general it may not be a valid assumption.

Since the thermocouple well acts as a sink for heat:

$$(\rho c_p)_5 \pi (R_4^2 - R_5^2)\frac{\delta T_1}{\delta t} = k_4 \cdot 2\pi R_4^2 \left.\frac{\delta T_2}{\delta r}\right|_{r = R_4}$$

or

$$\gamma t_5 = \zeta \left.\frac{\delta v}{\delta \zeta}\right|_{\zeta = 1} \qquad 2.7$$

where $t_5 = (\rho c_p)_5 (R_4^2 - R_5^2)/2k_4$

Continuity of the temperature profile and heat flux at the inner boundaries lead to the relations:

$$v(\eta, t) = y(1, t) \qquad 2.8$$

$$y(\eta', t) = z(1, t) \qquad 2.9$$

$$\eta\phi \left.\frac{\delta v}{\delta \zeta}\right|_{\zeta = \eta} = \left.\frac{\delta y}{\delta \zeta'}\right|_{\zeta' = 1} \qquad 2.10$$

$$\eta'\phi' \left.\frac{\delta y}{\delta \zeta'}\right|_{\zeta' = \eta'} = \left.\frac{\delta z}{\delta \zeta''}\right|_{\zeta'' = 1} \qquad 2.11$$

where $\eta = R_3/R_4$ $\quad \phi = k_4/k_3$

$\eta' = R_2/R_3$ $\quad \phi' = k_3/k_2$

$\eta'' = R_1/R_2$

Finally, at the outer boundary, the temperature rises linearly with time

$$z(\eta'', t) = \gamma (t + t_o) \qquad 2.12$$

The reference temperature, γt_o, has been taken to be the temperature of the thermocouple well at zero time, $T_5(0)$.

These equations can be integrated directly to yield:

$$\begin{aligned} v &= \gamma \tau \zeta^2/4 + A \ln \zeta + B \\ y &= \gamma \tau' \zeta'^2/4 + C \ln \zeta' + D \\ z &= P \ln \zeta'' + Q \end{aligned} \qquad 2.13$$

where A, B, C, D, P and Q are independent of r and may be evaluated from Equations 2.7 through 2.12 to obtain

$$\begin{aligned} v(\zeta, t) = {} & \gamma (t + t_o) - \frac{\gamma\tau}{4}(\eta^2 - \zeta^2) - \frac{\gamma\tau'}{4}(\eta'^2 - 1) \\ & + \frac{\gamma}{2}(2t_5 - \tau) \ln \frac{\zeta}{\eta} - \frac{\gamma}{2}[2\phi t_5 + \phi\tau(\eta^2 - 1) - \tau'] \ln \eta' \\ & - \frac{\gamma}{2}[2\phi t_5 + \phi\tau(\eta^2 - 1) + \tau'(\eta'^2 - 1)] \phi' \ln \eta'' \end{aligned} \qquad 2.14$$

$$y(\zeta', t) = \gamma(t + t_o) - \frac{\gamma\tau'}{4}(\eta'^2 - \zeta'^2)$$

$$+ \frac{\gamma}{2}[2\phi t_5 + \phi\tau(\eta^2 - 1) - \tau'] \ln\frac{\zeta'}{\eta'} - \frac{\gamma}{2}\phi' \ln\eta'' [2\phi t_5$$

$$+ \phi\tau(\eta^2 - 1) + \tau'(\eta'^2 - 1)] \qquad 2.15$$

$$z(\zeta'', t) = \gamma(t + t_o) + \frac{\gamma\phi'}{2}[2\phi t_5 + \phi\tau(\eta^2 - 1) + \tau'(\eta'^2 - 1)] \ln\frac{\zeta''}{\eta''}$$

$$2.16$$

Lastly, the overall temperature lag across the system may be computed.

$$\gamma t_o = z(\eta'', t) - v(1, t) = \frac{\gamma\tau}{4}(\eta^2 - 1) + \frac{\gamma\tau'}{4}(\eta'^2 - 1)$$

$$+ \frac{\gamma}{2}(2t_5 - \tau)\ln\eta + \frac{\gamma}{2}[2\phi t_5 + \phi\tau(\eta^2 - 1) - \tau'] \ln\eta'$$

$$+ \frac{\gamma}{2}[2\phi t_5 + \phi\tau(\eta^2 - 1) + \tau'(\eta'^2 - 1)] \phi' \ln\eta'' \qquad 2.17$$

For a typical set of parameters:

$\eta = 1.56$	$\tau = 1.83$ sec	$\phi = 3.13$
$\eta' = 1.30$	$\tau' = 26.6$ sec	$\phi' = 35.7$
$\eta'' = 1.0384$	$t_5 = 1.06$ sec	$\gamma = 0.05^{\circ}K/sec$

a value of $1.30^{\circ}K$ was found for γt_o, of which $1.08^{\circ}K$ was contributed by the gas film (N_2), $0.17^{\circ}K$ by the silica tube, and $0.05^{\circ}K$ by the sample (InSb).

The thermal conductance, defined in Equation 1.9 as the heat flowing across the system per unit height per unit temperature difference, may also be computed. Using the results in Equations 2.14 through 2.16:

$$G = \frac{2\pi k_4 \zeta \left.\frac{\delta v}{\delta \zeta}\right|_{\zeta = 1}}{z(\eta'', t) - v(1, t)} = 2\pi k_4 t_5 / t_o \qquad 2.18$$

For the above set of parameters, G is found to be 0.0161 cal/sec-cm-^{o}C.

Heat Conduction During Melting - Regime B

In this case it is assumed that the sample is melting as the temperature of the nickel block increases linearly with time. The heat conduction in the sample is ignored as its temperature is assumed to remain uniformly at the melting point T_f. Taking $T_o = T_f$, the differential equations which must be solved are:

$$\frac{\delta^2 y}{\delta \zeta'^2} + \frac{1}{\zeta'} \frac{\delta y}{\delta \zeta'} = \tau' \frac{\delta y}{\delta t} \qquad 2.19$$

$$\frac{\delta^2 z}{\delta \zeta''^2} + \frac{1}{\zeta''} \frac{\delta z}{\delta \zeta''} = 0 \qquad 2.20$$

At the inner boundary,

$$y(1, t) = 0 \qquad 2.21$$

Initially, let us take the condition:

$$y(\zeta', 0) = 0 \qquad 2.22(a)$$

$$z(\zeta'', 0) = 0 \qquad 2.22(b)$$

The remaining three boundary conditions are given by Equations 2.9, 2.11, and 2.12, respectively with γt_o in Equation 2.12 being replaced by T_f.

The solution to Equation 2.20 is:

$$z(\zeta'', t) = A(t) \ln \zeta'' + B(t) \qquad 2.23$$

Taking the Laplace transform of Equation 2.23 with respect to time:

$$\bar{z}(\zeta'', s) = \bar{A}(s) \ln \zeta'' + \bar{B}(s) \qquad 2.24$$

Equation 2.19 may be likewise transformed:

$$\bar{y}'' + \frac{1}{\zeta'} \bar{y}' = \tau' s \bar{y} \qquad 2.25$$

Equation 2.25 is the modified Bessel equation, whose solution is:

$$\bar{y}(\zeta', s) = \bar{C}(s) J_o(i\zeta' \sqrt{\tau' s}) + \bar{D}(s) Y_o(i\zeta' \sqrt{\tau' s}) \qquad 2.26$$

The nomenclature used for the Bessel functions is that used by Mickley, Sherwood, and Reed (59). The transformed boundary conditions are:

$$\bar{y}(1, s) = 0$$

$$\bar{y}(\eta', s) = \bar{z}(1, s)$$

$$\eta' \phi' \bar{y}(\eta', s) = \bar{z}'(1, s)$$

$$\bar{z}(\eta'', s) = \gamma / s^2 \qquad 2.27$$

Combining Equations 2.27, 2.24 and 2.26, four equations in $\bar{A}$, $\bar{B}$, $\bar{C}$ and $\bar{D}$ may be obtained:

$$\bar{C} J_o(\beta) + \bar{D} Y_o(\beta) = 0$$

$$\bar{C} J_o(\eta' \beta) + \bar{D} Y_o(\eta' \beta) = \bar{B}$$

$$\bar{C} \beta J_1(\eta' \beta) + \bar{D} \beta Y_1(\eta' \beta) = \bar{A} / \eta' \phi'$$

$$\bar{A} \ln \eta'' + \bar{B} + \gamma / s^2 \qquad 2.28$$

where $\beta \equiv i \sqrt{\tau' s}$

Solving Equations 2.28 for $\bar{A}$, $\bar{B}$, $\bar{C}$ and $\bar{D}$, the transformed variables $\bar{y}$ and $\bar{z}$ become:

$$\bar{y}(\zeta',\beta) =$$

$$\frac{\gamma\tau'^2}{\beta^4} \frac{J_o(\beta)Y_o(\zeta'\beta) - Y_o(\beta)J_o(\zeta'\beta)}{J_o(\beta)Y_o(\eta'\beta) - Y_o(\beta)J_o(\eta'\beta) - \eta'\phi' \ln\eta'' [\beta J_o(\beta)Y_1(\eta'\beta) - \beta Y_o(\beta)J_1(\eta'\beta)]} \qquad 2.29$$

$$\bar{z}(\zeta'',\beta) =$$

$$\frac{\gamma\tau'^2}{\beta^4} \frac{J_o(\beta)Y_o(\eta'\beta) - Y_o(\beta)J_o(\eta'\beta) - \eta'\phi' \ln\zeta'' [\beta J_o(\beta)Y_1(\eta'\beta) - \beta Y_o(\beta)J_1(\eta'\beta)]}{J_o(\beta)Y_o(\eta'\beta) - Y_o(\beta)J_o(\eta'\beta) - \eta'\phi' \ln\eta'' [\beta J_o(\beta)Y_1(\eta'\beta) - \beta Y_o(\beta)J_1(\eta'\beta)]} \qquad 2.30$$

Equations 2.29 and 2.30 cannot be easily inverted because they contain terms of the form $Y_o(\beta)$ and $Y_1(\eta'\beta)$. The series expansion of each of these Bessel functions contains a term in $\ln i\sqrt{s}$, and therefore $\bar{y}(\zeta', s)$ and $\bar{z}(\zeta'', s)$ have a branch cut along the negative real axis. In order to perform the inversion

$$y(\zeta', t) = \frac{1}{2\pi i} \int_{M-i\infty}^{M+i\infty} \bar{y}(\zeta', s) \exp(st)\, ds$$

A contour in in the s-plane must be chosen which excludes the negative real axis. This is a very difficult problem, and efforts to achieve a solution were finally abandoned.

Instead the analogous problem of linear heat flow between infinite parallel planes was considered. The differential equations simplify to:

$$\frac{\delta^2 T_3}{\delta x^2} = \frac{(\rho c_p)_3}{k_3} \frac{\delta T_3}{\delta t} \qquad 2.31$$

$$\frac{\delta^2 T_2}{\delta x^2} = 0 \qquad 2.32$$

Or, in terms of the parameters defined previously:

$$\frac{\delta^2 y}{\delta \zeta'^2} = \tau' \frac{\delta y}{\delta t} \qquad 2.33$$

$$\frac{\delta^2 z}{\delta \zeta''^2} = 0 \qquad 2.34$$

where $\zeta' = x/R_3$, $\zeta'' = x/R_2$, etc.

Although the parameters η', τ', etc. are defined unambiguously in the cylindrical case, since the region is fixed by the axis of the cylinder, the same is not true in the case of infinite parallel planes. It is convenient, however, to retain this notation in order to preserve the analogy, realizing that the choice of the origin is not arbitrary but fixed. That is, the origin is chosen such that

$$r = R_3 \qquad \text{(cylindrical)}$$

corresponds exactly to

$$x = R_3 \qquad \text{(parallel planes)}$$

The boundary conditions are then unchanged and are given by Equations 2.9, 2.11, 2.12, 2.21 and 2.22, with γt_o in 2.12 being replaced by T_f. Equations 2.33 and 2.34 may be written in operational form as before and solved to give

$$\bar{y}(\zeta', s) = \bar{C}(s) \sinh \zeta' \sqrt{\tau' s} + \bar{D}(s) \cosh \zeta' \sqrt{\tau' s} \qquad 2.35$$

$$\bar{z}(\zeta'', s) = \bar{A}(s)\, \zeta'' + \bar{B}(s) \qquad 2.36$$

The coefficients $\bar{A}$, $\bar{B}$, $\bar{C}$ and $\bar{D}$ are found by using the boundary conditions, with the final expressions being given by:

$$\bar{y}(\zeta', s) =$$

$$\frac{\gamma}{s^2} \; \frac{\sinh (1 - \zeta') \sqrt{\tau' s}}{\sinh (1 - \eta') \sqrt{\tau' s} + \eta' \phi' (1 - \eta'') \sqrt{\tau' s} \cosh (1 - \eta') \sqrt{\tau' s}} \qquad 2.37$$

$$\bar{z}(\zeta', s) =$$

$$\frac{\gamma}{s^2} \; \frac{\sinh (1 - \eta') \sqrt{\tau' s} + \eta' \phi' (1 - \zeta'') \sqrt{\tau' s} \cosh (1 - \eta') \sqrt{\tau' s}}{\sinh (1 - \eta') \sqrt{\tau' s} + \eta' \phi' (1 - \eta'') \sqrt{\tau' s} \cosh (1 - \eta') \sqrt{\tau' s}} \qquad 2.38$$

Equations 2.37 and 2.38 are well behaved; that is, they do not have any branch cuts. The inversion integral may thus be evaluated by the method of residues (18). Complete inversion yields:

$$y(\zeta' t) = a_o(\zeta') + a_1(\zeta')\, t + \sum_{n=1}^{\infty} b_n \sin \left(\frac{\zeta' - 1}{\eta' - 1}\right) \alpha_n \exp \left[- \frac{\alpha_n^2 t}{(\eta' - 1)^2 \tau'} \right] \qquad 2.39$$

and

$$z(\zeta'', t) = c_o(\zeta'') + c_1(\zeta'')\, t +$$

$$\sum_{n=1}^{\infty} b_n \left\{ \sin \alpha_n + \frac{\zeta'' - 1}{\eta' - 1} \eta' \phi' \alpha_n \cos \alpha_n \right\} \exp - \frac{\alpha_n^2 t}{(\eta' - 1)^2 \tau'} \qquad 2.40$$

where α_n are the positive roots (all real and simple) of:

$$\alpha \cot \alpha + \frac{\eta'-1}{\eta'\phi'(\eta''-1)} = 0 \qquad 2.41$$

and where

$$a_1(\zeta') = \frac{\gamma(\zeta'-1)}{\eta' - 1 + \eta'\phi'(\eta''-1)}$$

$$c_1(\zeta'') = \frac{\gamma\{(\eta'-1) + \eta'\phi'(\zeta''-1)\}}{\eta' - 1 + \eta'\phi'(\eta''-1)}$$

$$a_o(\zeta') = \frac{\gamma\tau'}{6} \frac{(\zeta'-1)\{(\zeta'-1)^2 - (\eta'-1)^2\}}{\eta' - 1 + \eta'\phi'(\eta''-1)}$$

$$- \frac{\gamma\tau'}{3} \frac{\eta'\phi'(\zeta'-1)(\eta'-1)^2(\eta''-1)}{\{\eta' - 1 + \eta'\phi'(\eta''-1)\}^2}$$

$$c_o(\zeta'') = - \frac{\gamma\tau'}{3} \frac{\eta'\phi'(\zeta''-\eta'')(\eta'-1)^3}{\{\eta' - 1 + \eta'\phi'(\eta''-1)\}^2}$$

and

$$b_n = \frac{2\gamma\tau'(\eta'-1)^2 \alpha_n^{-3}}{\frac{\eta'\phi'(\eta''-1)}{\eta'-1} \alpha_n \sin \alpha_n - \cos \alpha_n - \frac{\eta'\phi'(\eta''-1)}{\eta'-1} \cos \alpha_n}$$

The general solution of Equations 2.31 and 2.32 with the time derivative included in Equation 2.32 is discussed in Appendix V, and it is concluded that the error introduced by neglecting the time derivative is small.

For large values of the time Equations 2.39 and 2.40 become:

$$y = \left[\frac{\zeta' - 1}{\eta' - 1 + \eta'\phi'(\eta''-1)}\right] \gamma t \qquad 2.42$$

$$z = \left[\frac{\eta' - 1 + \eta'\phi'(\zeta''-1)}{\eta' - 1 + \eta'\phi'(\eta''-1)}\right] \gamma t \qquad 2.43$$

The corresponding approximations for the cylindrical case may be found by replacing $\zeta' - 1$ by $\ln \zeta'$, etc. Moreover, because of the curvature of the bounding surfaces, the factors $\eta'\phi'$ become simply ϕ'. This analogy yields:

$$y = \frac{\gamma t \ln \zeta'}{\ln \eta' + \phi' \ln \eta''} \qquad t \text{ large} \qquad 2.44$$

$$z = \frac{\gamma t (\ln \eta' + \phi' \ln \zeta'')}{\ln \eta' + \phi' \ln \eta''} \qquad t \text{ large} \qquad 2.45$$

Equations 2.44 and 2.45 are in agreement with all of the boundary conditions. Furthermore, the conductance for heat transfer is defined by

$$G = \frac{2\pi k_3 r \frac{\delta T_3}{\delta r}\Big|_{r = R_3}}{T_4(R_5) - T_3(R_3)} = \frac{2\pi k_3 \cdot \zeta' \frac{\delta y}{\delta \zeta'}\Big|_{\zeta'=1}}{\gamma t} \qquad 2.46$$

Using 2.44, it is evident that:

$$G = \frac{2\pi k_3}{\ln \eta' + \phi' \ln \eta''} \qquad t \text{ large}$$

$$= \left\{ \frac{\ln \eta'}{2\pi k_3} + \frac{\ln \eta''}{2\pi k_4} \right\}^{-1} \qquad 2.47$$

That is, as time becomes large, the conductance for heat transfer during melting approaches its steady state value, as would be expected. For the set of parameters used in the preceding section a value of 0.0225 cal/sec-cm-^{o}K is found for the steady state value of G during melting.

Heat Conduction Following Melting - Regime C

In this regime, it is assumed that melting is completed, and the sample temperature is rising more rapidly than the nickel block temperature. The differential equations whose solutions are examined in this section are:

$$\frac{\delta^2 v}{\delta \zeta^2} + \frac{1}{\zeta} \frac{\delta v}{\delta \zeta} = \tau \frac{\delta v}{\delta t} \qquad 2.3$$

$$\frac{\delta^2 y}{\delta \zeta'^2} + \frac{1}{\zeta'} \frac{\delta y}{\delta \zeta'} = \tau' \frac{\delta y}{\delta t} \qquad 2.4$$

$$\frac{\delta^2 z}{\delta \zeta''^2} + \frac{1}{\zeta''} \frac{\delta z}{\delta \zeta''} = 0 \qquad 2.20$$

The initial temperature profile may be found from the large time approximation in regime (B).

$$v(\zeta, 0) = 0$$

$$y(\zeta', 0) = \gamma t_f \left[\frac{\ln \zeta'}{\ln \eta' + \phi' \ln \eta''} \right]$$

where t_f is the time interval over which melting takes place.

As in Regime (A), the thermocouple well is assumed to behave as a sink for heat:

$$\bar{v}(1, t) = \frac{\nu}{\tau} \int_0^t \zeta \frac{\delta v}{\delta \zeta} \Big|_{\zeta=1} dt \qquad 2.48$$

where $\nu = \tau / t_5$.

The remaining boundary conditions are given by Equations 2.8 through 2.12, with t_f replacing t_o in Equation 2.12.

Equation 2.3 becomes, after taking Laplace transforms with respect to time:

$$\bar{v}'' + \frac{1}{\zeta} \bar{v}' = \tau s \bar{v} \qquad 2.49$$

which has the solution:

$$\bar{v}(\zeta, s) = \bar{A}(s) J_o (i\zeta \sqrt{\tau s}) + \bar{B}(s) Y_o (i\zeta \sqrt{\tau s}) \qquad 2.50$$

Similarly, Equation 2.4 may be transformed to give

$$\bar{y}'' + \frac{1}{\zeta'} \bar{y}' = \tau' s \bar{y} + \tau' \gamma t_f \left[\frac{\ln \zeta'}{\ln \eta' + \phi' \ln \eta''} \right] \qquad 2.51$$

whence

$$\bar{y}(\zeta', s) = \bar{C}(s) J_o (i\zeta' \sqrt{\tau' s}) + \bar{D}(s) Y_o (i\zeta' \sqrt{\tau s}) - \frac{\gamma t_f}{s} \frac{\ln \zeta'}{\ln \eta' + \phi' \ln \eta''} \qquad 2.52$$

Finally,

$$z(\zeta'', t) = P(t) \ln \zeta'' + Q(t) \qquad 2.53$$

or

$$\bar{z}(\zeta'', s) = \bar{P}(s) \ln \zeta'' + \bar{Q}(s) \qquad 2.54$$

The transformed boundary conditions are:

$$\bar{v}(1, s) = \frac{\nu}{\tau s} \zeta \frac{\delta \bar{v}}{\delta \zeta} \Big|_{\zeta=1}$$

$$\bar{v}(\eta, s) = \bar{y}(1, s)$$

$$\eta \phi \bar{v}(\zeta, s) = \bar{y}'(1, s)$$

$$\bar{y}(\eta', s) = \bar{z}(1, s)$$

$$\eta' \phi' \bar{y}'(\eta', s) = \bar{z}'(1, s)$$

$$\bar{z}(\eta'', s) = \gamma \left[\frac{t_f}{s} + \frac{1}{s^2} \right] \qquad 2.55$$

The boundary conditions, Equation 2.55 together with Equations 2.50, 2.52 and 2.54 yield six equations in the coefficients $\bar{A}$, $\bar{B}$, $\bar{C}$, $\bar{D}$, $\bar{P}$, and $\bar{Q}$, viz.:

$$\bar{A} J_o(\beta) + \bar{B} Y_o(\beta) = \frac{\nu}{\tau s} \left[- \bar{A} \beta J_1(\beta) - \bar{B} \beta Y_1(\beta) \right]$$

$$\bar{A} J_o(\eta\beta) + \bar{B} Y_o(\eta\beta) = \bar{C} J_o(\epsilon\beta) + \bar{D} Y_o(\epsilon\beta)$$

$$\bar{C} J_o(\epsilon\eta'\beta) + \bar{D} Y_o(\epsilon\eta'\beta) - \frac{\gamma t_f}{s} \left[\frac{\ln \eta'}{\ln \eta' + \phi' \ln \eta''} \right] = \bar{Q}$$

$$\bar{A} \beta J_1(\eta\beta) + \bar{B} \beta Y_1(\eta\beta) =$$

$$\frac{1}{\eta\phi} \left[\bar{C} \epsilon \beta J_1(\epsilon\beta) + \bar{D} \epsilon \beta Y_1(\epsilon\beta) + \frac{\gamma t_f}{s(\ln \eta' + \phi' \ln \eta'')} \right]$$

$$\bar{C} \epsilon \beta J_1(\epsilon\eta'\beta) + \bar{D} \epsilon \beta Y_1(\epsilon\eta'\beta) + \frac{\gamma t_f}{s\eta'(\ln \eta' + \phi' \ln \eta'')} + \frac{\bar{P}}{\eta'\phi'} = 0$$

$$\bar{P} \ln \eta'' + \bar{Q} = \gamma \left[\frac{t_f}{s} + \frac{1}{s^2} \right] \qquad 2.56$$

where $\beta \equiv i\sqrt{\tau s}$ and $\epsilon \equiv \sqrt{\tau'/\tau}$.

The simultaneous solution of six linear equations, Equations 2.56, for the coefficients $\bar{A}$, $\bar{B}$, $\bar{C}$, $\bar{D}$, $\bar{P}$ and $\bar{Q}$, subsequent determination of the transformed variables $\bar{v}$, $\bar{y}$, and $\bar{z}$, and inversion are not practically feasible. Furthermore, even if the above operations were carried out, the result would be of questionable value since it would be very complex indeed. On the other hand, past experience gives a clue as to the general form of the expected solution. It would be expected that the solution would contain a term dependent on the geometry and thermal properties of the system alone, a term linear in the time, and a term of the form

$$\sum_n C_n e^{-\beta_n^2 t/\tau} \qquad 2.57$$

where the C_n are complex functions of the geometry and thermal properties of the system, and the summation is taken over all the eigenvalues of the system.

Furthermore, the β_n are found from the roots of the principal determinant, D_p, formed from the Equations 2.56; that is:

$$D_p = F_1(\beta)\left\{\frac{\epsilon}{\eta\,\eta'\,\phi\,\phi'}\ F_2(\beta) - \frac{\beta\epsilon^2\ \ln\eta''}{\eta\,\phi}\ F_3(\beta)\right\}$$

$$+\ F_4(\beta)\left\{\epsilon\beta\ \ln\eta''\ F_5(\beta) - \frac{1}{\eta'\phi'}\ F_6(\beta)\right\} \qquad 2.58$$

where

$$F_1(\beta) = \Delta_1(\beta)\,Y_o(\beta\eta) - \Delta_2(\beta)\,J_o(\beta\eta)$$

$$F_2(\beta) = J_1(\epsilon\beta)\,Y_o(\epsilon\eta'\beta) - Y_1(\epsilon\beta)\,J_o(\epsilon\eta'\beta)$$

$$F_3(\beta) = J_1(\epsilon\beta)\,Y_1(\epsilon\eta'\beta) - Y_1(\epsilon\beta)\,J_1(\epsilon\eta'\beta)$$

$$F_4(\beta) = \Delta_1(\beta)\,Y_1(\eta\beta) - \Delta_2(\beta)\,J_1(\eta\beta)$$

$$F_5(\beta) = J_o(\epsilon\beta)\,Y_1(\epsilon\eta'\beta) - Y_o(\epsilon\beta)\,J_1(\epsilon\eta'\beta)$$

$$F_6(\beta) = J_o(\epsilon\beta)\,Y_o(\epsilon\eta'\beta) - Y_o(\epsilon\beta)\,J_o(\epsilon\eta'\beta)$$

$$\Delta_1(\beta) = \beta\,J_o(\beta) - \nu\,J_1(\beta)$$

$$\Delta_2(\beta) = \beta\,Y_o(\beta) - \nu\,Y_1(\beta)$$

$$\nu = \tau/t_5 = 2\,\frac{(\rho c_p)_4}{(\rho c_p)_5}\ \frac{R_4^2}{R_4^2 - R_5^2}$$

Now it is experimentally known that after melting, the DTA curve decays back to the baseline in an exponential fashion, which means that only the leading term of the sum, Equation 2.57, need be considered. In other words the theoretical expression for the time constant of exponential decay becomes:

$$\tau_{exp} = \tau/\beta_1^2 \qquad 2.59$$

where β_1 is the smallest root of the principal determinant, Equation 2.58. Equation 2.59 does in fact predict the correct order or magnitude of the time constant of exponential decay. For example, using the following typical set of parameters:

$\eta = 1.56$	$\tau = 1.83$ sec	$\phi = 3.13$
$\eta' = 1.30$	$\tau' = 26.6$ sec	$\phi' = 35.7$
$\eta'' = 1.0384$	$t_5 = 1.06$ sec	

β_1 was found to be 0.270, which leads to a value of $\tau_{exp} = 1.83/(0.270)^2$ = 25.1 sec, which is the correct order of magnitude.

The Thermal Conductance

It is now possible to examine the behavior of the thermal conductance during the course of a DTA experiment. Consider Figure 2.2 which depicts the variation of the thermal conductance side by side with the DTA curve. Just prior to melting and a few minutes after melting the value of the thermal conductance will be well below its steady state value.* Upon the initiation of melting the conductance will immediately rise to its steady state value with a time constant of about one second.** It will remain at this value throughout melting which may take about ten minutes. Immediately following the completion of melting the conductance will revert to the value it had before melting with a decay constant of about 25 seconds.

Based on these considerations it is evident that the steady state approximation will be quite valid because

$$\frac{\int_0^{t_2} G\,dt}{\int_0^{t_2} dt} \cong G_{ss}$$

---

* Cf. Equations 1.10 through 1.13 as well as the discussion following Equations 2.17 and 2.45.

** Cf. Appendix V.

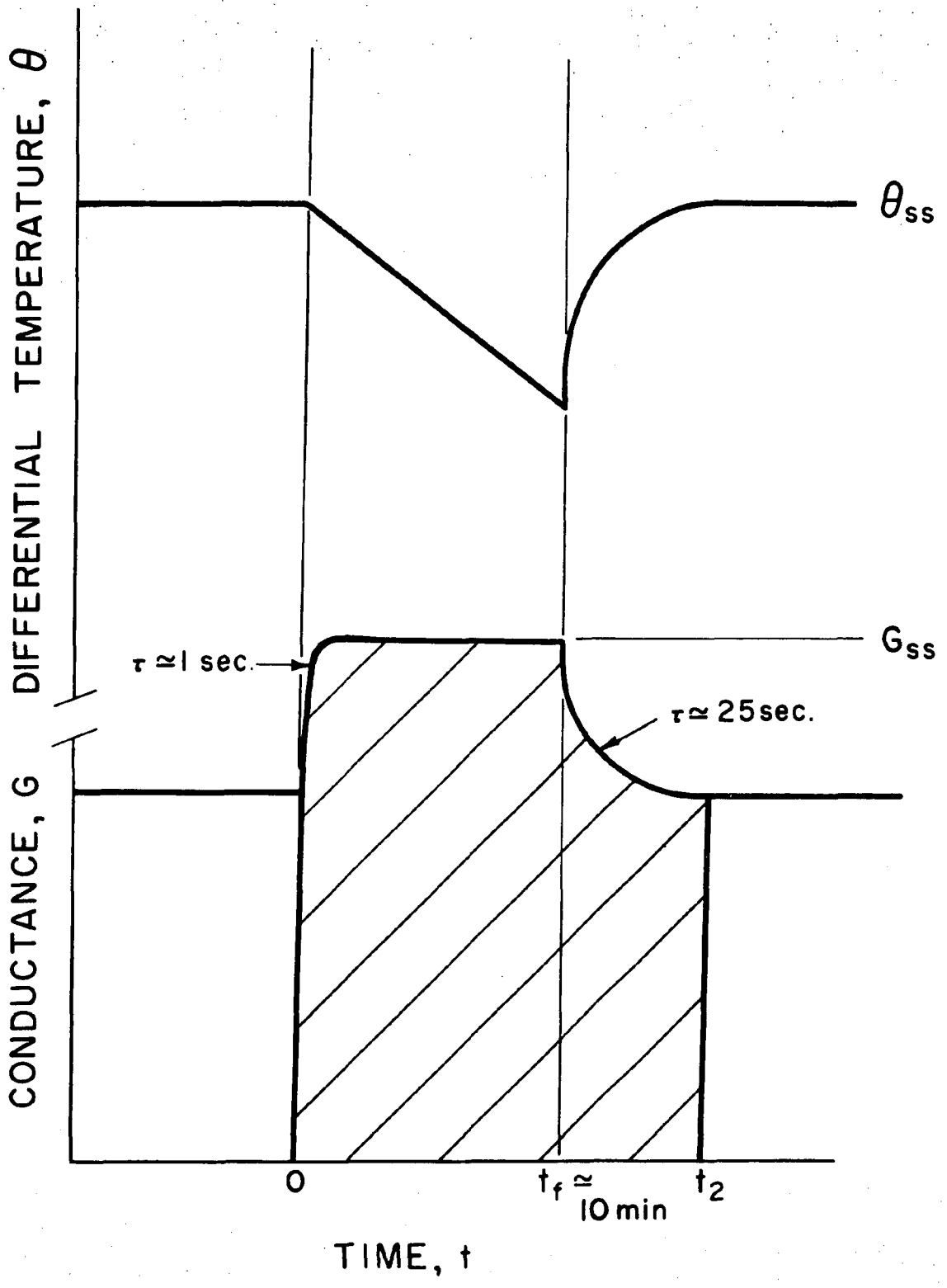


Figure 2.2. Relationship between the Differential Temperature, θ, and the Thermal Conductance, G, during DTA (Not to Scale).

as can be seen from Figure 2. 2.

In the foregoing, it was tacitly assumed that thermal conduction was the only mechanism by which heat could be transferred across the DTA system. At high temperatures, however, it would appear that thermal radiation would also contribute even though the temperature gradient is small (ΔT across the gas film is only about $1^{\circ}K$ before melting and may increase to about $30^{\circ}K$ during melting). These matters will be examined next.

Radiation in the DTA System

In this section the equations governing the transfer of heat by means of thermal radiation are considered and expressions are derived for this contribution to the thermal conductance. Consider Figure 2. 1 where radiation is emanating from the "gray" oxidized nickel surface and reflects diffusely from the surfaces of regions (4) and (1). It is assumed that radiation which is absorbed is absorbed at the surface of each region, that the reflectivity of the silica tube is zero ($\rho_3 = 0$), that the transmissivity of the sample is zero ($\tau_4 = 0$), and that only wavelengths less than 3. 7 microns pass through the silica tube, so that multiple reflections of wavelengths greater than 3. 7 microns need not be considered; that is to say none of the radiation which reflects from region (4) will be absorbed by region (3). With these assumptions, together with Planck's distribution function for black body radiation, it is possible to estimate an effective emissivity for fused silica as a function of temperature.

Keeping this in mind, denoting $\sigma A_i T_i^4$ by X_i, and noting that $f_{43} = f_{31} = 1$, where f_{jk} is the fraction of the radiation from j which is "seen" by k, the following relations are readily found:

Radiation emitted by 1, 3, and 4 respectively:

$$X_1 \epsilon_1$$

$$X_3 \epsilon_3$$

$$X_4 \epsilon_4$$

Radiation reflected by 1:

$$X_3\epsilon_3(1-\epsilon_1) + X_4\epsilon_4(1-\epsilon_3)(1-\epsilon_1) +$$

$$(1-\epsilon_1)(1-\epsilon_3)(1-\epsilon_4) f_{14} (X_1\epsilon_1 + X_3\epsilon_3(1-\epsilon_3) + X_4\epsilon_4(1-\epsilon_1)) +$$

$$\epsilon_1(1-\epsilon_1)(1-\epsilon_3)(1-\epsilon_4)^2 f_{14}^2 (X_1\epsilon_1 + X_3\epsilon_3(1-\epsilon_3) + X_4\epsilon_4(1-\epsilon_1))$$

$$+ \ldots\ldots\ldots$$

Radiation absorbed by 1:

$$X_3\epsilon_3\epsilon_1 + X_4\epsilon_4(1-\epsilon_3)\epsilon_1 +$$

$$\epsilon_1(1-\epsilon_3)(1-\epsilon_4) f_{14} (X_1\epsilon_1 + X_3(1-\epsilon_1)\epsilon_3 + X_4(1-\epsilon_1)\epsilon_4) +$$

$$\epsilon_1(1-\epsilon_1)(1-\epsilon_3)(1-\epsilon_4)^2 f_{14}^2 (X_1\epsilon_1 + X_3(1-\epsilon_1)\epsilon_3 + X_4(1-\epsilon_1)\epsilon_4)$$

$$+ \ldots\ldots\ldots$$

Radiation transmitted by 3:

$$X_1\epsilon_1(1-\epsilon_3) f_{13} + X_3\epsilon_3(1-\epsilon_1)(1-\epsilon_3) f_{13} + X_4\epsilon_4(1-\epsilon_3)$$

Radiation absorbed by 3:

$$X_1\epsilon_1\epsilon_3 f_{13} + X_3\epsilon_3^2(1-\epsilon_1) f_{13} + X_4\epsilon_4\epsilon_3$$

Radiation reflected by 4:

$$(1-\epsilon_4)(1-\epsilon_3) f_{14} (X_1\epsilon_1 + X_3(1-\epsilon_1)\epsilon_3) +$$

$$X_4(1-\epsilon_4)\epsilon_4(1-\epsilon_3)(1-\epsilon_1) f_{14} +$$

$$(1-\epsilon_1)(1-\epsilon_3)(1-\epsilon_4)^2 f_{14}^2 (X_1\epsilon_1 + X_3(1-\epsilon_1)\epsilon_3 + X_4(1-\epsilon_1)\epsilon_4)$$

$$+ \ldots\ldots\ldots$$

Radiation absorbed by 4:

$$\epsilon_4 (1-\epsilon_3) f_{14} (X_1\epsilon_1 + X_3\epsilon_3 (1-\epsilon_1)) + X_4\epsilon_4^2 (1-\epsilon_3)(1-\epsilon_1) f_{14} +$$

$$\epsilon_4 (1-\epsilon_1)(1-\epsilon_3)(1-\epsilon_4) f_{14}^2 (X_1\epsilon_1 + X_3 (1-\epsilon_1) \epsilon_3 + X_4 (1-\epsilon_1) \epsilon_4) +$$

$$\epsilon_4 (1-\epsilon_1)^2 (1-\epsilon_3)(1-\epsilon_4)^2 f_{14}^3 (X_1\epsilon_1 + X_3 (1-\epsilon_1) \epsilon_3 + X_4 (1-\epsilon_1) \epsilon_4)$$

+ .....

The net radiation transferred to 3 is:

Q'_5 = Radiation absorbed by 3 - Radiation emitted by 3

$$= X_1\epsilon_1\epsilon_3 f_{13} + X_3\epsilon_3^2 (1-\epsilon_1) f_{13} + X_4\epsilon_4\epsilon_3 - X_3\epsilon_3$$

But $Q'_5 = 0$ when $T_1 = T_3 = T_4$ so that:

$$f_{13} = \frac{a - b\epsilon_4}{\epsilon_1 + a\epsilon_3 (1-\epsilon_1)} \qquad 2.60$$

where $a = A_3/A_1 = 2\pi R_2 L / 2\pi R_1 L = R_2/R_1 = D_2/D_1$ and

$$b = A_4/A_1 = R_3/R_1 = D_3/D_1. \qquad 2.61$$

Substituting the value of f_{13} back into the expression for Q'_5 and assuming that $T_3 \cong T_4$ it is readily found that:

$$Q'_5 = \sigma A_1 \frac{\epsilon_1\epsilon_3 (a-b\epsilon_4)}{\epsilon_1 + a\epsilon_3 (1-\epsilon_1)} (T_1^4 - T_3^4)$$

$$Q'_5 = \sigma A_1 F_5 (T_1^4 - T_3^4)$$

where

$$F_5 = \frac{\epsilon_1\epsilon_3 (a - b\epsilon_4)}{\epsilon_1 + a\epsilon_3 (1-\epsilon_1)} \qquad 2.62$$

The thermal conductance for radiation to 3 may be defined as:

$$G_5 = Q'_5 / L(T_1 - T_3)$$

and if $T_1 \cong T_3$:

$$G_5 = 8\pi \sigma R_1 T^3 F_5 \qquad 2.63$$

The analogous procedure when applied to the net radiation transferred to region 4 is somewhat more complex because an infinite series results. The situation is rapidly solved, however, since the series obtained is of the form:

$$1 + z + z^2 + z^3 + \ldots .$$

where $z = (1-\epsilon_1)(1-\epsilon_4) f_{14} < 1$, so that:

$$1 + z + z^2 + \ldots \equiv \frac{1}{1 - z}$$

Rather than going through the complete derivation, however, as it is lengthy, only the results will be stated. They are:

$$f_{14} = \frac{b}{(1-\epsilon_3)(\epsilon_1 + a(1-\epsilon_1)\epsilon_3 + b(1-\epsilon_1)\epsilon_4) + b(1-\epsilon_1)(1-\epsilon_4)} \qquad 2.64$$

$$Q'_6 = \sigma A_1 F_6 (T_1^4 - T_4^4)$$

$$F_6 = \frac{b\epsilon_1\epsilon_4}{\epsilon_1 + a(1-\epsilon_1)\epsilon_3 + b(1-\epsilon_1)\epsilon_4} \qquad 2.65$$

$$G_6 = \frac{Q'_6}{L(T_1 - T_4)} \cong 8\pi \sigma R_1 T^3 F_6 \qquad 2.66$$

All these factors are combined in the following chapter to formulate procedures for measuring latent heats of transformation and fusion.

CHAPTER III

APPLICATION OF THE THEORY

In this chapter the equations which were derived in Chapters I and II will be applied to the determination of latent heats in the DTA calorimeter. It may be recalled that two methods of obtaining the thermal conductance were proposed: 1) theoretical calculation from the properties and geometry of the system; and 2) calculation from the experimental time constant of exponential decay of the DTA curve plus the thermal capacity of the system.

Furthermore, in the first method, it was noted that direct measurements of the dimensions of the gas film thickness were imprecise, necessitating the use of an indirect method. Two such methods were proposed: 1) calculation of the film thickness by comparison of the experimental time constant of exponential decay of the DTA curve with its theoretical counterpart; and 2) calculation from two different measurements of the area underneath the DTA curve using two different gaseous atmospheres of widely different thermal conductivity, such as nitrogen and helium, in the system. These methods will now be developed in more detail.

Calculation of the Thermal Conductance using the Theoretical Expression for the Time Constant to find the Gas Film Resistance

In this method the gas film thickness is found by a trial and error calculation wherein $\eta'' = R_1/R_2$* is varied until the time constant of exponential decay as computed from Equation 2.59 agrees with the experimentally measured value given by Equation 1.14 to within one percent. With this information it is then possible to compute the thermal conductance as follows.

It may be recalled that the individual conductance, G_i, is defined by the relation:

---

* See Figure 2.1.
$\eta'' \equiv \eta_2$.

$$G_i = \frac{Q_{il}}{L(T_{i0} - T_{il})} = K_i/L \qquad (3.1)$$

where Q_{il} is the net rate of heat flow across the conductance, L is the height of the sample which is a measure of the effective heat transfer area, T_{i0} is the temperature at the outside radius and T_{il} is the temperature at the inside radius.

For thermal conduction across the gas film and the silica tube the value of the individual conductance may be obtained from the steady state formula:*

$$G_i = 2\pi k_i/\ln \eta_i \qquad (3.2)$$

where η_i represents the radius ratio, R_{i-1}/R_i. For the sample one obtains:

$$\bar{G}_4^{-1} = \frac{\int_{R_4}^{R_3} G_4^{-1}(r)\, dr}{R_3 - R_4} \qquad (3.3)$$

After integration and inversion the result is*

$$\bar{G}_4 = \frac{2\pi k_4}{1 - \left(\frac{\ln \eta}{\eta - 1}\right)} \qquad (3.4)$$

where the average is taken because the solid-liquid interface traverses the sample, starting at the outside diameter and ending at the inside diameter.

The overall conductance is obtained by combining the individual conductances according to the steady state formula:

---

* $\eta \equiv \eta_4$; $\eta' \equiv \eta_3$; $\eta'' \equiv \eta_2$.

$$\frac{1}{G} = \frac{1}{G_2} + \frac{1}{G_3} + \frac{1}{G_4} \qquad (3.5)$$

and the computation of the heat of fusion according to Equation 1.7 becomes a simple matter.

In order to perform the above computations, a computer program was devised for use with the IBM-7090 Data Processing System. The program (Number DTA-19) was written in the MAD* language and is reproduced in Appendix VI together with all of the data used in the computations. The estimation of the physical properties for use in these calculations and others to be soon described is discussed in Appendix IV. In order to test this method of computation, the DTA data for a number of standards whose latent heats of fusion are well known were processed. The results of this calculation are presented in Table 3.1. The values of η'' computed here agree quite well with the directly measured values (1.04 to 1.07), and the calculated heats of fusion agree with the values reported in the literature.

It may be noted that the contribution of thermal radiation was neglected in this analysis. Its effect, however, does not appear to influence the computation of the thermal conductance. Furthermore, the calculation of the thermal conductance by this method does not require precise values for the thermal properties of the various components of the system. Reasonable estimates are usually sufficient.

The uncertainties which result from the neglect of thermal radiation in the model and from the use of approximate values for thermal properties show up in the calculation of a radius ratio for the gas film which is somewhat different from its true value without greatly affecting the computation of the thermal conductance or the heat of fusion. In this respect this method is self-compensating and relatively insensitive to experimental errors and to estimations of the parameters which appear in the calculation.

---

* Michigan Algorithm Decoder, 1963 Version, University of Michigan Computing Center, Ann Arbor, Michigan.

Table 3.1

Results of Computer Program Number DTA-19 for Standards

Material	T_f °K	Run Number	Cycle	η''	L_f cal/g	L_f, lit* cal/g
Ag	1234	C-4	1C-N2	1.066	19.4	24.9
			2H-N2	1.055	22.8	
		C-5	1C-N2	1.065	21.4	
			2H-N2	1.060	22.3	
		C-13	2H-N2	1.037	21.8	
In	430	C-12	2C-N2	1.049	6.6	6.8
			3H-N2	1.047	6.8	
Pb	600	C-3	1C-N2	1.080	4.8	5.9
			2H-N2	1.071	5.8	
			4H-N2	1.072	5.3	
Sb	904	C-2	2C-N2	1.059	33.3	39.0
			3H-N2	1.057	34.4	
Te	723	C-1	2H-N2	1.076	33.6	32.7
			2C-N2	1.084	33.9	

* Kubaschewski and Evans (47).

Calculation of the Thermal Conductance using Two Measurements of the Area under the DTA Curve to find the Gas Film Resistance

In this method the gas film thickness is found by means of a double trial and error calculation wherein the two unknowns, η'' and G, are evaluated from two pieces of experimental data: 1) the area under the DTA curve when a gas of known thermal conductivity (e.g. nitrogen) fills the system; and 2) the change in the area under the DTA curve when a second gas of different thermal conductivity (e.g. helium) replaces the first. A double trial and error calculation is necessary because an estimate of G is required in order to calculate η''.

Figure 2.1 schematically depicts the physical system under consideration and also illustrates the nomenclature to be used in the following discussion. It is assumed that the nickel block due to its high thermal conductivity has a uniform temperature and due to its high total heat capacity (about 240 cal/^{o}C) acts as a source for heat while the melting interface acts as a sink.

It is assumed that two parallel mechanisms contribute to the overall thermal conductance of this system: conduction of heat from the nickel block through a series of intervening media to the solid-liquid interface, and exchange of radiation between the oxidized nickel surface and the silica tube and sample. Note that subscripts 2, 3, and 4 refer to the conductances of the gas film, the silica tube, and the sample, respectively, whereas the subscripts 5 and 6 refer to equivalent conductances for radiation.

The individual conductances for thermal conduction of heat across the system are given by Equations 3.2 and 3.4. It may be recalled that the parallel conductances for thermal radiation are given by:

$$G_i = 8\pi R_1 F_i \sigma T^3 \qquad i = 5, 6 \qquad (2.63;\ 2.66)$$

$$F_5 = \frac{\epsilon_1 \epsilon_3 (R_2 - R_3 \epsilon_4)}{R_1 \epsilon_1 + R_2 \epsilon_3 (1-\epsilon_1)} \qquad (2.62)$$

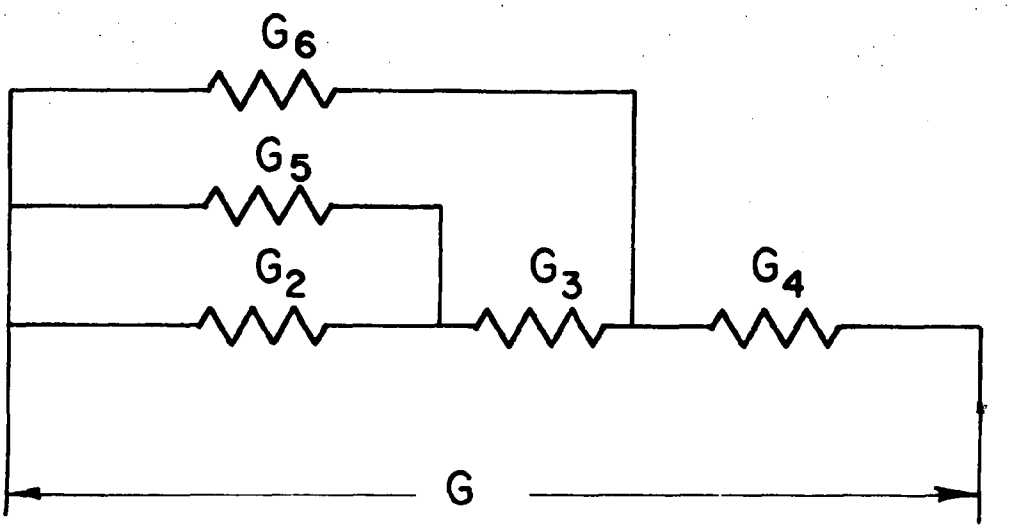


Figure 3.1. Analogous Electrical Circuit for Calculation of the Overall Thermal Conductance.

$$F_6 = \frac{R_3 \epsilon_1 \epsilon_4}{R_1 \epsilon_1 + R_2 \epsilon_3 (1 - \epsilon_1) + R_3 \epsilon_4 (1 - \epsilon_1)} \tag{2.65}$$

where σ is the Stefan-Boltzmann constant and F_5 and F_6 represent the fractions of the total radiation emitted from the oxidized nickel surface which are absorbed by the silica tube and sample, respectively.

In order to combine the individual conductances into a working formula for the overall conductance, it is useful to consider the analogous electrical circuit depicted in Figure 3.1. Combining the individual conductances in the usual fashion, the final equation which represents the overall thermal conductance is readily obtained, viz:

$$G = \frac{G_6 + (G_2 + G_5)(1 + G_6/G_3)}{1 + (G_2 + G_5)\left(\frac{1}{G_3} + \frac{1}{G_4} + \frac{G_6}{G_3 G_4}\right)} \tag{3.6}$$

The radius ratio of the gas film may be found from two different measurements of the area under the DTA curve as follows:

$$\ln \eta'' = \ln \left(1 + \frac{R_1 - R_2}{R_2}\right)$$

$$\ln \eta'' = \frac{-2\pi \beta^2 k_2 k_2^*}{k_2^* - k_2} \left\{ \frac{(G - G^*)}{(G - \alpha)(G^* - \alpha)} \right\} \tag{3.7}$$

where α and β include the effect of radiation, and are defined by the relationships:

$$\beta = \frac{1}{1 + \frac{G_5}{G_3} + \frac{G_5 + G_6}{G_4} + \frac{G_5 G_6}{G_3 G_4}} \tag{3.8}$$

$$\alpha = \beta (G_5 + G_6 + G_5 G_6 / G_3) \tag{3.9}$$

For $G_5 = G_6 = 0$, then $\beta = 1$ and $\alpha = 0$. In the above equations the starred and unstarred values refer to helium and nitrogen gases, respectively, and $G = K/L$ is obtained from Equation 1.7. It may be noted that at sufficiently low temperatures Equation 3.7 reduces, as it should, to:

$$\lim_{G_5, G_6 \to 0} \ln \eta'' = 2\pi \left\{ \frac{\Delta (1/G)}{\Delta (1/k)} \right\} \qquad (3.10)$$

Thus the increase in complexity introduced by the radiation terms is evident.

In order to solve Equations 1.7, 2.63, 3.2, 3.4, 3.6, and 3.7 simultaneously a computer program (Number DTA-16) in the MAD language was devised. The program listing is presented in Appendix VI.

Unfortunately, it was not possible to check this method as thoroughly as the previous method because much of the data was unsuitable. Nearly all of the data was taken by alternating the flows of nitrogen and helium into the system. It was found, however, that in replacing the nitrogen with helium, not all of the nitrogen could be removed in this manner. Thus the data with helium as the gas atmosphere really represent data with a mixture of helium and nitrogen of uncertain composition. Furthermore, the calculation which has been described requires that the exact thermal conductivity of the gas be known, since otherwise quite erroneous values for the film thickness were obtained.

It was decided, therefore, to reconstruct the DTA furnace so that it could be evacuated and backfilled with the desired gas. The system has not as yet been fully perfected, but some data has been obtained (DTA run number C-32 with sample number 152, indium) which substantiates the above conclusions. In this DTA run it was estimated that about 90% of the nitrogen was removed and replaced by helium. Brokaw's rule (70) was used to estimate the thermal conductivity of the mixture. It was found that at 430°K, the melting point of indium, the thermal conductivity of helium was reduced by 20% if 10% nitrogen was present as an impurity. Using this correction, the calculation of η'' and the heat of fusion by this method

(Program DTA-16) agreed quite well with the values obtained by the previously described method (Program DTA-19).

Calculation of the Thermal Conductance from the Time Constant and the Thermal Capacity

It was pointed out in Chapter I that the application of Equations 1.4 and 1.14 to the calculation of the thermal conductance depends on the estimation of the thermal capacity, C, and that some questions arise in regard to the constitution of C. These questions may now be examined. In considering the DTA data on standards whose latent heats of fusion are known, a value of the thermal capacity may be computed as follows:

$$C = \frac{\tau_{exp}\,\Delta E}{\int \theta \cdot dt} \tag{3.11}$$

and a value may also be estimated by summing the heat capacities of the sample and the silica in contact with the sample:

$$C' = m_s c_{p,s} + m_Q c_{p,Q} \tag{3.12}$$

Let Z denote the ratio C/C' which may be computed for each standard. If the theory and experiment were completely matched then Z would be equal to unity. The results of such a calculation* are given in Table 3.2. It is evident that, within the precision of the data, Z may be considered to be a constant dependent only on the geometry of the system, and then used to compute the heats of fusion of other materials. For the Series B runs $Z_B = 1.30 \pm 0.274$, and for the Series C runs $Z_C = 1.115 \pm 0.187$.

Of course, it may be argued that this approach is naive, and so it is. In the first place, the system is one containing distributed parameters, that is distributed thermal resistance and distributed thermal capacitance, so that the model through which Equation 1.4 was derived is in fact oversimplified. In the second place, it is known that after melting the

* See Appendix VI; MAD program Number DTA-17.

Table 3.2

The Correlation Factor $Z = C/C'$

Series B DTA Runs

Material	Number of Cycles N	Mean Value Z	Standard Deviation σ_Z
Ag	6	1.310	0.132
Cu	14	1.345	0.202
In	20	1.240	0.256
Pb	8	1.425	0.306
Sb	6	1.285	0.140
Te	8	1.235	0.244
Overall	62	1.300	0.274

Series C DTA Runs

	N	Z	σ_Z
Ag	10	1.085	0.071
In	4	1.090	0.145
Pb	5	1.195	0.191
Sb	4	1.232	0.080
Te	4	1.005	0.113
Overall	27	1.115	0.187

conductance is not constant and is not identical to the conductance during melting.*

Notwithstanding these objections, however, within the precision of the data, this method of finding the thermal conductance is satisfactory. The pragmatic viewpoint is taken that the use of this method does provide useful and realistic estimates of the latent heats and is therefore justified.

These two methods for measuring the latent heats of fusion are used in the following chapter to analyze the data on about 20 semiconducting compounds and to determine their latent heats of fusion and latent heats of transformation.

---

* See Figure 2.2.

CHAPTER IV

HEATS OF FUSION AND TRANSFORMATION BY DTA CALORIMETRY

In this chapter the methods described in the preceding chapter are applied to the determination of the latent heats of fusion and transition of twenty compound semiconductors: $Ag_2In_8Se_{13}$, Ag_2Se, Ag_2Te, Bi_2Se_3, Bi_2Te_3, CdSe, CdTe, GaAs, GaSb, InAs, InSb, In_2Se_3, InTe, In_2Te_3, PbSe, PbTe, Sb_2Se_3, Sb_2Te_3, SnTe and ZnTe.

Experimental Data

The experimental data consists in the tracings from a recording potentiometer which portray the difference in temperature between the DTA sample and reference as the amplified millivoltage output of a differential thermocouple versus time. A few typical DTA curves are shown in Figure 4.1 with the shaded region representing the area under the DTA curve. The melting point was chosen as the temperature of the sample over the time interval that the DTA curve was linear.

Three basic types of DTA curves have been observed: 1) those for very pure materials, such as silver, which have a very sharp melting point, and the decay of the differential temperature after melting is truly exponential for both heating and cooling curves; 2) those for impure materials or compounds which contain an excess of one of the constituents, such as CdTe, wherein melting occurs gradually at first and then more rapidly; although the decay of the heating curve may yield the true time constant, the cooling curve generally will not because of the continued evolution of latent heat; and 3) those for materials which undergo a large volume decrease on melting, such as the III-V compounds, Ge, and Bi. The latter curves often contain "wiggles", and may or may not be useful for finding the time constant for exponential decay.

The time constant may be found from a plot of $\log | \theta - \theta_{ss} |$ versus time. A few such typical plots are shown in Figure 4.2. The experimental time constant, τ_{exp}, may be found from the slope of such graphs via Equation 1.14.

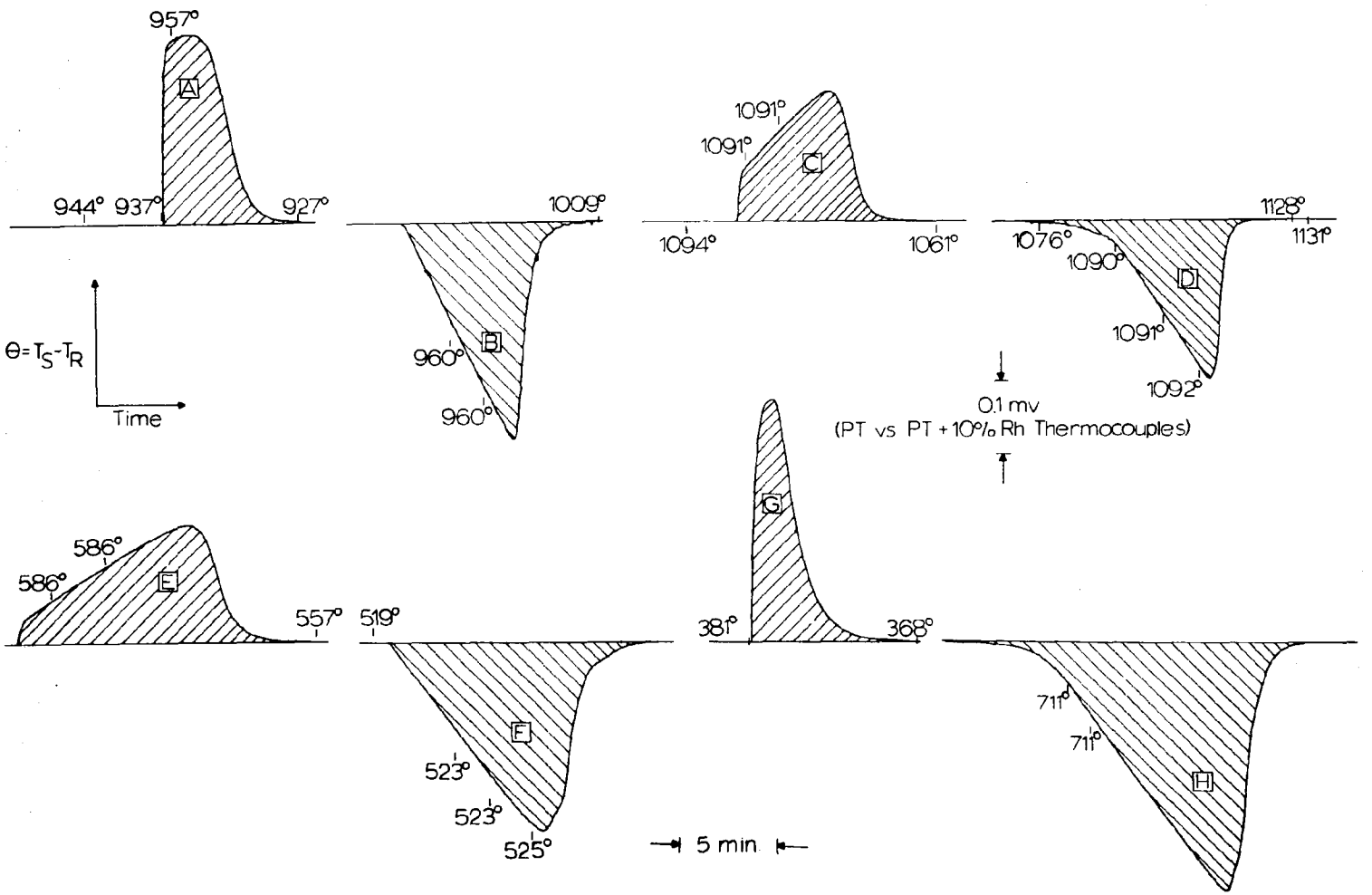


Figure 4.1. Some Typical DTA Curves Showing Differential Temperature vs Time, and Selected Sample Temperatures: A- No. 115, Ag, Run C-13, Cycle IC-N_2; B- No. 93, Ag, Run C-4, Cycle II H-N_2; C- No. 104, CdTe, Run C-10, Cycle I C-N_2; D- No. 104, CdTe, Run C-10, Cycle II H-N_2; E- No. 110, Bi_2Te_3, Run C-9, Cycle II C-N_2; F- No. 126, InSb, Run C-18, Cycle II H-N_2; G- No. 92, Te, Run C-1, Cycle II C-N_2; H- No 102, GaSb, Run C-6, Cycle II H-N_2.

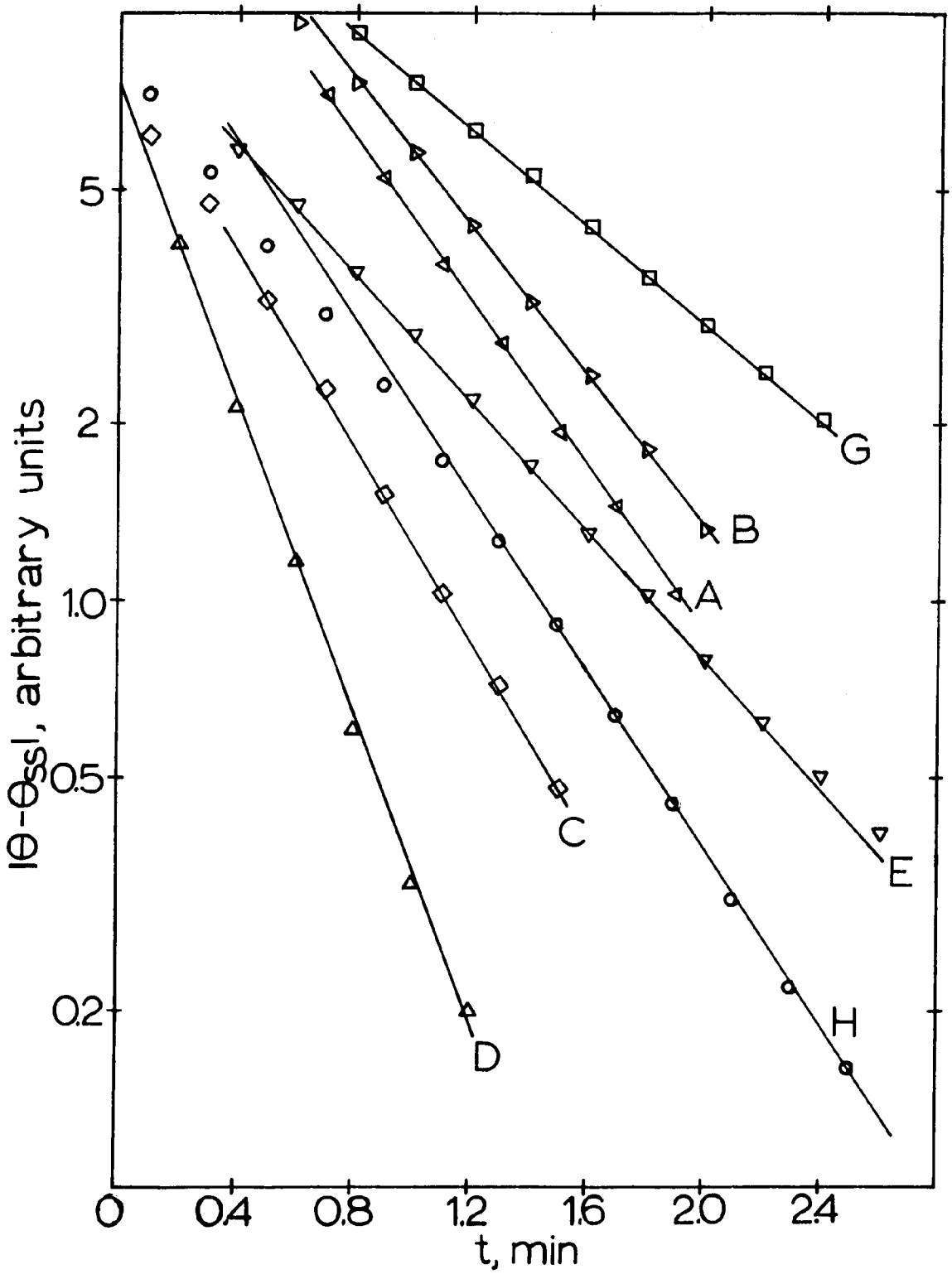


Figure 4.2. Some Typical Semilogarithmic Plots for Finding the Time Constant for Exponential Decay of the DTA Curve. The Legends Correspond to the DTA Curves of Figure 4.1.

The remainder of the experimental data consists in the measurement of the dimensions of the silica sample tubes by means of a micrometer and calipers during their fabrication. The estimation of the physical properties of the components of the system is discussed in Appendix IV, and all the numerical values used in the calculations are listed side by side with the computer programs in Appendix VI.

Experimental Results

The heats of fusion calculated from the DTA data via computer programs DTA-17 (using Z values of 1.300 and 1.115 for the series B and C DTA runs, respectively) and DTA-19 appear in Table 4.1 where they are compared with the values reported in the literature and with the values computed from the heats of fusion of the elements according to the method of Kubaschewski and Evans (47):

$$L_f = T_f \Delta S_f = T_f \left[\sigma + \sum_i \frac{N_i L_{f,i}}{T_{f,i}} \right] \qquad 4.1$$

$$\sigma = -R \sum_i N_i \ln N_i \qquad 4.2$$

where T_f = melting point of compound, ^{o}K

$T_{f,i}$ = melting point of element i, ^{o}K

L_f = heat of fusion of compound, cal/mean gram atom

$L_{f,i}$ = heat of fusion of element i, cal/g-atom

ΔS_f = entropy of fusion of compound, cal/m.g.a.-^{o}K

N_i = atom fraction of element i in the compound

R = gas constant = 1.987 cal/g-atom-^{o}K

The heats of transition are summarized in Table 4.2. The confidence intervals given in columns IV and V of Table 4.1 and in columns III and IV of Table 4.2 are simply the standard deviations from the mean

Table 4.1

Heats of Fusion of Compound Semiconductors

Material	Latent Heat of Fusion - Calories/gram					
	I	II	III	IV	V	VI
$Ag_2In_8Se_{13}$	-	-	49.8*	20.2±3.3	19.1± 2.8	20±3
Ag_2Se	-	-	44.4*	9.3±1.1	7.9±0.8	8±2
Ag_2Te	-	-	50.1*	8.9±3.0	7.0±1.3	8±2
Bi_2Se_3	-	-	37.9	39.2±3.0	32.2±3.1	36±6
Bi_2Te_3	36.2	(8)	35.8	31.6±4.4	31.4±2.7	33±4
CdSe	-	-	71.5	56.5±15.0	53.5±14.2	55±15
CdTe	-	-	63.3	(62.2)	46.3±5.8	50±8
GaAs	-	-	-	192.	199 ± 23	200±25
GaSb	62.6	(73)	63.7	90.8±3.5	75.8±15.3	85±12
InAs	-	-	-	98.0±15.6	95.5±9.7	96±12
InSb	47.3;51.5	(62, 73)	33.4	46.3±1.0	51.7±6.0	50±5
In_2Se_3	-	-	48.2*	30.0±1.8	35.0±7.1	30±4
InTe	-	-	41.2	(36.7)	24.7±2.6	28±8
In_2Te_3	-	-	42.5*	19.7±5.1	18.4±4.3	19±5
PbSe	-	-	36.7	64.6±23.0	32.2±5.8	38±12
PbTe	-	-	37.3	37.4±12.6	25.0±3.2	28±9
Sb_2Se_3	-	-	48.5	36.6±3.5	31.8±4.8	35±5
Sb_2Te_3	-	-	42.1	45.1±8.5	33.4±4.1	37±6
SnTe	-	-	40.2	31.3±0.1	33.2±1.5	32±3
ZnTe	-	-	89.7	-	80.7±11.0	81±11

Code: I.-Heat of Fusion from Literature

II - Literature reference

III - Value calculated from Heats of Fusion of Elements; after Kubaschewski and Evans (47).

IV - Program DTA-19; $L_f \pm \sigma_{L_f}$

V - Program DTA-17; $L_f \pm \sigma_{L_f}$

VI - Recommended Value.

* For compounds with transitions, this estimate includes heat of fusion and heats of transition.

Table 4.2

Heats of Transition of Compound Semiconductors

Material	T_t °K	Heats of Transition - Calories/gram				
		I	II	III	IV	V
$Ag_2In_8Se_{13}$	1022	-	-	6.0 ± 0.9	4.1 ± 1.0	5 ± 2
Ag_2Se	406	5.43	(47)	10.1 ± 1.7	6.5 ± 0.4	8 ± 3
Ag_2Te	420	-	-	5.9 ± 3.8	6.9 ± 0.5	7 ± 1
Ag_2Te	1072	-	-	1.1 ± 0.2	0.75 ± 0.12	1.0 ± 0.3
In_2Se_3	474	0.73	(94)	2.8	2.3 ± 0.2	2.5 ± 0.5
In_2Te_3	893	-	-	-	(0.8)	(0.8)

Code:

I- Literature Value

II- Literature Reference

III- Program DTA-19; $L_t \pm \sigma_{L_t}$

IV- Program DTA-17; $L_t \pm \sigma_{L_t}$

V- Recommended Value.

for the number of heating and cooling cycles used in computing the mean, and represent the scatter of the data. The confidence intervals quoted in column VI of Table 4.1 and column V of Table 4.2 represent, in this writer's judgment, the probable error associated with the recommended values cited.

An examination of Table 4.1 reveals that in most instances the method of Kubaschewski and Evans yields a high estimate of the heat of fusion, though in the case of the III-V compounds the estimate is low. Of course, some of the materials undergo crystalline transformation before they melt in which case the sum of the entropies of transition and melting must be compared with the value predicted from Equation 4.1. Such a comparison is provided in Table 4.3 wherein it is evident that the prediction of Equation 4.1 is still high. It is of interest to examine each transformation in more detail in order to learn as much as possible from the phenomena which occur.

$Ag_2In_8Se_{13}$

O'Kane (66) has investigated the thermal transformations in this compound and reported the melting point to be 815°C with a thermal transformation occurring at 753°C on heating and 745°C on cooling. In this work, DTA measurements were obtained on samples of high resistivity ($> 10^5$ ohm-cm), zone refined $Ag_2In_8Se_{13}$. Initial melting was somewhat gradual, but the constant melting point, 812°C, was quickly attained about one to two minutes after the first deflection from the baseline. The thermal transition was moderately sharp and occurred at 748°C on heating but supercooled to 743°C on cooling. These figures are in general agreement with the findings of O'Kane.

The heats of fusion calculated by both of the methods described agreed with one another quite well, and the recommended value is 43.5 ± 6.5 kcal/g mol. The heats of transition by the two methods disagreed somewhat, and the average value of 11 ± 4 kcal/g mol is recommended.

Table 4.3

Comparison of the Sum of the Entropies of Transition and Fusion with the Theoretical Prediction

Material	Melting or Transition Temperature ^{o}K	ΔS_f or ΔS_t $\frac{cal}{g - {}^{o}K}$	$\sum_j \Delta S_j$ * $\frac{cal}{g - {}^{o}K}$	$\sum \Delta S_j$ Theoretical ** $\frac{cal}{g - {}^{o}K}$
$Ag_2In_8Se_{13}$	1022	0.0049		
	1088	0.0184	0.023	0.0409
Ag_2Se	406	0.0197		
	1170	0.0068	0.027	0.0380
Ag_2Te	420	0.0167		
	1072	0.0009		
	1232	0.0065	0.024	0.0406
In_2Se_3	474	0.0053		
	1158	0.0259	0.031	0.0417
In_2Te_3	(893)	(0.0009)		
	940	0.0203	0.021	0.0453

* j refers to the number of transformations, including melting.

** After Kubashewski and Evans (47).

Ag_2Se

Walsh, Art and White (89) who have measured its heat capacity from 16-300°K have reported the true composition of this compound to be $Ag_{1.99}Se$. These authors report no anomalies in the specific heat in this temperature range. The crystalline transformation at 133°C and the melting point of 894°C have been well established (31, 39, 47, 58) and the heat of transition has been reported to be 1.6 ± 0.4 kcal/mole (47).

These figures have been confirmed by our measurements which indicate that the transition occurs sharply at 133-136°C on heating at 2.5°C/min and supercools to 122°C on cooling at a rate of 0.5°C/min, and that the melting point, also quite sharp, occurs at 894°C. The heat of transition measured here, however, is somewhat higher than that reported in the literature, being $2.3_6 \pm 0.5_9$ kcal/g mol where the average of the two measurements has been chosen. The heats of fusion found by the two methods agree within experimental precision, and the recommended value is $2.3_6 \pm 0.5_9$ kcal/g mol. It is probably fortuitous that the heat of transition is substantially equal to the latent heat of fusion.

Ag_2Te

The investigations of Miyatani (60) indicate that two compounds of nearly identical composition, $Ag_{2.00}Te$ and $Ag_{1.93}Te$ exist in the silver-tellurium system at room temperature. Walsh, Art, and White (89) report that the composition of the latter phase is actually $Ag_{1.88}Te$ and have measured its heat capacity from 16-300°K finding no anomalies. The existence of a thermal transition in Ag_2Te at 147°C has been established (31) and its melting point has been reported to be 959°C (31, 39).

In this work it was found that the low temperature transition occurs very sharply at 147-149°C on heating at 2.5°C/min, but supercools to 143°C on cooling at 0.7°C/min. A second, previously unreported, thermal transition has also been observed which occurs very sharply

on both heating and cooling at 799°C. Melting was somewhat gradual, beginning at about 951°C with a constant melting point of 960°C being established within a few minutes. The heats of fusion computed by the two methods described agree within experimental precision and a value of $2.7_4 \pm 0.6_9$ kcal/g mol is recommended. The heats of transition at 147°C found by the two methods disagree somewhat and a larger value of $2.4_0 \pm 0.3_5$ kcal/g mol is preferred because the experimental scatter is much lower. The heat of transition at 799°C is equal to 0.34 kcal/g mol.

Bi_2Se_3, Bi_2Te_3, Sb_2Se_3 and Sb_2Te_3

These four compounds melt congruently and no crystalline transformations have been reported for them. Hansen (31) gives their melting points as 706°C, 585°C, 622°C and 617°C, respectively. Offergeld and Cakenberghe (65) have investigated the stoichiometry of three of the compounds and list the true compositions as $Bi_{40.065}Te_{59.935}$, $Bi_{40.02}Se_{59.98}$ and $Sb_{40.40}Te_{59.60}$.

Except for the sample of Bi_2Te_3 which was zone refined, the materials measured here exhibited somewhat gradual initial melting. Our melting points for Bi_2Se_3, Bi_2Te_3, Sb_2Se_3 and Sb_2Te_3 are 700°C, 586°C, 613°C and 617°C, respectively. Bolling (8) has measured the heat of fusion of Bi_2Te_3 and found a value of 29.0 ± 3.2 kcal/g mol which compares favorably with the value of 26.4 ± 3.2 kcal/g mol found in this work. The values found by the two methods for the remaining three materials differ somewhat. Where the standard deviations were equal the recommended value was found by simply averaging the two measurements, but if the standard deviations were unequal, the preferred value was found by adjusting to a point where the standard deviations overlap. In this manner the heats of fusion for Bi_2Se_3, Sb_2Se_3 and Sb_2Te_3 are found to be 23.6 ± 3.9, 16.8 ± 2.4, and 23.5 ± 3.8 kcal/g mol, respectively.

GaAs, GaSb, InAs and InSb

Hansen (31) gives the melting points of these compounds, each of which melts congruently and undergoes no crystalline transformations, as 1238°C, 706°C, 943°C and 525°C, respectively. Nachtrieb and Clement (62) have measured the heat of fusion of InSb which they report as 11.2 ± 0.4 kcal/g mol; and Schottky and Bever (73) report the heats of fusion of InSb and GaSb to be 12.2 ± 0.7 and 12.0 ± 0.7 kcal/g mol, respectively.

In this work, the melting points of GaAs, GaSb, InAs, and InSb were found to be 1236°C, 712°C, 942°C and 524°C with all occurring sharply except GaSb which was somewhat gradual.* Our heat of fusion for InSb, 11.7 ± 1.2 kcal/g mol, is in good agreement with the previous measurements, but our value for GaSb, 16.3 ± 2.3 kcal/g mol is substantially higher. Furthermore, the two measurements for GaSb disagree substantially, the higher value being preferred because of less scatter. The two measurements of the heat of fusion of InAs and GaAs are in good agreement with one another with the preferred values being 18.2 ± 2.3 and 28.9 ± 3.6 kcal/g mol, respectively.

CdSe, CdTe and ZnTe

These compounds melt congruently and do not undergo crystalline transformation on heating. The melting points of CdSe and ZnTe have been reported by Mason and O'Kane (58) to be 1258° and 1300°C, respectively, whereas that of CdTe has been variously reported as 1090°C (63), 1092°C (54), 1098°C (57, 58) and 1106°C (49).

In this work all three materials were observed to melt gradually at first with a constant melting point being achieved a few minutes after melting was initiated.* The corresponding melting points and heats of fusion of CdSe, CdTe, and ZnTe were found to be 1250°C and

---

* Cf. Figure 4.1.

10.5 ± 2.9 kcal/g mol; 1091°C and 12.0 ± 1.9 kcal/g mol; and 1290°C and 15.6 ± 2.1 kcal/g mol. The heats of fusion of CdTe and ZnTe represent primarily the results of the calculation from the time constant for exponential decay plus an estimate of the thermal capacity via Program DTA-17, as only one data point, that being for CdTe, was available for processing by the second method. The two methods yielded values in good agreement with one another for CdSe, although the standard deviation was high.

In_2Se_3

Miyazawa and Sugaike (61) have investigated the crystal structure of In_2Se_3 at room temperature and the thermal properties by DTA, and found that α - In_2Se_3, the stable phase at room temperature, is hexagonal and undergoes sharp heat absorption at 200°C on heating but below 100°C on cooling. Semiletov (74) has extended the crystallographic investigation to higher temperatures and reports four crystalline modifications of In_2Se_3: 1) an α, graphite-like, hexagonal phase which is stable below 200°C; 2) a β, hexagonal phase which is stable above 200°C; 3) a γ, cubic modification which exists above 500-600°C; and 4) a possible δ, monoclinic phase whose region of stability is uncertain. He further reports that the $\alpha \rightarrow \beta$ transformation is sluggish, requiring a seven to eight hour anneal at 350°C for completing the transformation of a thin film 400-600 A thick. O'Kane (66) has observed a thermal transformation 210°C and also reports a small transition at 740°C. The melting point of In_2Se_3 has been well established (58, 66) and has been reported to be 888°C. Yoshioka (94) has studied the thermal properties of In_2Se_3 in the range 20-300°C and has estimated the heat of the $\alpha \rightarrow \beta$ transformation from heat capacity measurements and found it to be 0.34 kcal/g mol.

In this work, the low temperature phase change was observed to occur very abruptly on heating at 201-202°C, and supercooled to below 100°C on cooling. Melting began gradually about 5°C below the melting

point which was 885°C, and as soon as the melting point was achieved, proceeded at constant temperature. Our value for the latent heat of transition at 202°C is 1.17 ± 0.23 kcal/g mol which is larger than that reported by Yoshioka by a factor of three. There is good agreement between the two methods of calculating the heat of transition from our data.

The alleged phase transformation at 740°C, although it was observed, is thought not to belong to the compound, which is believed to be non-stoichiometric and deficient in selenium. The basis for this judgment is the phase diagram study of the InSe system which is reported in Chapter V, and which exhibits a peritectic reaction at 745°C which extends from nearly pure selenium to In_2Se_3. This explanation would also account for the anamalous δ-phase postulated by Semiletov. Finally, the $\alpha \rightarrow \beta$ reaction did not seem to be as sluggish as Semiletov has suggested. It is conceded, however, that the value of the heat of transition reported here would be too low if all of the latent heat were not absorbed during the five to ten minutes required to traverse the transition peak in our DTA experiments. This probability, however, appears slim.

The two methods of calculation yield values for the latent heat of fusion which are in good agreement with one another. The preferred value is 14.0 ± 1.9 kcal/g mol.

InTe and In_2Te_3

Hansen (31) gives the melting points of these compounds as 696°C and 667°C, respectively. Zaslavskii and Sergeyeva (95) have investigated polymorphism in In_2Te_3 and report that two phases exist: an α-phase which is stable at low temperatures and decomposes between 500° and 600°C into a β-phase. The In-Te phase diagram has been recently investigated by Grochowski and Mason (29) who give the exact compositions of these compounds as $In_{49.2}Te_{50.8}$ and $In_{40.3}Te_{59.7}$.

Unlike In_2Se_3, the $\alpha \rightarrow \beta$ transformation in In_2Te_3 is an order-disorder transition, not accompanied by a large change in the crystal

structure (95) and has been almost too elusive to detect in our equipment. Minute deflections in the neighborhood of 580°C have been observed, however, and they may or may not be associated with this transformation. A more substantial heat absorption of about 0.5 kcal/mole has, however, been detected at about 620°C on heating. This is presently believed to be associated with the peritectic decomposition of the compound In_3Te_5 which decomposes at 625°C. Both InTe and In_2Te_3 have been observed to melt gradually with their respective melting points being 693° and 667°C.

The two methods for finding the heat of fusion yield results for In_2Te_3 which are in good agreement with one another, but only one data point, that for InTe, was available for processing by the second method (Program DTA-19). The recommended heats of fusion are 6.9 ± 1.9 kcal/g mol InTe and 11.6 ± 3.1 kcal/g mol In_2Te_3. In the case of InTe, it was impossible to obtain time constants from the cooling curves because of continued evolution of heat as freezing continued. This was due to the deviation of the composition from the In-deficient compound. Similar troublesome behavior was encountered with SnTe.

PbSe, PbTe and SnTe

These three compounds all melt congruently and do not undergo any other phase transformations above room temperature. Hansen (31) has listed their melting points as 1088°, 917°, and 790°C. In this work, PbSe has been observed to melt sharply at 1083°C while PbTe and SnTe melted gradually at 923° and 804°C, respectively.

Umeda, Jeong and Okada (85) have found the true composition of SnTe to be $SnTe_{1.038}$. A large number of tin vacancies have also been inferred from the anomalous thermal conductivity data of Damon (19).

The heat of fusion of SnTe has been determined from heating data to be 7.9 ± 0.8 kcal/g mol. The cooling curves could not be used because the discrepancy of the composition of our material from the tin-deficient compound resulted in continued evolution of latent heat during the

the decay portion of the DTA curve, and thus the true time constant could not be extracted. The two measurements for PbSe and PbTe did not agree with one another very well. The lower values were favored because the scatter was less, so that the recommended values are 10.9 ± 3.4 kcal/g mol PbSe and 9.4 ± 3.0 kcal/g mol PbTe.

Experimental Precision

The melting points and transition temperatures reported here are considered to be accurate, for the materials measured, to within ± 2°C. The largest sources of variability are changes in thermocouple calibration and the melting of samples over a range of temperature which is occasioned by a deviation from the congruent composition.

The precision in the measurement of quantities of heat is not particularly high, perhaps ± 15% on the average. Numerous sources for this variability may be cited: error in the measurements of the dimensions of the system or of the area under the DTA curve, error in the values of the physical property estimates, error in the measurement of the time constant, improper choice of a physical model on which to base the calculations, etc., but it is not apparent that one of these choices should be preferred over the others. It is presumably a combination of all of them which leads to the observed variability.

The question arises as to which of the two methods for finding latent heats is to be preferred. In this writer's judgment, it is the first, that is direct calculation of the thermal conductance from a knowledge of the geometry and physical properties of the system with calculation of the dimensions of the gas film by matching the time constant for exponential decay of the DTA curve with its theoretical counterpart. This statement nevertheless must be qualified because, although the method is moderately insensitive to the estimate of the thermal conductivity of the sample, the latter may not be chosen indiscriminately, particularly when it is low. This fact is borne out by the results on PbSe and PbTe where large discrepancies between the two methods appear. The method

of direct calculation is also preferred because it is constructed on a much firmer theoretical foundation and does not depend on any calibration of the equipment.

Discussion

A comparison of the entropies of fusion plus transition of these twenty compounds in Table 4.4 reveals that they can be grouped as follows:

ΔS = 2-3 $Ag_2In_8Se_{13}$, Ag_2Se, Ag_2Te, In_2Se_3, In_2Te_3

ΔS = 3-5 CdSe, CdTe, ZnTe, InTe, PbSe, PbTe, SnTe

ΔS = 4-7 Bi_2Se_3, Bi_2Te_3, Sb_2Se_3, Sb_2Te_3

ΔS = 7-10 GaAs, GaSb, InAs, InSb.

These entropy changes represent changes in the state of order of the compound in transforming from the crystalline state at room temperature to the liquid state. The compounds having low values of ΔS undergo less pronounced configurational changes than those having high values of ΔS. It is known, for example, that the coordination number of the III-V compounds in the crystalline state is 4 whereas in the liquid the coordination number is about 6 (25). Furthermore, the change in density for these materials on melting is large, being about 11.6% for InSb and 7.3% for InAs (37). Thus the change in the state of order on melting is large for these materials, and the entropy of fusion is correspondingly large. Finally, it may be pointed out that the variations exhibited in Table 4.4 are great -- from 2.2 for $Ag_2In_8Se_{13}$ to 9.6 for GaAs. It is clear that no simple correlation can be found for predicting heats of fusion from entropies of fusion which would be analogous to Trouton's rule for heats of vaporization. This conclusion has been reached on numerous occasions before* and is confirmed by our data.

* E.g. see Kubaschewski and Evans (47).

Table 4.4

Entropies of Transition and Fusion of Semiconducting Compounds

Compound	T_t °K	ΔS_t cal/g-at-°K	T_f °K	ΔS_f cal/g-at-°K	$\sum_{i=t,f} \Delta S_i$
$Ag_2In_8Se_{13}$	1020	0.4_7	1085	1.7_4	2.2
Ag_2Se	408	1.9_3	1169	0.6_8	2.6
Ag_2Te	420	1.9_1	1233	0.7_4	2.7
	1072	0.1_0			
Bi_2Se_3			973	4.8_5	4.9
Bi_2Te_3			859	6.1_5	6.2
Sb_2Se_3			886	3.8_0	3.8
Sb_2Te_3			890	5.2_8	5.3
GaAs			1508	9.6_0	9.6
GaSb			985	8.2_5	8.3
InAs			1216	7.5_0	7.5
InSb			797	7.3_4	7.3
CdTe			1364	4.4_0	4.4
CdSe			1523	3.4_5	3.5
ZnTe			1563	4.9_9	5.0
In_2Se_3	474	0.5_0	1158	2.4_2	2.9
In_2Te_3			940	2.4_7	2.5
InTe			966	4.1_0	4.1
PbSe			1356	4.0_2	4.0
PbTe			1196	3.9_3	3.9
SnTe			1077	3.6_7	3.7

Finally it is of interest to compare the entropies of fusion of these compounds with values for other materials. The entropies of fusion of metals are about 2.2 cal/g at-^{o}K whereas those of ordered and disordered alloy phases are about 3.5 and 2.2 cal/g at-^{o}K, respectively (47). Dworkin and Bredig (21) have measured the heats of fusion of the alkali halides and have found that the corresponding entropy changes average 2.9 cal/mean gram atom-^{o}K. The entropies of fusion of Ge and Si are 6.7 (28, 71) and 7.2 (67) cal/g at-^{o}K, respectively, which are about the same order of magnitude as the III-V compounds.

CHAPTER V

SOLID-LIQUID EQUILIBRIUM STUDIES

In this chapter the results of studies on the systems cadmium-tellurium, zinc-tellurium, and indium-selenium are presented and discussed.

The System Cadmium-Tellurium

This system was first studied by Kobayashi (42) who reported that the system contained one compound, CdTe, which was congruently melting at $\sim 1050^{\circ}C$ and the two eutectics between the pure elements and CdTe which occur very close to the Cd and Te ends of the diagram at 322° and $437^{\circ}C$, respectively. He was unable to measure the liquidus curve for compositions wherein the mole percent of cadmium was greater than 50% because of the high vapor pressure and evaporation of his samples.

The discrepancies in the melting point of CdTe* and the unavailability of liquidus data and vapor pressure data especially for high percentages of cadmium in solution prompted several reinvestigations of this phase diagram (54, 57, 58, 63). Our work (57, 58) has not been formally published in detail as yet because it was desired to determine the heat of fusion of CdTe so as to be able to make thermodynamic calculations from the liquidus data. Estimates of the heat of fusion by two different methods, calculation from the liquidus data and calculation from the entropies of fusion of the elements (47) did not agree with one another and necessitated an experimental determination.

Our experimental data** for the cadmium-tellurium phase diagram are presented in Table 5.1 and are plotted in Figure 5.1 together with

---

* Cf. Chapter IV.

** See Appendix I for discussion of the interpretation of the DTA curves.

Table 5.1

Experimental Data for the Cd-Te Phase Diagram

Sample Number	Composition Atom % Te	Maximum Fusion Temperature °C	Eutectic Temperature °C	Liquidus Temperature °C
----	0	----	---	321
376	1.0	980	(333)	730
380	3.0	970	(340)	808
379	10.0	975	322	895
384	25.0	1050	323	963
385	40.0	1100	325	1035
402	45.0	1150	325	1067
104-F	50.0	1200	---	1091
520	50.0	1200	---	1091
389	54.0	1100	450	1075
383	62.5	1100	450	1000
375	75.0	1000	450	885
382	85.0	900	449	755
381	95.0	750	450	602
388	98.2	850	448	480
396	98.7	800	450	480
92-F	100	----	---	449
151-F	100	----	---	449

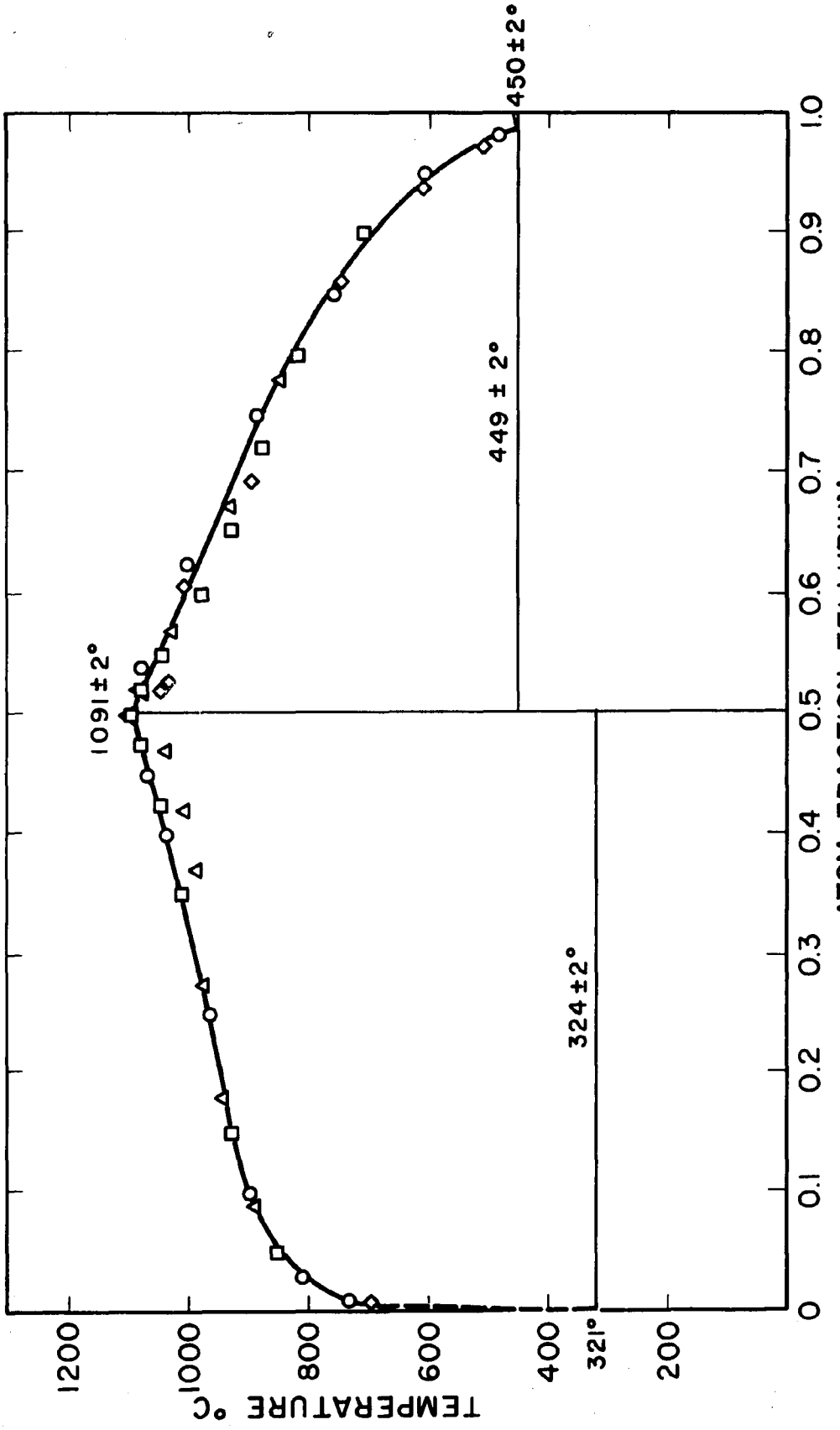


Figure 5.1. The Phase Diagram for the Cadmium-Tellurium System.
◆ Data of Kobayashi; △ de Nobel; ◘ Lorenz; O This Work.

the data of other workers. In the regions of high cadmium and high tellurium concentrations, the agreement is quite good, but in the neighborhood of 40-50% Te our liquidus temperatures are substantially higher than those reported by de Nobel, (63) and in the neighborhood of 60-70% Te they are substantially higher than the results of Lorenz (54). The cadmium-rich eutectic temperature was 324 ± 2°C and the eutectic composition was practically pure cadmium. The tellurium-rich eutectic was found to be 449 ± 2°C and 98.7 atom percent tellurium.

Knowing the liquidus curves and the thermodynamic properties of the constituents it is possible to make some thermodynamic calculations in order to gain some insight into the nature of the system. For example, Wagner (88) has derived equations for computing the excess free energy of a liquid phase from the liquidus of a compound. If a term associated with the excess molar entropy of the liquid is neglected, his Equation 61 for the case of an equimolar compound becomes

$$F^E = -\frac{1}{2}\left[N_A \int_0^{N_B} I_1(N_B)\, dN_B + N_B \int_{N_B}^{1} I_1(N_B)\, dN_B\right] \qquad 5.1$$

where N_A = atom fraction of element A in solution

$N_B = 1 - N_A$ = atom fraction of B

F^E = excess molor free energy of the solution, kcal/mean gram atom

and the integrand $I_1(N_B)$ is defined by

$$I_1(N_B) = \frac{\Delta S_f [\, T_f - \phi(N_B)\, T]}{(N_B - \frac{1}{2})^2} \qquad 5.2$$

where ΔS_f is the entropy of fusion of the compound in cal/mean gram atom - °K, T_f the melting point of the compound in °K, T the liquidus temperature and $\phi(N_B)$ is defined as:

$$\phi(N_B) = 1 + \frac{1}{2}\frac{R}{\Delta S_f} \ln \frac{1}{4 N_A N_B} \qquad 5.3$$

where R is the gas constant.

Equation 5.3 also represents the liquidus curve of a hypothetical ideal liquid, that is

$$T_{id}(N_B) = T_f/\phi(N_B) \qquad 5.4$$

where the standard state is chosen as the pure, completely dissociated, equimolar solution.

The function $I_1(N_B)$ is plotted in Figure 5.2 wherein it is apparent that the excess free energy exhibits a steep minimum at the compound CdTe. This would infer that CdTe molecules are very stable in solution, which is remarkable in view of the fact that the compound dissociates completely in the gas phase (44, 63) as do the rest of the II-VI compounds (44, 92, 93). Further support to this argument is given by the fact that the two liquidus lines intersect at 50% Te rather than joining in a single smooth curve. This behavior is also characteristic of a compound which exists as such in solution.*

Integration of Equation 5.1 for $N_B = \frac{1}{2}$ gives the excess free energy of liquid CdTe at the melting point to be -16.0 kcal/g mol which, when used with Wagner's Equation 34, results in a value for the standard free energy of formation of the compound from the pure solid elements at the melting point of CdTe of -24.4 kcal/g mole. Using the thermodynamic properties listed in the Handbook of Chemistry and Physics (30) a corresponding figure of -26.5 kcal/g mole is obtained. The agreement is good in view of the high probable error associated with drawing the curve $I_1(N_B)$ in the neighborhood of the compound.

It should be noted that a value of 11.2 kcal/g mol for the heat of fusion of CdTe has been used in these calculations. Although this figure is slightly lower than the value recommended in the preceding chapter (12.0 ± 1.9 kcal/g mol), it is within the probable error cited,

* See Lewis and Randall (52) p. 220; for a more quantitative discussion of the effect of interactions in solution on the curvature of the liquidus, see also Bonnier and Desre (10).

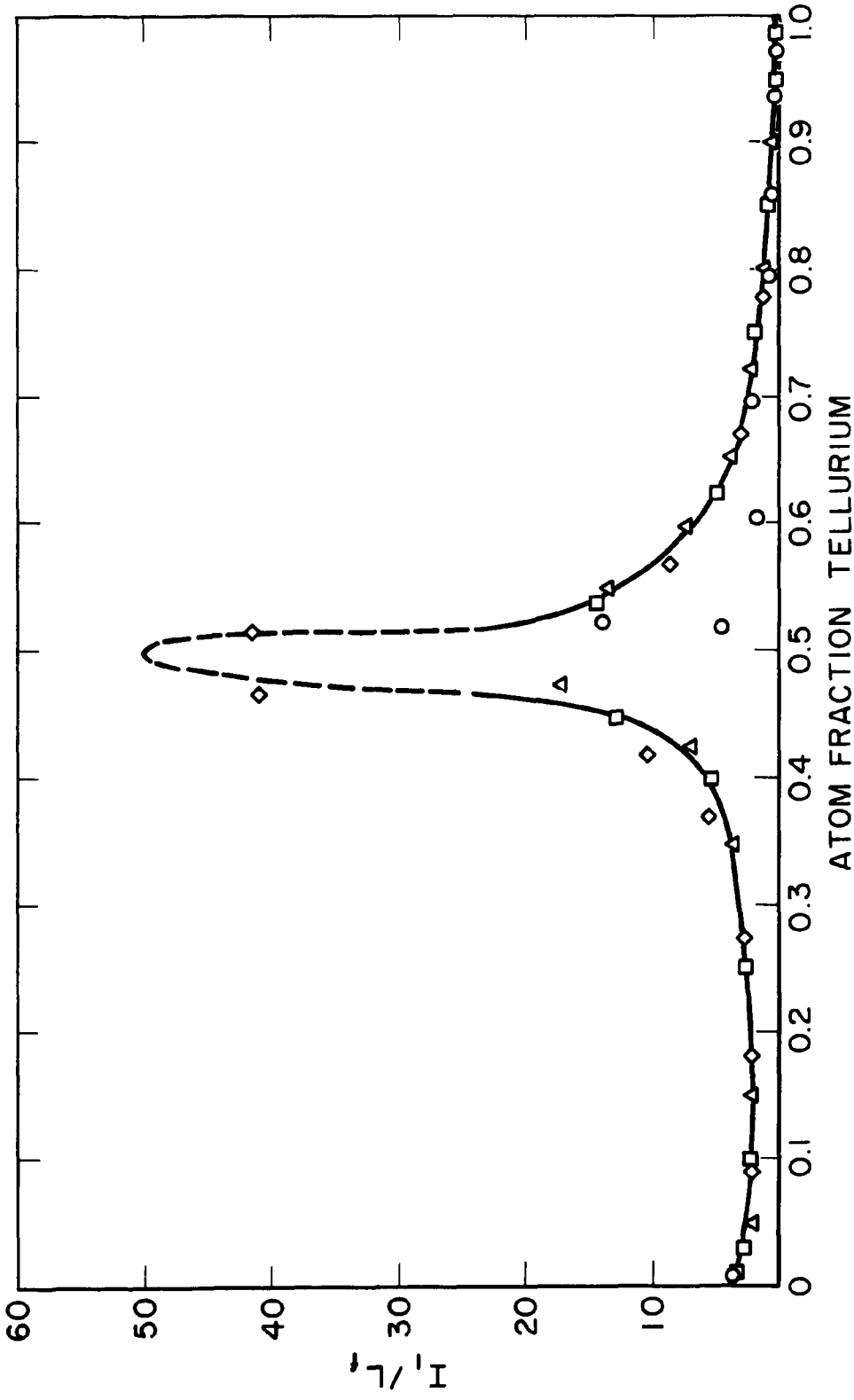


Figure 5.2. The Integrand of the Excess Free Energy Function versus Composition for the Cadmium-Tellurium System. O Data of Kobayashi; ◆ de Nobel; △ Lorenz; ■ This Work.

and the use of the slightly higher value would not substantively alter the conclusions.

Bonnier and Desre (11) have derived an expression for computing the heat of mixing at infinite dilution from liquidus data in binary systems containing a compound and a eutectic close to the pure element. Their expression for the case where the compound is equimolar is:

$$\overline{\Delta H}_{\infty A(B)} = \Delta H^{o}_{AB} - L_{f,B} - L_{f,A} - R \left. \frac{d \ln N_A N_B}{d(1/T)} \right|_{B} \qquad 5.5$$

where

$\overline{\Delta H}_{\infty A(B)}$ = partial molar enthalpy of mixing of 1 mole of A and an extremely large quantity of B.

ΔH^{o}_{AB} = standard enthalpy of formation of compound AB

$L_{f,A}$ = latent heat of fusion of A

$L_{f,B}$ = latent heat of fusion of B

and the last term represents the gas constant times the slope of the liquidus curve in the region of dilute A when plotted as $\ln N_A N_B$ versus reciprocal temperature. Such a plot for the cadmium-tellurium system appears in Figure 5.3 where the straight, dashed line represents the liquidus of a hypothetical ideal solution based on Equation 5.4. A brief calculation using $\Delta H^{o}_{CdTe} = -24.52$ kcal/g mol, $L_{f,Cd} =$ 1.53 kcal/g atom and $L_{f,Te} = 4.18$ kcal/g atom (47), yields $\overline{\Delta H}_{\infty Cd(Te)} = -19.0$ kcal/g atom and $\overline{\Delta H}_{\infty Te(Cd)} = +4.4$ kcal/g atom These figures indicate that dissolution of Te in Cd requires the expenditure of energy whereas the dissolution of Cd in Te releases energy, or in other words the liquidus for the system CdTe-Te exhibits negative deviations from Raoult's law while the system Cd-CdTe exhibits positive deviations.

Finally it might be noted that correlation of the liquidus data by means of the sub-regular solution theory of Thurmond and Kowalchik

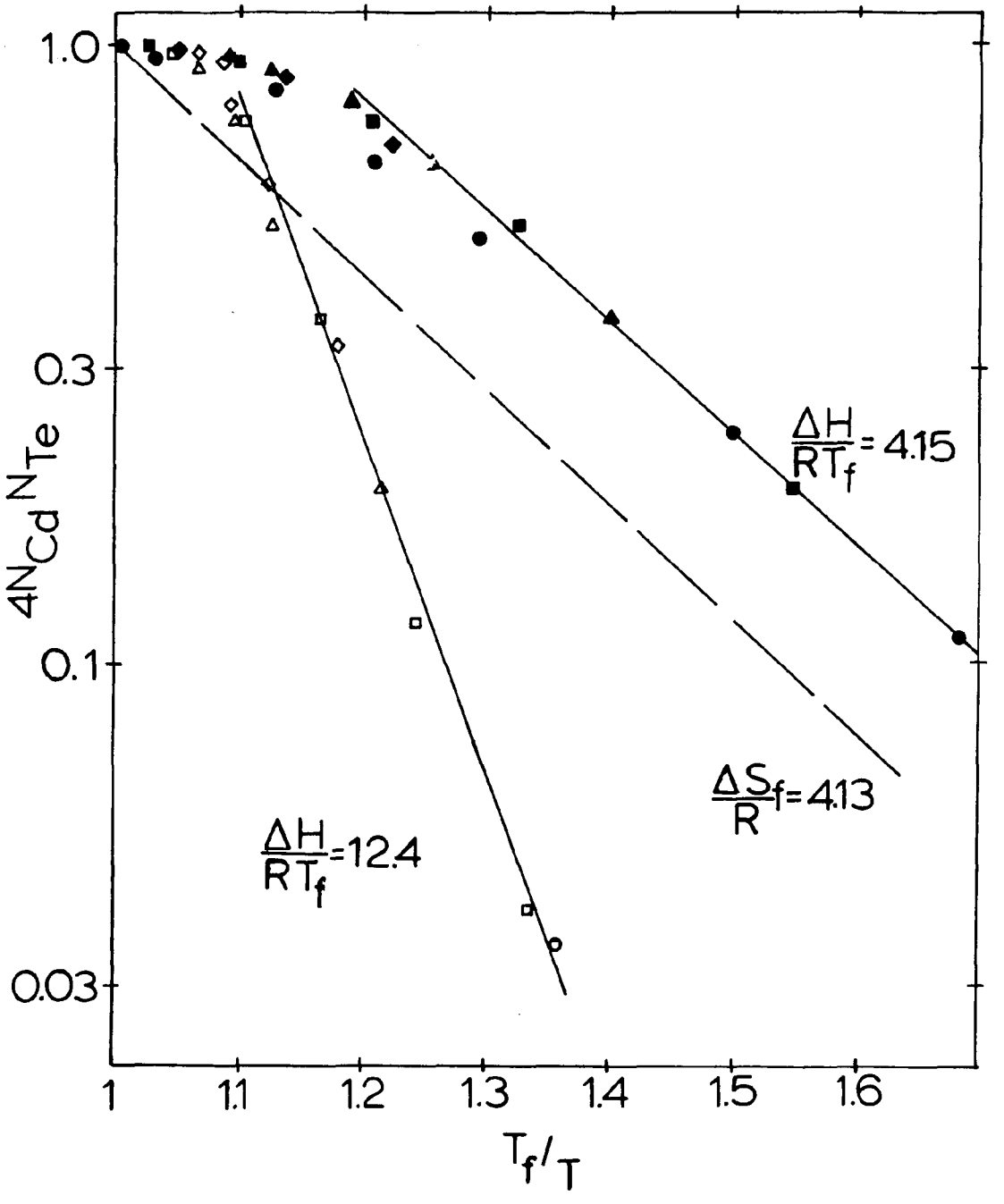


Figure 5.3. The Liquidus Curves for the Cadmium-Tellurium System Plotted as log 4 $N_{Cd}N_{Te}$ versus Reciprocal Reduced Temperature.
O Data of Kobayashi; ◇ de Nobel; △ Lorenz;
□ This Work. For Open Symbols $N_{Te} < 1/2$ and for Closed Symbols $N_{Te} > 1/2$. The Dashed Line Represents Equation 5.4.

(83) was tried. These authors found that the solubility of many elements in silicon and germanium could be explained by such a correlation. This method requires that a plot of the quantity $RT \ln \gamma/(1 - x)^2$ be a linear function of T, where x is the mole fraction of the compound in solution and

$$\ln \gamma = -\ln x + \frac{L_f}{R}\left(\frac{1}{T_f} - \frac{1}{T}\right)$$

These equations are based on a standard state of pure undissociated, supercooled liquid compound, so that the activity coefficient γ represents the deviation of the liquidus from that given by Van't Hoff's equation

$$\ln x = \frac{L_f}{R}\left(\frac{1}{T_f} - \frac{1}{T_{id}}\right)$$

rather than from Equation 5.4. When these plots were prepared for the systems Cd-CdTe and CdTe-Te, however, they were highly non-linear.

The System Zinc-Tellurium

The only previous study of this system is due to Kobayashi (43) who found that one congruently melting compound, ZnTe, exists as do two eutectics whose compositions are very close to the pure elements. His measurements were performed in an open system, however, so that evaporation of the alloys at high temperatures was a problem, and therefore he was unable to measure liquidus temperatures of mixtures containing less than 50 atom percent tellurium.

In this work eighteen DTA runs were performed on alloys containing from 3.0 to 100 atom percent tellurium, and the results are presented in Table 5.2 and Figure 5.4. On the high-tellurium side of the phase diagram, the liquidus temperatures were found to occur from 30°-70°C higher than the values found by Kobayashi. They are higher partly because our measurements were taken at constant volume while his were taken at constant pressure, but more probably because our elements

Table 5.2

Experimental Data for the Zn-Te Phase Diagram

Sample Number	Composition Atom % Te	Maximum Fusion Temperature °C	Eutectic Temperature °C	Liquidus Temperature °C
---	0	----	---	419.5
407	3.0	1175-1200	424	1190 ± 10
447	10.0	1130	423	1208 ± 5
461	20.0	1310	420	1215 ± 5
475	30.0	1280	420	1223 ± 5
466	40.0	1300	421	1250 ± 5
476	45.0	1310	420	1270 ± 5
125	50.0	----	---	1290 ± 3
432	50.0	1350	---	1290 ± 3
531	50.0	1350	---	1290 ± 2
477	55.0	1310	449	1260 ± 5
436	60.0	1250	445	1205 ± 5
457	70.0	1250	448	1100 ± 15
478	78.0	1100	449	996 ± 5
404	85.0	1100	446	915 ± 5
484	92.5	980	449	790 ± 15
401	95.0	1025	448	740 ± 20
92-F	100	----	---	449 ± 2
151-F	100	----	---	449 ± 2

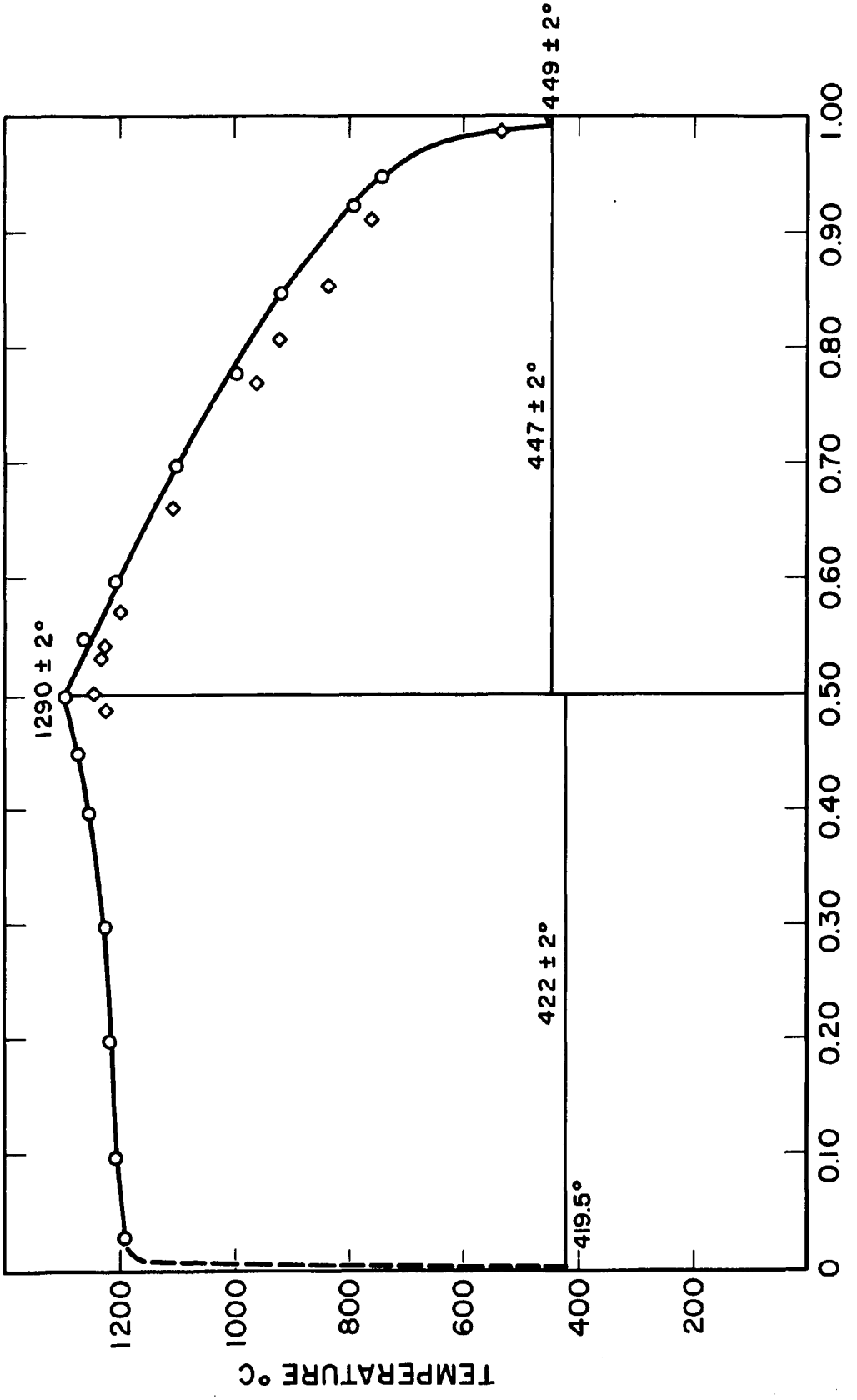


Figure 5.4. The Phase Diagram for the Zinc-Tellurium System.
◇ Data of Kobayashi; O This Work.

were much purer and less likely to become contaminated by oxidation.

The tellurium-rich eutectic was observed to occur at 447 ± 2°C and greater than 99 atom percent Te. The decomposition of the liquid phase at the solidus was observed to occur by peritectic reaction as the arrest temperatures were 422 ± 2°C - higher than the melting point of pure zinc (419.5°C) - with the composition at the peritectic point being indistinguishable from pure zinc.

The liquidus curve for alloys containing less than 50 atom percent Te was very flat, but it is felt that the possibility of the presence of a monotectic is remote, since no range of constant arrest temperatures was observed. The liquidus temperature also increases continuously from the pure Zn to the ZnTe compound. It should be pointed out that the exact composition of the samples containing 30-45% Te was somewhat different from the nominal composition reported here, because of the difficulty in recovering a substantial portion of the sample which stuck to the quartz tube on fusion. This error is tolerable, however, because of the relative flatness of the liquidus curve in this region.

One additional point should be mentioned. It may be noted that the liquidus curve shows a point of inflection. That this is the case is supported by the fact that the DTA curves for the 40 and 45% Te samples show double peaks in the neighborhood of the liquidus. The lever rule demands that, at equilibrium, in a two phase region, the two phases are present in a given mass ratio which is determined in part by the position of the liquidus curve. The shape of the DTA curve will depend on how this mass ratio varies with time. When the liquidus curve is very flat and contains a point of inflection, as is the case here, the ratio of solid/liquid will change as follows. On heating a sample whose composition lies to the right of the inflection point but to the left of ZnTe, the above ratio will be approximately constant from 423° to about 1200°; as the bend of the liqudus curve is passed, this ratio will decrease very rapidly; as the inflection point is passed the decrease will become less rapid; finally, on approaching the liquidus the decrease will become

more and more rapid until no more solid is left at the liquidus point.

Granted that this analysis is merely a qualitative one as other factors also influence the shape of the DTA curve (e.g., the rate of energy input to the sample, and the variation of the heat of dissolution with temperature and composition), it is nonetheless evident that such a double peak should not be entirely unexpected. In this case the above explanation appears to be the most plausible one.

As regards the thermodynamics of Zn-Te solutions, it may be stated that, as with Cd-Te solutions, the excess free energy of the solution exhibits a sharp minimum at the 50% composition which fact indicates that ZnTe molecules are stable in the liquid phase. The heats of mixing at infinite dilution may also be computed as described in the previous section (See Figure 5.5). We find $\overline{\Delta H}_{\infty Zn(Te)} = -21.7$ kcal/g atom and $\overline{\Delta H}_{\infty Te(Zn)} = +300.$ kcal/g atom. It is evident that the positive deviation from ideality in the Zn-ZnTe system is exceedingly strong indeed, which fact is also indicated by the extreme flatness of the liquidus in this region. Finally, it may be noted that as with the previous systems, the liquidus temperature data for the systems Zn-ZnTe and ZnTe-Te could not be explained by sub-regular solution theory based on the non-dissociative solubility of ZnTe in atomic zinc and atomic or diatomic tellurium.

The Indium-Selenium Phase Diagram

The only data reported on this system as yet have been a few selected studies on isolated compositions (31, 61, 74, 94) within the system, and no liquidus temperatures, other than the melting points of InSe, $660 \pm 10^{\circ}$ and In_2Se_3, $890 \pm 10^{\circ}C$ (31) have been reported. In this work sixteen thermograms have been obtained on compositions from 10.0 to 90.0 atom percent selenium. The DTA results are summarized in Table 5.3, and the proposed phase diagram is depicted in Figure 5.6. Five compounds are believed to exist -- two which melt congruently, and three which decompose pertectically. The congruently melting compounds,

Table 5.3

Experimental Data for the In-Se Phase Diagram

Sample Number	Atom % Se	Maximum Fusion Temperature* °C	Transition Temperature °C	Liquidus Temperature °C
---	0	----	----	157
493	10.0	950	158, 521	521
494	20.0	950	157, 518	518
495	30.0	950	157, 520	520
496	40.0	950	159, 520, 554	(560)
844	45.0	950	521, 553	598
497	50.0	950	Melts gradually, beginning at 605°	613
509	54.0	1000	663	686
510	56.0	950	659	765
846	58.0	1000	(195), 660	850
676	60.0	950	201, 745	885
294	62.0	1000	201, 220, 640, 744	865
533	64.0	1000	220, 742	-
275	66.0	975	201, 270, 650, 744, (760)	795
499	70.0	900	214-220, 745, 759	759
500	80.0	625	201, 220, 650, 745, 759	759
501	90.0	625	220, 658, 743	822
---	100	---	----	217

* All samples were water quenched.

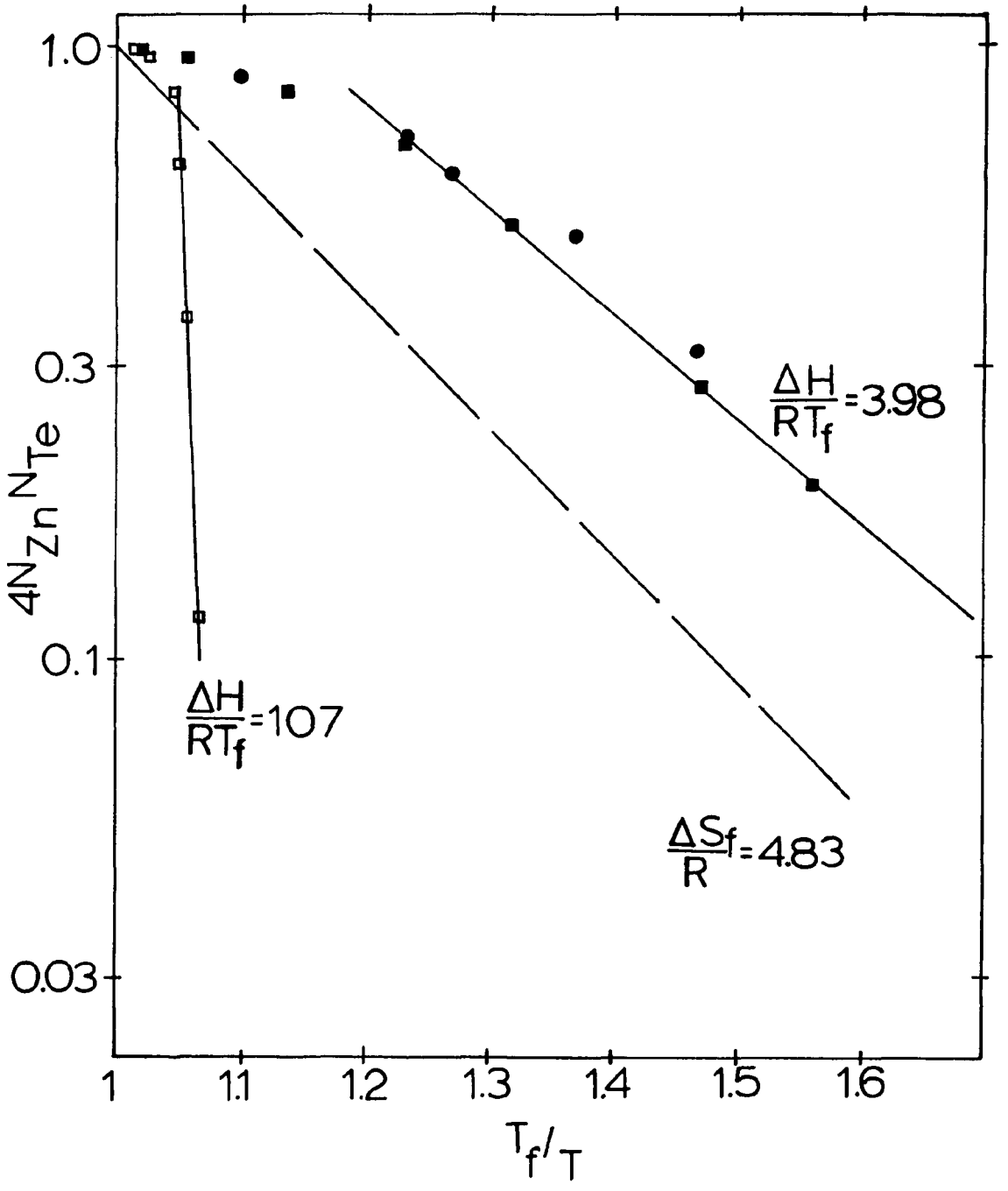


Figure 5.5. The Liquidus Curves for the System Zinc-Tellurium Plotted as log $4N_{Zn}N_{Te}$ versus Reciprocal Reduced Temperature.
O Data of Kobayashi; ◘ This Work.
For Open Symbols $N_{Te} < 1/2$ and for Closed Symbols $N_{Te} > 1/2$. The Dashed Line Represents Equation 5.4.

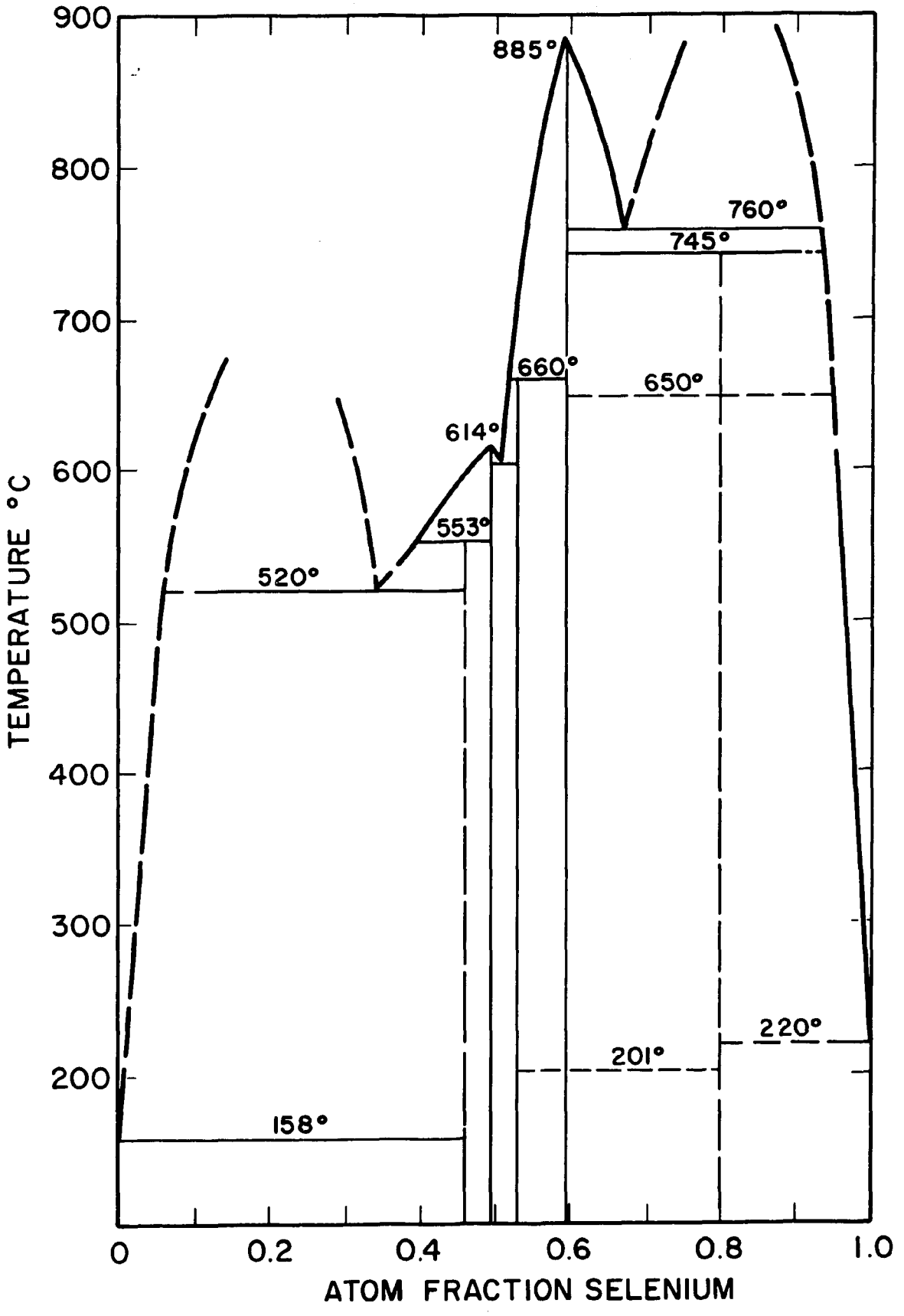


Figure 5.6. The Proposed Phase Diagram for the Indium-Selenium System.

InSe (M. P. = 614°C) and In_2Se_3 (885°C), both appear to be deficient in selenium. The first peritectic compound contains about 46 atom percent selenium and decomposes at 553°C. The second contains about 53% Se and decomposes at 660°C, the previously reported melting point of InSe. The location of the third compound which decomposes at 745°C is uncertain, but it probably contains about 80% Se. There appears to be crystalline transformations associated with In_2Se_3, at 201°C, and $InSe_4$ (?), at 650°C.

The indium-rich eutectic (?) occurs at 158°C and is thought to have a composition of nearly pure indium. The selenium-rich liquid decomposes by a peritectic reaction at 220°C (vs 217° for the melting point of pure Se) and contains nearly pure selenium. The anomalous variations in the low temperature transition* for alloys containing 60-100% Se are ascribed to non-equilibrium, local variations in the composition of the ingots, since they were prepared by quenching in water from the two-liquid region, and were not annealed prior to DTA.

Two monotectic ($S + L_1 \rightarrow L_1 + L_2$ on heating) transformations were observed. In the first, two liquid phases of nominally 5% and 35% selenium form at 520°C, and in the second, two liquid phases of nominally 68% and 95% Se form at 760°C.

Clearly, more work is indicated in order to completely characterize the nature of this system as there are many uncertainties which still must be resolved. Yet, with relatively few thermograms it has been possible to formulate a fairly complete, qualitative picture of the phase diagram.

Discussion

In attempting to correlate the liquidus data for the Cd-Te and Zn-Te systems it has been observed that sub-regular solution theory based on the non-dissociative dissolution of the compound in either

---

* See Table 5.3.

element does not suffice. Furthermore, regular solution theory based on the complete dissociation of the compound is also insufficient, for it requires that the integrand I_1 be constant,* and this is obviously untrue. The phase diagrams are, however, of a simple type which would infer that their theoretical explanation would also be reasonably uncomplicated. In this regard the following scheme was tried.

Consider the following model: the compound AB dissolves as the molecular species in element B which exists in the form of a cluster of n atoms on the average, B_n, thereby forming an ideal solution of the Van't Hoff type.

$$\ln x = \frac{\Delta S_f}{R}\left(1 - \frac{T_f}{T}\right) \qquad 5.6$$

where ΔS_f is the entropy of fusion of the compound, T_f is its melting point, R is the gas constant, and x the mole fraction of AB in a solution containing AB and B_n. Equation 5.6 may also be written as follows:

$$x = \exp \frac{\Delta S_f}{R}\left\{1 - \frac{T_f}{T}\right\} \qquad 5.7$$

Now x may also be found by material balance as follows. Let N_B denote the atom fraction of B in solution, whence

$$x = \frac{n(1 - N_B)}{n - 1 - (n-2)N_B} \qquad 5.8$$

Solving Equation 5.8 for n, Equation 5.9 is obtained:

$$n = \frac{x}{x - 1}\quad\frac{2N_B - 1}{1 - N_B} \qquad 5.9$$

Thus for each liquidus point, x may be found from Equation 5.7 and n from Equation 5.9.

---

* See Wagner (88); also Equation 5.1 ff. and Figure 5.2.

Applying this calculation to the liquidus curves of the systems Cd-Te and Zn-Te using $\Delta S_f = 8.8$ and 10.0 cal/g mol ^{o}K for CdTe and ZnTe respectively, the results which appear in Figure 5.7 are readily obtained. The indicated correlations may also be stated as follows:

System				
CdTe-Te	n	=	constant	= 1.5_3
ZnTe-Te	n	=	constant	= 1.3_5
Cd-CdTe	n	=	1.6_2	exp $8.3_8[(T_f/T) - 1]$
Zn-ZnTe	n	=	0.30	exp $75._8[(T_f/T) - 1]$

Hence this model does provide a simple, two parameter, correlation for the liquidus curves of these two systems. In fact, for the systems CdTe-Te and ZnTe-Te only one parameter is needed, for n is constant. Admittedly the theoretical basis for these results is shaky, but on the other hand the idea of atoms clustering is comprehensible. Perhaps the theory presented is a simplification of a more general hypothesis. It cannot be said at this time. The results are only presented here as being interesting.

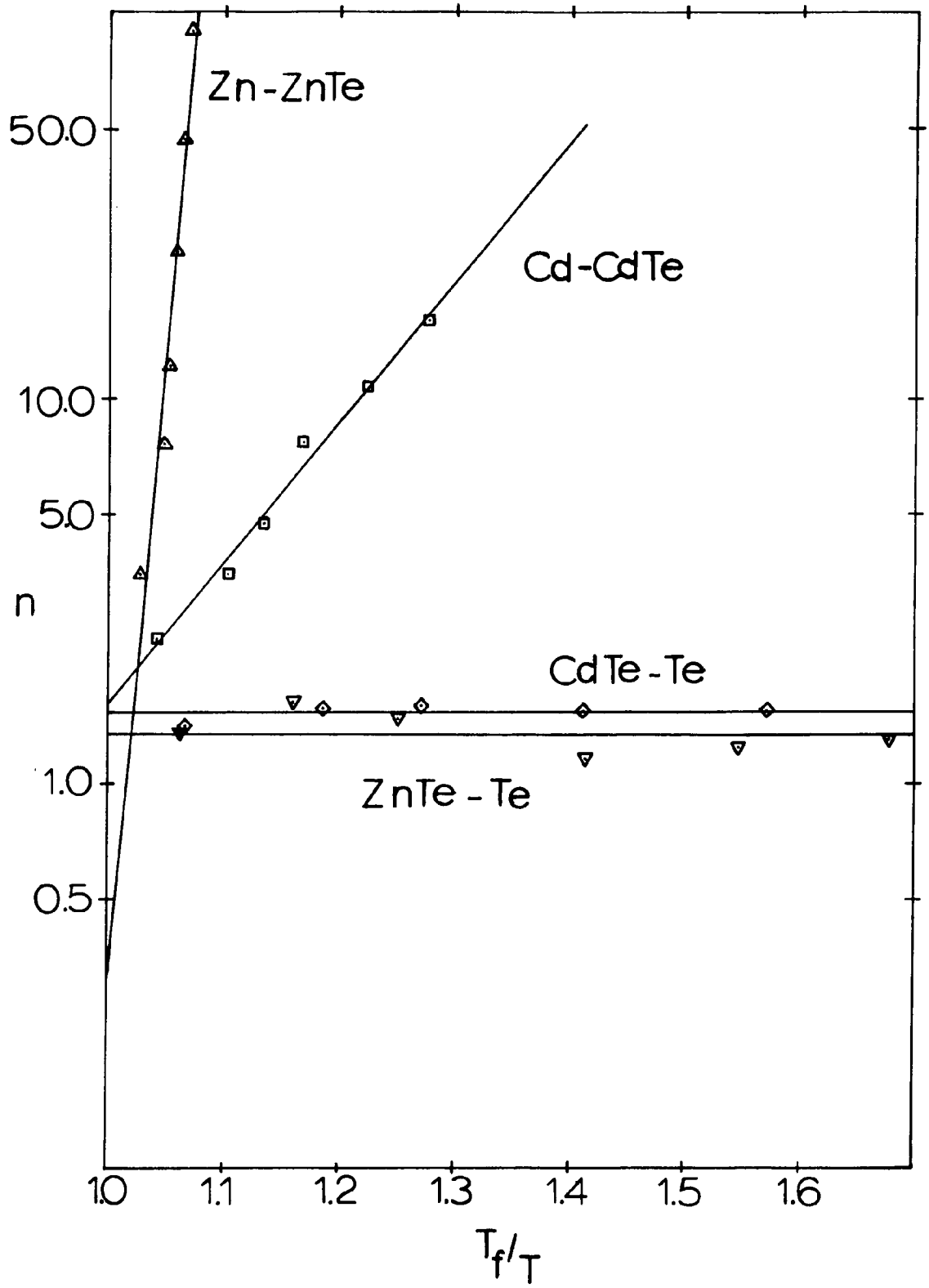


Figure 5.7. Semilogarithmic Plot of the Average Cluster Size, n, versus Reciprocal Reduced Temperature.

CHAPTER VI

CONCLUSION

In this final chapter, the results of the work are summarized and evaluated, and recommendations are made for possible future work.

Summary

In Chapter I several methods for determining the thermal conductance for the transfer of heat to the DTA sample were discussed. Of these, two--direct calculation from the geometry and physical properties of the system and calculation from the time constant plus the thermal capacity--appeared to be well suited to our system, but the first method was imperiled because direct observation of the dimensions of the gas film yielded imprecise values for its thickness. Subsequently, two indirect methods for calculating the thickness were proposed, viz. comparison of the theoretical time constant for the exponential decay of the DTA curve and comparison of the areas under the DTA curve when two gases of widely different thermal conductivity filled the system.

Next, in Chapter II the problems of heat conduction in the system prior to melting, during melting, and immediately following the completion of melting were considered. From these studies two significant facts emerged. The first important result was that the steady state formulae for the conductances could indeed be used to predict the thermal conductance of the system. The second result of significance was the extraction of expressions which would allow a theoretical computation of the time constant for exponential decay of the DTA curve, and thereby afford a method for evaluating the thickness of the gas film.

In Chapter III the methods proposed were further developed and applied to data on standards whose latent heats of fusion were well known. The agreement between the calculated heats of fusion and those taken from the literature was good, but it was learned that a calibration of the apparatus was necessary in order to apply the second method --

calculation of the thermal conductance from the observed time constant plus the thermal capacity.

The two methods via computer programs DTA-19 and DTA-17 were applied to the measurement of latent heats of fusion and transition of twenty compounds in Chapter IV. The entropies of fusion plus transition were found to vary from 2.2 cal/g atom ^{o}K for $Ag_2In_8Se_{13}$ to 9.6 cal/g atom ^{o}K for GaAs. It was further found that the compounds could be grouped into broad categories on the basis of their entropies of fusion and that similar compounds could be placed in the same category.

In Chapter V the phase diagrams for the systems Cd-Te, Zn-Te, and In-Se were presented and discussed, and the measured values of the heats of fusion of cadmium telluride and zinc telluride were used in performing thermodynamic calculations with the liquidus data for these systems. It was concluded that cadmium telluride and zinc telluride exist as the molecular species in solution although some dissociation is probable. A speculative model which correlates the liquidus data of these two systems was also proposed. This model was based on the formation of an ideal solution of the Van't Hoff type between undissociated compound AB and clusters of atoms of type B, B_n, where n represents the average number of B atoms in a cluster and is a function of temperature.

Advantages and Disadvantages of the Methods Used to Measure Latent Heats

It is clear that a principal advantage of both methods for measuring latent heats is that they permit the measurement over a very wide temperature range, from 300^{o} to 1560^{o}K. Secondly, the large thermal resistances of the gas film and the silica sample tube minimize uncertainties due to the properties of the sample which may not be well known.

As to the two methods proposed, the first, direct calculation of the thermal conductance from the geometry and thermal properties of the system, is clearly preferred because no calibration of the apparatus

is required. It does require an estimate of the thermal conductivity of the sample, however, and the estimate must be reasonably precise if the thermal conductivity of the sample is low. With regard to experimental precision, both methods leave a great deal to be desired since the probable error in the measured heats is 15% or more.

Recommendations

Three avenues for further work along these lines are open. In the first place, efforts would have to be made to determine the major sources of variability which contribute to the probable error associated with the latent heats measured. This would have to be accomplished by a process of elimination and would entail considerable effort.

Secondly, the method for evaluating the gas film dimensions by alternating the gas atmospheres in the system should be examined more closely. At the same time the contribution of thermal radiation to the heat transfer mechanism could be studied. In order to carry out these studies the DTA furnace would have to be modified so that it could be evacuated and backfilled with the desired gas. This appears to be the only way in which one can be sure that one gas is completely replaced by another.

Finally, the methods could be adapted to the study of other types of heat effects such as heats of reaction and heats of solution. These areas provide a fertile field for future research activity. It is felt that DTA will perform a useful role in the field of calorimetry in the future because it is rapid, the measurements are performed with ease, and the equipment required is simple, easily constructed, and relatively inexpensive.

APPENDIX I

DTA EQUIPMENT AND PROCEDURE

Two different sample arrangements were used: A) Crushed samples were sealed under vacuum below 0.1 micron in specially cleaned, clear fused silica tubes which were 11 mm in inside diameter by about 10 cm long. The sample tubes contained concentric thermocouple wells 6 mm in outside diameter by about 2.5 cm deep. The tubes were placed in holes drilled in the nickel holder, with a concentric graphite spacer being inserted between the sample tube and the nickel block. The weight of each sample was adjusted in accordance with its density so as to maintain about the same sample volume from one run to the next, a volume of about three cubic centimeters being chosen as the norm. This volume corresponds to a sample weight of from 15 to 35 grams. Chromel-P versus alumel thermocouples were used. B) The second sample arrangement utilized is depicted in Figure A-I-1. In this arrangement 10 mm (rather than 11 mm) tubes were used in which the thermocouple well was 6 cm (rather than 2.5 cm) deep. The graphite spacer was eliminated; and the nickel block was oxidized by heating in air at 1100°C. Platinum-platinum + 10% rhodium thermocouples were used. Sample arrangement A corresponds to the series B DTA runs, whereas sample arrangement B corresponds to the series C DTA runs.

The DTA furnace was designed around a 3" diameter, 2.5 kva Kanthal furnace winding which was installed in a vertical position, surrounded with bubble alumina insulation, and contained inside a 12" diameter stainless steel shell. Copper cooling coils were soft-soldered to the shell in order to control the cooling rate at lower temperatures. With this arrangement it is possible to maintain a heating rate of 2.5°C/min. from room temperature to 1100°C and a cooling rate of 2.5°C/min. from 1300-500°C. Above 1100°C and below 500°C the maximum heating and cooling rates, respectively are limited by the time constant of the system, the latter being about 200 min. at room temperature and decreasing to about 120 min. at 1300°C.

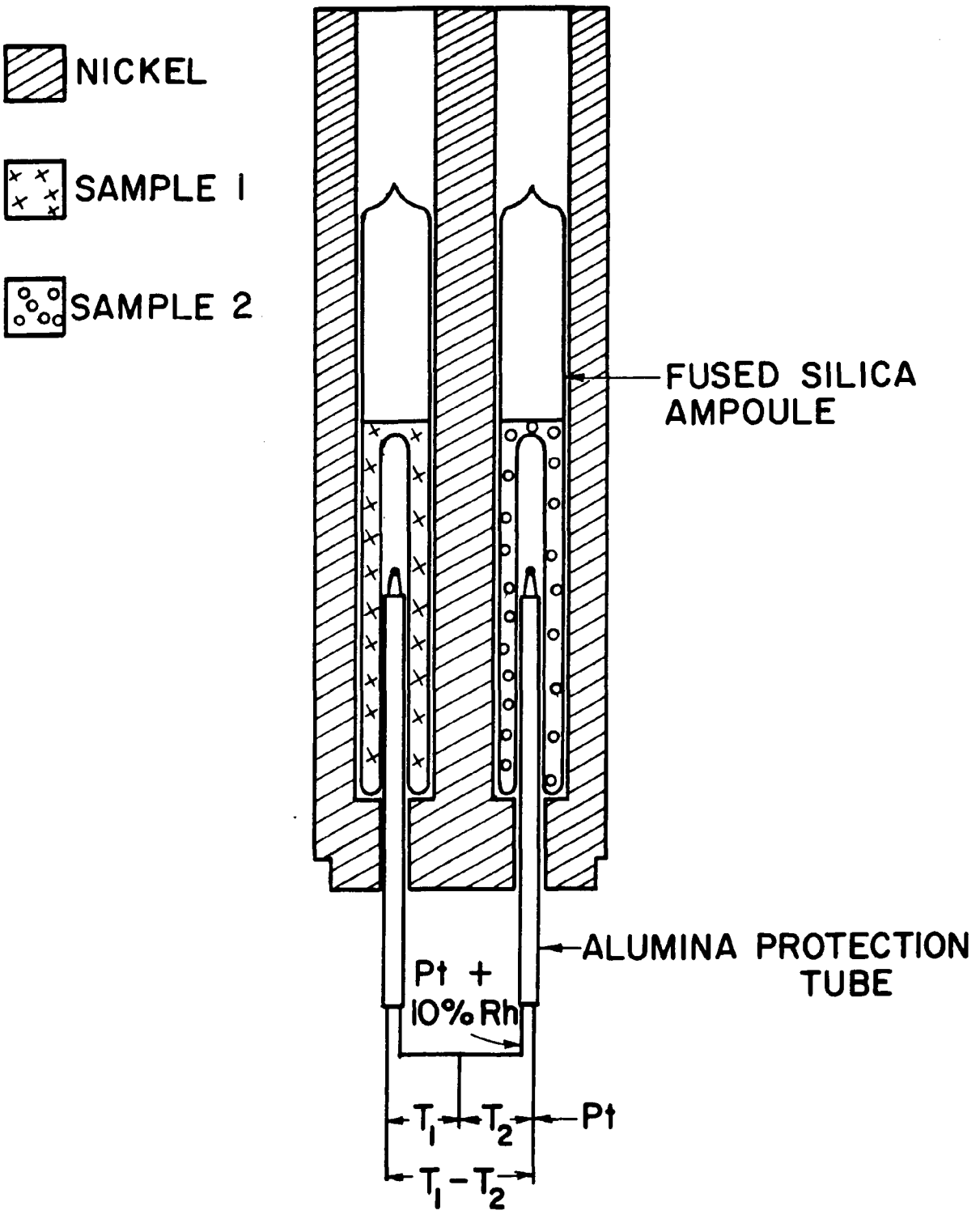


Figure A-I-1. DTA Samples inside the Nickel Block for Sample Arrangement B.

A 2-1/2" diameter by 21" long alumina (McDanel AV-30) tube which is sealed at the top is mounted inside the winding. The sample holder consists of a nickel block, 2" in diameter by 6" long, which contained two or three symmetrically located sample wells. The nickel block is supported inside the furnace by an alumina tube (McDanel AV-30) which is 2" in diameter by 12" long and flanged at the bottom to accommodate an arrangement for holding the assembly in the furnace. This tube also serves as a holder for the thermocouples and contains a port for introducing the helium or nitrogen purge gases. It too is filled with bubble alumina for insulation.

A block diagram showing the salient features of the temperature control and measurement circuit is shown in Figure A-I-2. All the operations in the system are actuated by a pulse generator. A short 110 volt, 60 cycle, AC pulse, about 1/4 to 1/3 second in duration is generated each 20 seconds by the microswitch which rides against a cam on a clock motor, which makes one revolution every 20 seconds.

The pulses are used to control a motor-driven autotransformer which feeds power to the Kanthal furnace so as to generate a substantially linear heating or cooling rate. The pulse length is adjusted so that each pulse can drive the autotransformer through about 1/200 of its full range. (It requires 64 seconds for the motor to drive the autotransformer through its full range.) If all the pulses were used to drive the autotransformer motor, the heating rate might be too rapid, and hence it was necessary to devise a Pulse Selector Circuit. With such a circuit it is possible to vary the time between the successive pulses which drive the autotransformer and thus to establish a heating rate of from $1^{\circ}C/min$ to $6^{\circ}C/min$. The pulse selector circuit uses a Guardian stepping relay, Model MER-115, which comprises a 21-point stepping circuit and a reset circuit. As the stepping coil is triggered by the pulse generator the contact arm advances along the various contacts from number 1 to number 21. Whenever the reset coil is triggered, the contact arm is returned by a detent spring to contact number 1. The short AC pulses are used not only to trigger the stepping coil but are

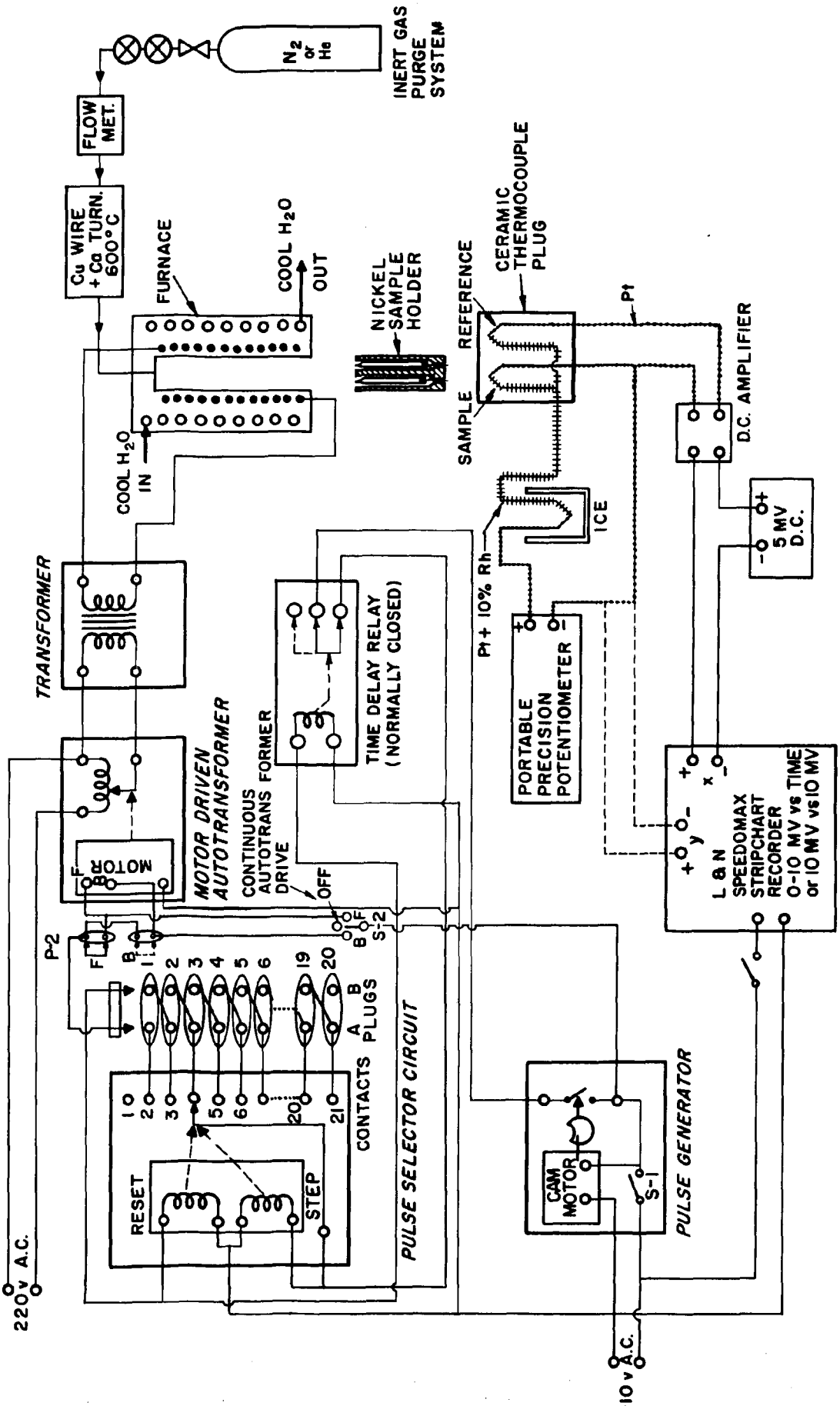


Figure A-I-2. Block Diagram Showing Operation of the DTA Equipment.

also fed through the contacts of the stepping switch. Each of the contacts on the stepping switch from contact number 2 to contact number 21 is connected on one terminal (A) on each of the 20 outlets on the panel. Hence, by connecting the autotransformer motor to the appropriate outlet the motor is activated only when the stepping switch has advanced sufficiently to feed the pulse to the outlet, and the time interval between each selected pulse can be varied in 20-second steps from 60 seconds to 420 seconds. A control switch is mounted in parallel with a pulsing switch so that the initial or final position of the autotransformer can be set as desired.

The second terminal (B) on each outlet is connected to the subsequent contact on the stepping switch, and leads to the reset coil. The next pulse then triggers the reset coil and returns the contact arm to contact number 1 for another cycle. For example, in order to select a pulse once every 60 seconds, the plug would be inserted into the second outlet. As the contact arm advances to contact number 3, the pulse is fed through terminal (A) of outlet number 2 and activates the autotransformer motor. The next pulse advances the contact arm to contact number 4 which feeds the pulse to terminal (B) of the second outlet. At this point the reset coil is triggered and the contact arm is returned to contact number 1 to start the cycle over again. An ordinary power control relay was required in the circuit as shown in order to open the stepping circuit for the duration of the resetting pulse, in order to allow the stepping contact to return all the way to contact number 1.

The measuring and recording circuits use a Leeds and Northrup Model G Speedomax strip chart recorder to read the differential emf. The differential thermocouple is connected through a Leeds and Northrup DC amplifier to the x-axis of the recorder and the differential emf was shifted to read zero at mid-scale, by providing a 0-10 mv auxiliary variable emf in series with the output from the DC amplifier. The thermocouple used to measure the sample temperature (with

respect to the reference junction temperature) was monitored by means of a portable precision potentiometer.

By using a 10 mv x 10 mv x-y recorder (not shown) a plot of differential emf versus sample temperature can be obtained directly, by introducing the sample thermocouple directly to the y-axis of the x-y recorder. The portable potentiometer is retained in the circuit. At low temperatures corresponding to less than 10 mv output from the sample thermocouple, the potentiometer output is set at zero. Above 10 mv output, the x-y recorder was reset onto the next 10" of chart, and the first 10 mv of thermocouple emf is balanced out with the auxiliary precision potentiometer. In this way the record of sample thermocouple emf is plotted on a scale of 1.0 mv per inch, which permits good separation of the transitions and careful indication of the transitions points, using either chromel-alumel or platinum-platinum rhodium thermocouples. In studying phase equilibria the x-y recorder was found to be considerably more convenient and records the data in a form which permits ready interpretation.

The following procedure was carried out for each heat of fusion run. First, both samples were melted so that each would present substantially the same effective heat transfer area. Then each sample in turn was frozen and re-melted with a nitrogen purge atmosphere in the DTA furnace and the procedure was repeated with a helium purge atmosphere in place of nitrogen. In each case the melting point and the heating rate were noted. The differential emf versus time curves were then graphically integrated so as to obtain the area under the curve. Upon removal of the samples from the DTA furnace the height of the sample material in each tube was noted. During each run, the furnace chamber was purged with an inert gas, the flow rate being maintained at about 2 cc/sec (at STP).

The liquidus temperatures of the binary alloys were estimated from both the heating and cooling curves. In the former case the temperature at which the last deflection returned to baseline was noted, and in the latter, the first deflection on cooling was used.

In most cases these temperatures agreed with one another to within less than 5°C. Difficulty in establishing the liquidus temperature was encountered in two instances: 1) for very high concentrations of tellurium, nucleation of the solid phase on cooling was sometimes suppressed to below the eutectic temperature; and 2) in regions where the liquidus curve was very steep, nucleation of the solid phase at the liquidus produced only a small deflection which sometimes could not be detected precisely. The latter behavior is a consequence of the lever rule, since in such a region the amount of solid which nucleates at the liquidus will be very small and thus the heat evolved will also be very small.

APPENDIX II

DYNAMICS OF THE DTA FURNACE

Determination of the Time Constant

The dynamics of the furnace can be determined by placing a thermocouple into the thermocouple well of a sample which is contained in the nickel block and establishing a constant temperature in the furnace. When the power input to the furnace is changed abruptly to a new constant value, it is assumed that a new source temperature is established instantaneously and the sample thermocouple temperature is measured as a function of time.

The differential equation describing a single time constant system which is absorbing heat by both conduction and radiation is

$$V \rho C_V \, dT/dt = UA(T_\infty - T) + \epsilon \sigma A(T_\infty^4 - T^4) \qquad \text{(A-2.1)}$$

where

V = volume of the system, cm^3

ρ = density, gm/cm^3

C_V = specific heat, $cal/gm\,^oC$

U = heat transfer coefficient $cal/cm^2\,^oK$ min

A = area of heat transfer, cm^2

ϵ = emissivity of receiver

σ = Stefan-Boltzmann constant

T_∞ = heater (source) temperature

T = thermocouple temperature.

Over small temperature ranges the radiation term can be factored and an average temperature defined such that

$$T_\infty^4 - T^4 = T_m^3 (T_\infty - T) \qquad \text{(A-2.2)}$$

where $T_m = \frac{1}{1.59}(T_\infty^3 + T_\infty^2 T + T_\infty T^2 + T^3)^{1/3} \approx \frac{1}{2}(T_\infty + T)$.

Substitution and rearrangement of the differential equation gives

$$K \frac{dT}{dt} + T = T_{\infty} \qquad \text{(A-2.3)}$$

where $K = a/(T_m^3 + b)$ = effective time constant of the system. This has the solution

$$\frac{T - T_o}{T_{\infty} - T_o} = Z = 1 - \exp -t/K \qquad \text{(A-2.4)}$$

Therefore plots of log (1 - Z) vs. t should give a straight line of slope -1/K. If there is an initial lag, then this must be subtracted from the time. Alternately the point where 63.2% of the change is complete also can be used as a time constant. Actually all three methods were used in this work. By carrying out several step function experiments over the temperature range, K can be evaluated as a function of T_m. In the furnace described, different results were obtained from heating and cooling experiments. For heating

$$K_h = 667/[(T_m/1000)^3 + 3.60] \qquad \text{(A-2.5)}$$

and for cooling

$$K_c = 667/[(T_m/1000)^3 + 2.94] \qquad \text{(A-2.6)}$$

When steady state operating conditions were established for each setting of the autotransformer, then the furnace temperature was found as a function of autotransformer setting. This relationship is

$$T_{\infty} = 20 + 0.8\, Y^{5/3} \quad (^{o}C) \qquad \text{(A-2.7)}$$

where

Y = autotransformer position, % of full scale.

These results now can be used to determine the operating conditions which are required for the DTA runs.

Operating Conditions and Procedures

In DTA measurements it is usually desirable to maintain a uniform heating or cooling rate, m. That is

$$T_{\left[\frac{h}{c}\right]} = T_b \pm \left(\frac{dT}{dt}\right)(t - t_b) = T_b \pm \frac{T_\infty - T_{\left[\frac{h}{c}\right]}}{K_{\left[\frac{h}{c}\right]}}(t - t_b) \qquad \text{(A-2.8)}$$

where

$dT/dt = m$ = constant, $^{o}C/min$

t_b = time at beginning of DTA run, min

T_b = temperature at beginning of DTA run, ^{o}C.

The upper sign (+) is chosen for heating and the lower value (-) for cooling. When the expressions for T_∞ and K are combined, then the final expression is

$$T_{\left[\frac{h}{c}\right]} = T_b \pm m(t - t_b) = \qquad \text{(A-2.9)}$$

$$20 + 0.8Y^{5/3} \mp m\left[\frac{667}{\begin{bmatrix}3.60\\2.94\end{bmatrix} + \left(\frac{566 + T_{\left[\frac{h}{c}\right]} + 0.8Y^{5/3}}{2000}\right)^3}\right]$$

This equation is unique for the particular furnace and sample arrangement, and must be solved by trial and error. For heating and cooling rates of $2.5^{o}C/min$, the solutions are plotted in Figure A-II-1 along with the correlation for T_∞ as a function of Y.

It is apparent then that for heating, the original setting of the autotransformer must be almost at midscale, but the rate of motion of the autotransformer (dY/dt) is less than that required to maintain T_∞. The slope of the Y vs. t curve then defines the rate of motion for the autotransformer, which must be established by the Pulse selector circuit.

Discussion

The time constant and equilibrium temperature correlations are functions of the furnace and sample designs, and must be determined experimentally for any particular system. Although similar sample geometries should be used for any consistent series of runs, there is

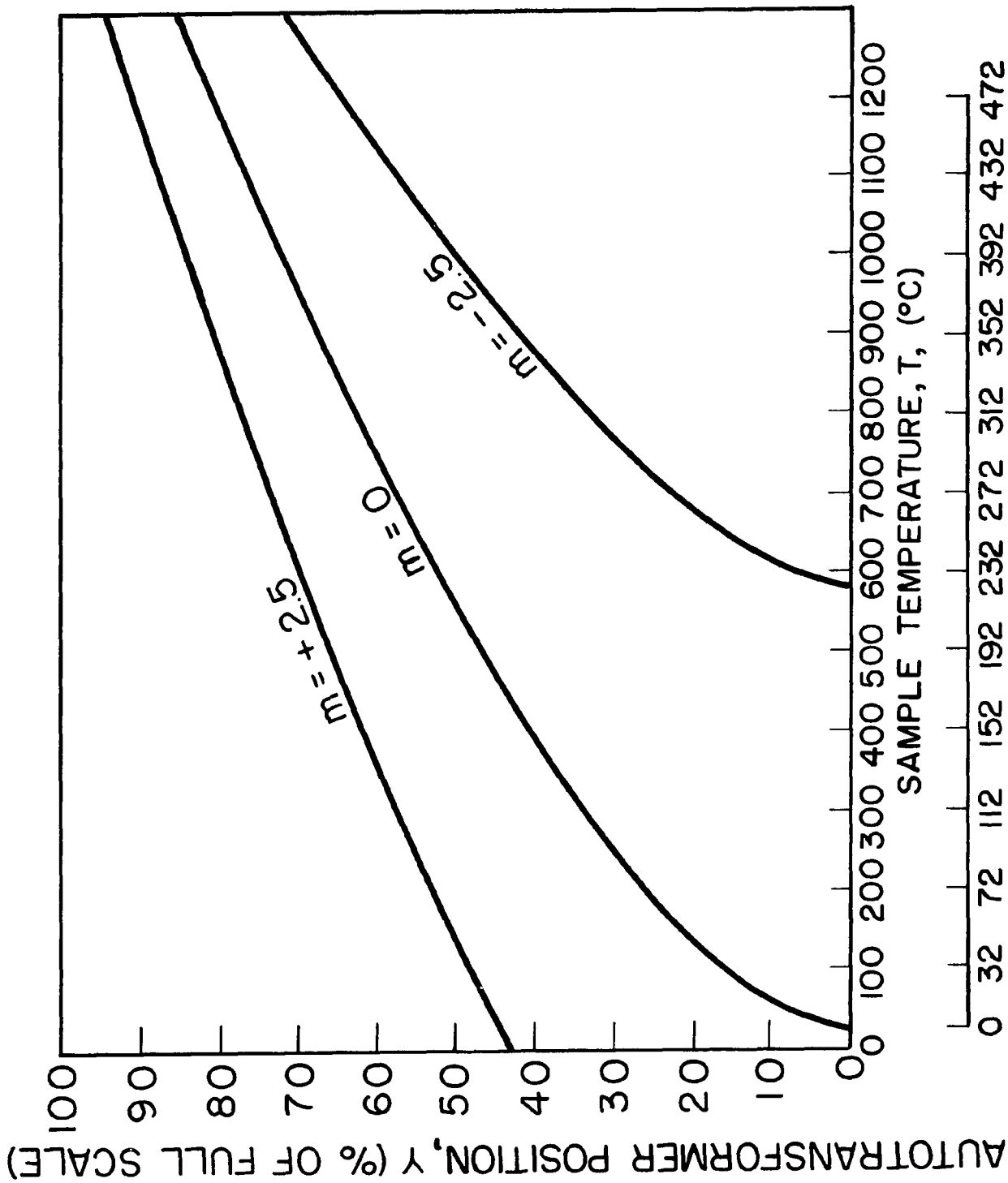


Figure A-II-1. Plot of Equation A-2.9 Showing Relationships between Furnace Temperature and and Autotransformer Setting for Heating and Cooling at Rates of 2.5°C/min and Steady State Conditions.

no need to retain a particular sample holder if it is found to be unsatisfactory for any reason. A new calibration can be obtained, and in general will be found not to vary significantly for a particular furnace.

Although the apparatus requires careful attention at each change point on the y-scale, it represents a good compromise between reliability, accuracy, cost and ease of operation. No temperature controller or precision program circuit is required, and the only expensive items in the system are the recorder, the DC amplifier, the motor-driven autotransformer, and the precision potentiometer. The rest of the system, being built from small, standard components, is relatively inexpensive.

APPENDIX III

SAMPLE PREPARATION

Materials

The materials used in this work originated from three sources. Samples of the III-V compounds, GaAs, GaSb, InAs, and InSb were donated by Texas Instruments, Inc. These samples were either portions of Czochralski grown single crystals, or portions of zone refined ingots. One sample of GaSb was received in the form of a "button" formed by direct fusion from the elements. Specimens of a number of compounds, including Ag_2Se, Ag_2Te, PbTe, PbSe, and SnTe, were donated by Dr. Alan J. Strauss of Lincoln Laboratories. Exact sample histories for the preparation of the samples mentioned above are largely unavailable. A qualitative measure of their purity, however, may be ascertained from their respective melting points and their thermal behavior (sharp versus gradual) during melting. The remainder of the samples were prepared in our laboratory by direct fusion from the elements. Table A-III-1 contains a summary of all of the elements, whether used as standards or used in the preparation of compounds, together with their respective sources and purities. And Table A-III-2 contains a list of all the DTA samples used for the measurement of heats of transformation.

Specimens of Bi_2Te_3, Bi_2Se_3, CsSe, CdTe, In_2Se_3, InTe, In_2Te_3, PbSe, PbTe, SnTe, ZnTe, and $Ag_2In_8Se_{13}$ were prepared from the elements in our laboratory. First, the elements were wherever possible etched with nitric acid or aqua regia in order to remove any surface oxide, and then weighed out to ±0.25 mg (total weight of sample = 25 to 70 g) by means of an analytical balance using standardized weights. In each case the stoichiometric composition was assumed. Thus in the following, $Ag_2Te \equiv Ag_{2.00}Te_{1.00}$, $In_2Te_3 \equiv In_{2.00}Te_{3.00}$, etc.* That is, the compounds

* Hodgkinson (32) has pointed out, however, that the maximum melting point does not in general correspond to the stoichiometric composition. This behavior is borne out experimentally. Thus, InTe, In_2Te_3, Ag_2Se, Bi_2Te_3, Bi_2Se_3, Sb_2Te_3 and SnTe are really $In_{49.2}Te_{50.8}$, $In_{40.3}Te_{59.7}$, (29) $Ag_{66.56}Se_{33.44}$ (89), $Bi_{40.065}Te_{59.935}$, $Bi_{40.02}Se_{59.98}$, $Sb_{40.40}Te_{59.60}$ (65) and $Sn_{49.06}Te_{50.94}$ (85).

TABLE A-III-1

ELEMENTS USED AS STANDARDS IN THE PREPARATION OF COMPOUNDS

Element	Source	Purity
Ag	Cominco Products, Inc.	5N, deoxidized
Bi	American Smelting and Refining Co.	5N
Cd	American Smelting and Refining Co.	4N
Cu	American Smelting and Refining Co.	5N
Ge	Zone-levelled single crystal	2-4 ohm-cm.
In	Indium Corp. of America	5N
Pb	Cominco Products, Inc.	High Purity
Sb	Johnson, Matthey and Co., Ltd.	High Purity
Se	American Smelting and Refining Co.	5N
Sb	Johnson, Matthey and Co., Ltd.	High Purity
Sn	Johnson, Matthey and Co., Ltd.	High Purity
Te	American Smelting and Refining Co.	5N
Zn	American Smelting and Refining Co.	4N

5N = 99.999%

4N = 99.99%

prepared here did not necessarily correspond precisely to the composition at the maximum melting point. An exception was $Ag_2In_8Se_{13}$*, which was purified by zone refining.

The elements were then placed in specially cleaned, clear, fused silica tubes, subsequently evacuated to below 0.1 micron and sealed. The encapsuled sample was next reacted by controlled heating to well above the melting point or liquidus temperature. For most samples, the heating and cooling cycles were accomplished in a digitally programmed resistance furnace. The latter equipment has been described by Hozak, Cook, and Mason (33). For cadmium and zinc telluride, however, it was found more convenient to use a much more rapid reaction cycle than could be achieved with the resistance furnace. For these compounds, the encapsuled elements were placed in a graphite susceptor and heated by radio frequency induction to a temperature about 50-100°C above the melting point of the compound. The entire heating cycle could be consummated within 3-5 minutes, thus suppressing any reaction with or wetting of the silica sample tube. The compound $Ag_2In_8Se_{13}$, the existence of which has been reported by O'Kane (66), was prepared as follows. 70 grams of Ag, In, and Se, in the proper stoichiometric ratios, were placed in a 10 mm I.D. silica tube. The Ag was placed in the bottom of the tube and the In and Se were cut into small pieces, mixed together and placed on top of the Ag. After seal-off the overall sample length was about 30 cm. The sample was reacted by carefully heating it in a rotating, rocking, resistance furnace. Extreme caution was taken as the temperature approached 245°C, since the In and Se react violently with one another at this point.** Following the exothermic reaction at 245°C, heating was continued until the sample was completely molten (MP. = 814°C). The molten sample was then transferred to a preheated zone

* In this case the composition $Ag_2In_8Se_{13}$ is approximate, since the exact influence of the zone refining process on the composition is as yet undetermined.

** This fact was confirmed by DTA experiments on a sample of 2In + 3Se. Secondary reaction peaks were observed at 610° and 835°C.

refiner and subjected to three or more passes, using a zone length of about 3.8 cm and a zone travel rate of about 1.9 cm/hr. Upon completion of zone refining, portions of high resistivity ($> 10^5$ ohm-cm) material were removed for further processing.

Preparation of Alloys

Alloys of Cd-Te and Zn-Te for the phase diagram determinations were prepared in much the same manner as the intermetallic compounds. In the case of Cd-Te alloys, the elements in the desired ratio were weighed into fused silica tubes and sealed under vacuum as described above. They were reacted by heating to temperatures well above the liquidus in a rotating, rocking resistance furnace, and were rapidly cooled or air-quenched to room temperature to obtain a homogeneous sample. In many instances the samples wet the fused silica tube and induced cracks and fractures in the containers during cooling. Only samples which remained bright, shiny and unoxidized after fusion were processed further.

In the case of the Zn-Te alloys, the R-F induction method described above was found to be much more satisfactory. Reaction with and wetting of the silica tube were completely suppressed. Although water-quenching of some samples proved satisfactory, a few materials, notably 30-50 a/o Te in Zn, were found to explode when rapidly plunged into cold water. As a result, most of the samples were rapidly cooled in air by turning off the power to the R-F unit.

Preparation of DTA Samples

Samples for the heat of transformation determinations were processed as described in Appendix I. For the phase diagram studies, the alloys were completely crushed and 15 grams of material were sealed under vacuum below 0.1 micron, in clear, specially cleaned, fused silica tubes which were 10 mm in I.D. and each of which contained a concentric thermocouple well about 2.5 cm deep. Exceptions were samples containing

more than 80 a/o Cd or Zn, in which case crushing was impossible. These materials were recovered in the form of a solid ingot which was rebottled in its entirety and rested on top of the thermocouple well until melting was initiated.

TABLE A-III-2

LIST OF SAMPLES USED IN THE HEAT OF TRANSFORMATION STUDIES

DTA Sample No.	Composition	Mass Grams	DTA Run Number(s)	Source/Purity	Melting Characteristic and Melting Point Observed
6	In	21.93	B-1; B-3	In Corp; 5N	sharp; 157°C
9	Cu	26.88	B-1	AS and R; 5N	sharp; 1082°C
12	Ge	15.96	B-2	2-4 ohm-cm	fairly sharp; 938°C
13	Te	18.72	B-3	AS and R; 5N	sharp; 450°C
14	CdTe	18.60	B-4	SL-479	gradual; 1092°C
16	InSb	17.37	B-5	TI; "P" ends	sharp; 526°C
17	InAs	17.10	B-5	TI; "N"; 0.02 ohm-cm	sharp; 943°C
18	GaAs	15.93	B-6	TI; zone-refined	fairly sharp; 1235°C
19	CdSe	17.43	B-7	SL-705+SL-717	gradual initial melting; 1251°C
20	ZnTe	16.62	B-6	SL-463	gradual; 1289°C
21	GaSb	16.86	B-7	TI; "button"	somewhat gradual; 712°C
22	Pb	34.02	B-10	Baker; Anal. Reag.	sharp; 327°C
23	Sb	19.04	B-8	Matthey	sharp; 631°C
24	Ge	15.96	B-8	2-4 ohm-cm	fairly sharp; 938°C
25	Te	18.72	B-11	AS and R; 5N	sharp; 450°C
26	Cu	26.88	B-14	AS and R; 5N	sharp; 1082°C

TABLE A-III-2 (Cont.)

DTA Sample No.	Composition	Mass Grams	DTA Run Number(s)	Source/Purity	Melting Characteristic and Melting Point Observed
27	CdTe	18.60	B-9	SL-479+SL-482	gradual; 1092°C
29	Sb	19.04	B-11	Matthey	sharp; 631°C
30	In	21.93	B-9; B-10	In Corp; 5N	sharp; 157°C
32	Ge	15.96	B-12	2-4 ohm-cm	fairly sharp; 937°C
33	CdTe	18.60	B-12	SL-479; SL-482	gradual; 1090°C
35	ZnTe	16.62	B-20	SL-1099	gradual; 1289°C
37	Sb	19.04	B-15	Matthey	sharp; 631°C
38	InAs	17.10	B-16	TI	sharp; 943°C
39	GaAs	15.93	B-17	TI	fairly sharp; 1235°C
40	Ag	31.53	B-14	Cominco; deoxidized	very sharp; 958°C
41	In	21.93	B-19	In.Corp; 5N	sharp; 158°C
42	InSb	17.37	B-15	TI; "P" ends	sharp; 524°C
43	Bi	29.40	B-16	AS and R; 5N	sharp; 275°C
45	Cu	26.88	B-18	AS and R; 5N	sharp; 1082°C
46	Ag	31.50	B-18	Cominco; deoxidized	very sharp; 960°C
47	CdTe	18.60	B-22	SL	gradual; 1092°C
48	Te	18.72	B-19	AS and R; 5N	sharp; 449°C
49	CdSe	17.43	B-24	SL	gradual initial melting; 1249°C

TABLE A-III-2 (Cont.)

DTA Sample No.	Composition	Mass Grams	DTA Run Number(s)	Source/Purity	Melting Characteristic and Melting Point Observed
52	GaSb	16.86	B-26	TI; "button"	somewhat gradual; 715°C
53	Pb	34.02	B-23	Cominco; 5N	sharp; 328°C
54	Bi_2Te_3	22.10	B-27	SL; zone refined	fairly sharp; 587°C
55	Bi_2Se_3	20.46	B-27	SL-489	somewhat gradual; 702°C
56	Sb_2Te_3	19.80	B-28	SL-491	somewhat gradual; 617°C
57	Sb_2Se_3	19.20	B-29	SL-490	somewhat gradual; 612°C
58	In_2Te_3	17.37	B-25	SL-488	gradual; 668°C
59	In_2Se_3	17.70	B-25	SL-492	slightly gradual; 885°C
61	Cu	26.88	B-24	AS and R; 5N	sharp; 1082°C
62	Ag_2Se	24.00	B-29	A.J.S.	sharp; 894°C
63	Ag_2Te	25.50	B-28	A.J.S.	sharp; 959°C
64	PbSe	24.30	B-30	A.J.S.	fairly sharp; 1085°C
65	PbTe	24.48	B-30	A.J.S.	slightly gradual; 926°C
68	InSb	17.37	B-33	TI; "P" ends	sharp; 527°C
69	InAs	17.10	B-33	TI; "N"; 0.02 ohm-cm	sharp; 944°C

TABLE A-III-2 (Cont.)

DTA Sample No.	Composition	Mass Grams	DTA Run Number(s)	Source/Purity	Melting Characteristic and Melting Point Observed
73	ZnTe	16.62	B-35	SL-463;SL-1099	gradual; 1286°C
90	Bi	29.70	C-1	AS and R; 5N	sharp; 271°C
91	Sb	19.50	C-2	Matthey	sharp; 931°C
92	Te	18.60	C-1	AS and R; 5N	sharp; 449°C
93	Ag	28.80	C-4	Cominco; deoxidized	very sharp; 960°C
94	Pb	32.40	C-3	Cominco; 5N	sharp; 326°C
96	Ge	16.20	C-2	Intrinsic	fairly sharp; 937°C
97	Ag	28.80	C-5	Cominco; deoxidized	very sharp; 961°C
99	In	21.30	C-12	In Corp; 5N	sharp; 157°C
100	InSb	18.30	C-6	TI	sharp; 524°C
101	InAs	17.70	C-7	TI	fairly sharp; 942°C
102	GaSb	17.40	C-6	TI; single crystal	slightly gradual; 712°C
103	SnTe	19.50	C-7	SL-512	gradual; 804°C
104	CdTe	18.60	C-10	SL	gradual; 1091°C
105	PbTe	24.60	C-8	A.J.S.	very gradual; 922°C
106	PbSe	24.30	C-8	A.J.S.	fairly sharp; 1083°C
107	GaAs	16.50	C-12	TI	sharp; 1236°C

TABLE A-III-2 (Cont.)

Sample No.	Composition	Mass Grams	DTA Run Number(s)	Source/Purity	Melting Characteristic and Melting Point Observed
110	Bi_2Te_3	23.10	C-9	SL-zone refined	fairly sharp; 586°C
111	Bi_2Se_3	20.40	C-9	SL-489	somewhat gradual; 700°C
112	Ag_2Te	25.50	C-10	A.J.S.	sharp; 958°C
113	Ag_2Se	24.00	C-11	A.J.S.	sharp; 894°C
115	Ag	28.80	C-13	Cominco, deoxidized	gradual; 957°C; oxide present
116	Sb_2Te_3	19.80	C-14	SL-515	somewhat gradual; 615°C
117	Sb_2Se_3	19.20	C-15	SL-516	somewhat gradual; 613°C
118	In_2Te_3	17.40	C-21	SL-522	gradual; 667°C
119	In_2Se_3	17.10	C-14	SL-492+SL-504	slightly gradual; 884°C
120	InTe	18.90	C-20	SL-529	gradual; 693°C
121	CdTe	18.60	C-15	SL-520	gradual; 1091°C
123	CdSe	17.50	C-16	SL-514	gradual initial melting; 1251°C
124	Ag	28.80	C-29	Cominco; deoxidized	sharp; 960°C
126	InSb	18.30	C-18	TI	sharp; 523°C

TABLE A-III-2 (Cont.)

DTA Sample No.	Composition	Mass Grams	DTA Run Number(s)	Source/Purity	Melting Characteristic and Melting Point Observed
127	InAs	17.70	C-18	TI	fairly sharp; 941°C
128	GaSb	17.40	C-19	TI	slightly gradual; 711°C
129	GaAs	16.50	C-19	TI	fairly sharp; 1236°C
130	Bi_2Te_3	23.10	C-22	SL-528	fairly sharp; 586°C
131	Bi_2Se_3	20.35	C-22	SL-523	somewhat gradual; 700°C
132	PbTe	24.60	C-23	SL-526	gradual; 923°C
133	PbSe	24.30	C-23	SL-527	fairly sharp; 1082°C
135	Ag_2Te	25.50	C-28	A.J.S.	sharp; 958°C
136	Ag_2Se	24.00	C-24	A.J.S.	sharp; 893°C
137	Sb_2Te_3	19.80	C-17	SL-515	somewhat gradual; 617°C
138	Sb_2Se_3	19.20	C-24	SL-521	somewhat gradual; 613°C
139	In_2Te_3	17.40	C-26	SL-522	gradual; 667°C
141	SnTe	19.50	C-16	A.J.S.	gradual; 804°C
142	InTe	18.90	C-17	SL-529	gradual; 693°C
145	CdSe	17.50	C-25	SL-498	gradual initial melting; 1248°C
146	ZnTe	16.60	C-28	SL-531	gradual; 1290°C

TABLE A-III-2 (Cont.)

DTA Sample No.	Composition	Mass Grams	DTA Run Number(s)	Source/Purity	Melting Characteristic and Melting Point Observed
148	$Ag_2In_8Se_{13}$	18.50	C-27	SL-281; zone refined; middle section; $>10^5$ ohm-cm	slightly gradual; 811°C
149	$Ag_2In_8Se_{13}$	18.50	C-29	SL-741; zone refined; middle section; $>10^5$ ohm-cm	slightly gradual; 813°C
150	In	21.30	C-30	In Corp; 5N	sharp; 157°C
151	Te	18.60	C-29	AS and R; 5N	sharp; 449°C

Code

5N = 99.999%
4N = 99.99+%
SL = Samples prepared by the Semiconductor Materials Laboratory, University of Michigan
A.J.S. = Samples donated by Dr. Alan J. Strauss, Lincoln Laboratories
TI = Samples donated by Texas Instruments, Inc.
AS and R = Materials purchased from American Smelting and Refining Co.
Matthey = Materials purchased from Johnson, Matthey and Company, Ltd.
Cominco = Materials purchased from Cominco Products, Inc.
In Corp = Materials purchased from the Indium Corporation of America

APPENDIX IV

PHYSICAL PROPERTIES AND THEIR ESTIMATION

In order to perform heat transfer calculations, values are needed for the heat capacities, thermal conductivities and so forth of the various components of the system. Furthermore, values are needed for the latent heats of fusion of the "standards" so as to have a basis for comparison of the results. For many of the components these properties are well known, but for most of the intermetallic compounds they have to be estimated. In this section, the values used will be summarized and the references given. Methods of estimation will also be discussed

Heats of Fusion and Transformation

The heats of fusion for all of the standards, except Ge, were taken from Kubaschewski and Evans (47). More recent values for Ge have been reported by Greiner and Breidt (28) as well as by de Roche (71). Among the intermetallic compounds, values are available only for Bi_2Te_3 (8), InSb (62, 73) and GaSb (73). Heats of transition have been reported for In_2Se_3 (94) and Ag_2Se (47).

Two methods are available for the estimation of heats of fusion. The first is based on a correlation between the entropy of fusion and the melting temperature by Turkdogan and Pearson (84). The data scatter considerably so that the probable error is high, perhaps ± 25% or more, but the correlation does point up a trend of increasing entropy of fusion with increasing melting temperature. Certain classes of compounds, such as those of zincblende structure, however, do not fit into this correlation. The second method, which is due to Kubaschewski and Evans (47), consists in additively combining the entropies of fusion of the elements to obtain the entropy of fusion of the compound. For disordered alloys, this method provides an excellent estimate. For ordered alloys and compounds it has been found that a better estimate is obtained if a factor

$$\sigma = -R[N_1 \ln N_1 + N_2 \ln N_2]$$

is added to the sum of entropies of fusion of the elements. Here N_1 and N_2 are the respective atom fractions of each element in a binary compound, R is the gas constant (1.987 cal/g atom $^{\circ}$K), and the units of σ are cal/mean gram atom $^{\circ}$K. If transitions occur below the melting point of the compound the above calculation would give an estimate of the sum of the entropies of transition and the entropy of fusion.

Densities

The densities are perhaps the best known of all the physical properties needed. The densities of nearly all of the materials of interest here are given in the standard handbook references (27, 30, 35, 48, 77). The density of α and β - In_2Te_3 at room temperature was measured by Zaslavskii and Sergeyeva (95), and those of the III-V compounds at high temperature were reported by Joffe and Regel (37). Although the values at high temperature are desired, corresponding measurements at room temperature usually provide a sufficiently precise estimate. If the density is unknown, it can be estimated from the crystal structure.

The density of silica is practically independent of temperature from 300°K to 1600°K and has a value of 2.20 grams per cubic centimeter. For the purge gases, the perfect gas law provides a good estimate:

$$\rho\,(g/cm^3) = 0.0122\ M/T\ (^{\circ}K)$$

where M is the molecular weight of the gas and the pressure is taken to be one atmosphere.

Heat Capacities

The specific heat of silica glass (77) in cal/g $^{\circ}$K is given as follows:

$$c_{p,\,SiO_2} = 0.223 + 0.0613\left(\frac{T}{1000}\right) - 0.00575\left(\frac{T}{1000}\right)^{-2}$$

$$T = {}^{o}K$$

A summary of the specific heats of a number of elements and compounds at their respective melting points appears in Table A-IV-1. Kubaschewski and Evans (47) have pointed out that the specific heat of many compounds is around 7.25 cal/mean gram atom ^{o}K at the melting point. The data reproduced here is in general agreement with this figure, so it was used to predict specific heat when they were unknown. The specific heats of some compounds at the transition temperature are reproduced in Table A-IV-2. These figures were used as a guide in estimating heat capacities of similar materials at the transition temperature.

Thermal Conductivity

The thermal conductivity of fused silica is a nearly linear function of temperature and may be represented by the following equation (27):

$$k_{SiO_2}\ (\text{cal/min cm } {}^{o}K) = 0.155 + 0.190\left(\frac{T}{1000}\right) \qquad T > 300^{o}K$$

The thermal conductivities of nitrogen (22) and helium (22, 90) are well approximated by the relations:

$$k_{N_2}\ (\text{cal/min cm } {}^{o}K) = 0.00060 + 0.01085\left(\frac{T}{1000}\right) - 0.00180\left(\frac{T}{1000}\right)^{2}$$

$$T > 300^{o}K$$

$$k_{He}\ (\text{cal/min cm } {}^{o}K) = 0.01163 + 0.03625\left(\frac{T}{1000}\right) - 0.00278\left(\frac{T}{1000}\right)^{2}$$

$$T > 300^{o}K$$

Table A-IV-1

Specific Heats of Elements and Compounds at the Melting Point

Material	T_f °C	c_p^s cal/m.g.a. - °C	c_p^l cal/m.g.a. - °C	Reference
Ag	961	7.63	7.3	(77)
Bi	271	7.43	7.29	(77)
Cu	1083	7.31	7.5	(77)
Ge	937	7.27		(47)
In	157	6.88	7.10	(77)
Pb	327	7.03	7.55	(77)
Sb	631	7.14	7.5	(77)
Te	450	8.40	9.0	(77)
AgBr	430	9.35	7.45	(47)
AgCl	455	7.50	8.00	(47)
Bi_2S_3	777	7.05		(47)
Bi_2Te_3	586	7.58		(9)
CdS	(1750)	(7.35)		(47)
InSb	525	6.55	7.4	(62, 72)
Sb_2S_3	547	6.98		(47)
SnS	881	7.05		(77)
ZnS	(1650)	7.26		(47)

Table A-IV-2

Specific Heats of Compounds at the Transition Point

Material	$T_{\alpha\rightarrow\beta}$ °C	c_p^{α} cal/m.g.a.°C	c_p^{β} cal/m.g.a.°C	$T_{\beta\rightarrow\gamma}$ °C	c_p^{β} cal/m.g.a.°C	c_p^{γ} cal/m.g.a.°C	Reference
Ag_2S	179	7.36	7.21				(47)
Ag_2Se	133	7.23	6.80				(47)
Ag_2Te	147	7.70	7.36	799			(47)
Cu_2S	103	6.50	7.75	350	7.75	6.77	(47)
Cu_2Se	110	7.07	6.73				(47)
In_2Se_3	200	9.35	9.35	725			(94)

The thermal conductivities of the standards near their melting points are well known and are summarized in Table A-IV-3. Those of the intermetallic compounds, on the other hand, are in general unknown. Moreover, due to the large number of processes which influence the thermal conductivity at high temperatures, their prediction is extremely difficult without detailed information about the electrical properties of each sample. The latter information was not available for our samples. As a result, a reasonable estimate of the thermal conductivity at the melting point could be made only in the case of the III-V compounds for which experimental data were available. For the remainder of the compounds, values of the thermal conductivity were selected in a somewhat arbitrary fashion and represent orders of magnitude only. Some of the estimates used in our calculations are given in Table A-IV-3.

Emissivities

Even though no calculations in which the equivalent conductances for radiation appear were performed in this work, the values of the emissivities and other methods available for their estimation are of interest because knowledge of them will be useful in future work where it may be desired to perform such calculations. The emissivity of oxidized nickel (30) may be expressed as follows

$$\epsilon_{NiO} = 0.143 + 0.48 \left(\frac{T}{1000}\right) \qquad > 300^{\circ}K$$

An effective emissivity for fused silica was found by assuming that all wavelengths less than 3.7 microns are totally transmitted through the quartz while all wavelengths greater than 3.7 microns are completely absorbed, and that this distribution is independent of temperature.*

* In truth the absorption spectrum is a complicated function of both wavelength and temperature. See, for example, ref. (27). It is a fact, however, that some radiation will penetrate the tube and impinge on the sample. As a zeroth approximation this factor may thus be taken into consideration.

Table A-IV-3

Thermal Conductivities of the Solid Near the Melting Point

Material or Property	Value Used cal/sec-cm-^{o}K	Temperature ^{o}C	Method of Estimation	References
In	0.053	156	A	(77)
Pb	0.070	327	E, A	(77)
Bi	0.018	270	E, A	(77)
Sb	0.052	630	E	(77)
Ag	0.65	960	E	(27)
Ge	0.042	937	E	(1, 5, 36, 75)
Te	0.009	450	E	(2, 20)
InAs	0.020	942	E	(13, 14)
InSb	0.018	525	E	(13, 15, 40, 81)
GaSb	0.013	706	E	(86)
GaAs	0.018	1237	L	--

Code:

E -- Extrapolated from experimental data.

A -- From the temperature coefficient of electrical resistance, α. $k_T/k_{300} = T/300\ (1 + \alpha(T - 300))$.

L-- From the extrapolation of the lattice component of thermal conductivity to the melting point and the Wiedemann-Franz law: $k = k_{ph} + L\sigma$.

Secondly, it is assumed that the reflectivity of the quartz is zero.* Kirchoff's law then takes the form

$$\epsilon = \alpha = 1 - \tau$$

The transmissivity as a function of temperature may then be found from the first assumption and the black-body radiation distribution function. The following empirical expression was obtained for the emissivity

$$\epsilon_{SiO_2} = \exp\left\{-\sqrt{\frac{T}{1000}}\left(\frac{0.93T}{1000} - 0.39\right)\right\} \quad T > 420^{\circ}K$$

Emissivities of the various intermetallic compounds are largely unknown. The reflectivity of GaAs has been measured (4) but data on the other compounds is nonexistent. Where sample emissivity data were not available, they were estimated, from the index of refraction according to the formula:

$$\epsilon \cong 4n/(n+1)^2$$

Use of this formula implies that the transmittance is effectively zero and that the extinction coefficient is small compared to n. It may be noted that this equation appears to work quite well for Ge and GaAs at room temperature, so that it might at least be expected to provide a reasonable estimate. Some values of the emissivity for standards as well as compounds are summarized in Table A-IV-4.

---

* In reality the reflectivity of fused silica varies from 17% at room temperature to 3% at 800°C (68).

Table A-IV-4

Emissivities of Elements and Compounds

Material or Property	Value Used	Method of Estimation	Reference
In	0.10	A	--
Pb	0.10	E	(77)
Ag	0.03	E	(77)
Bi	0.08	E	(77)
Te	0.45	E	(77)
Sb	0.35	E	(77)
Ge	0.52	E	(27)
GaSb	0.66	N	(16, 24, 34)
InSb	0.64	N	(16, 24, 34)
GaAs	0.70	E, N	(4, 16, 24, 34)
InAs	0.70	N	(24, 34)

Code: E - Experimental;
N - From index of refraction
A - Arbitrarily assumed.

APPENDIX V

CONDUCTION OF HEAT IN THE SYSTEM DURING MELTING*

In this Appendix, the complete temperature problem encountered during melting of a DTA sample [Regime (B)] is considered and the solution established for the case of semi-infinite planar bounding surfaces. A continuous solution of the following boundary value problem is to be found. The differential equation governing the temperature in regions (2) and (3)** is:

$$\frac{\delta}{\delta x}\left\{ k \frac{\delta T}{\delta x} \right\} = \rho c_p \frac{\delta T}{\delta t} \qquad \text{A-5.1}$$

$$X_3 < x < X_1 \, , \; t > 0$$

where k, ρ, and c_p are functions of x only and are defined in the region $X_3 < x < X_1$ such that

$$k(x) = \begin{cases} k_3 & \text{for } X_3 < x < X_2 \\ k_2 & \text{for } X_2 < x < X_1 \end{cases}$$

$$\rho(x) = \begin{cases} \rho_3 & \text{for } X_3 < x < X_2 \\ \rho_2 & \text{for } X_2 < x < X_1 \end{cases}$$

$$c_p(x) = \begin{cases} c_{p,3} & \text{for } X_3 < x < X_2 \\ c_{p,2} & \text{for } X_2 < x < X_1 \end{cases}$$

where k_3, k_2, ρ_3, ρ_2, etc. are constants, so that k, ρ, and c_p have a discontinuity of the first kind at $x = X_2$.

---

* The author is deeply indebted to Mr. A. N. Currim for his assistance in solving this problem.

** Cf. Figure 2.1, where x is written in place of r and X_i in place of R_i, since in this problem the bounding surfaces are planar.

The initial condition and the boundary conditions are:

$$\text{As } t \to 0+,\ T(x,t) \to 0\ ;\ X_3 < x < X_1 \qquad \text{A-5.2}$$

$$\text{As } x \to X_3+,\ T(x,t) \to 0\ ;\ t > 0 \qquad \text{A-5.3}$$

$$\text{As } x \to X_1-,\ T(x,t) \to \gamma t\ ;\ t > 0 \qquad \text{A-5.4}$$

The temperature is continuous at $x = X_2$:

$$\lim_{x \to X_2-} T(x,t) = \lim_{x \to X_2+} T(x,t)\ ;\ t > 0 \qquad \text{A-5.5}$$

The flux is continuous across $x = X_2$:

$$\lim_{x \to X_2-} k_3 \frac{\delta T}{\delta x} = \lim_{x \to X_2+} k_2 \frac{\delta T}{\delta x}\ ,\quad t > 0 \qquad \text{A-5.6}$$

The differential equation A-5.1 takes the following form in region (3) and region (2), respectively:

$$\frac{\delta^2 T}{\delta x^2} = \frac{1}{h_3^2} \frac{\delta T}{\delta t} \qquad X_3 < x < X_2\ ,\ t > 0 \qquad \text{A-5.7}$$

$$\frac{\delta^2 T}{\delta x^2} = \frac{1}{h_2^2} \frac{\delta T}{\delta t} \qquad X_2 < x < X_1\ ,\ t > 0 \qquad \text{A-5.8}$$

where

$$h_i^2 = \frac{k_i}{\rho_i c_{p,i}} \qquad i = 2, 3 \qquad \text{A-5.9}$$

is the thermal diffusivity.

$$\text{Let } q = \frac{x - X_3}{X_1 - X_3} \qquad \text{A-5.10a}$$

and

$$d = \frac{X_2 - X_3}{X_1 - X_3} \qquad \text{A-5.10b}$$

and write:

$$T(x, t) = T(q, t) = v(q, t) + \gamma q t \qquad \text{A-5.11}$$

Substituting Equations A-5.10 and A-5.11 into Equations A-5.7, A-5.8, and A-5.2 through A-5.6 transforms the inhomogeneous boundary problem for $T(x, t)$ into the following homogeneous boundary value problem for $v(q, t)$:

$$\frac{\delta^2 v}{\delta q^2} = H_3^2 \frac{\delta v}{\delta t} + \gamma H_3^2 q ; \quad 0 < q < d, \; t > 0 \qquad \text{A-5.12}$$

$$\frac{\delta^2 v}{\delta q^2} = H_2^2 \frac{\delta v}{\delta t} + \gamma H_2^2 q ; \quad d < q < 1, \; t > 0 \qquad \text{A-5.13}$$

$$\text{As } t \to 0+ , \; v(q, t) \to 0 ; \text{ for } 0 < q < 1 \qquad \text{A-5.14}$$

$$\text{As } q \to 0+ , \; v(q, t) \to 0 ; \text{ for } t > 0 \qquad \text{A-5.15}$$

$$\text{As } q \to 1- , \; v(q, t) \to 0 ; \text{ for } t > 0 \qquad \text{A-5.16}$$

$$\lim_{q \to d-} v(q, t) = \lim_{q \to d+} v(q, t) \qquad t > 0 \qquad \text{A-5.17}$$

$$\lim_{q \to d-} \left(k_3 \frac{\delta v}{\delta q} \right) + (k_3 - k_2) \gamma t = \lim_{q \to d+} \left(k_2 \frac{\delta v}{\delta q} \right) \qquad t > 0 \qquad \text{A-5.18}$$

where

$$H_i^2 = \frac{(X_1 - X_3)^2}{h_i^2} , \quad i = 2, 3 \qquad \text{A-5.19}$$

The solution of the boundary value problem given by Equations A-5.12 and A-5.18 is obtained by using the Laplace transform.

$$\text{Let} \quad L_t \left\{ v(q,t) \right\} = \int_0^\infty e^{-st} v(q,t)\, dt = V(q,s) \qquad \text{A-5.20}$$

Then Equations A-5.12 to A-5.18 become:

$$\frac{\delta^2 V}{\delta q^2} = H_3^2 V + \frac{\gamma H_3^2 q}{s}, \quad 0 < q < d \qquad \text{A-5.21}$$

$$\frac{\delta^2 V}{\delta q^2} = H_2^2 s V + \frac{\gamma H_2^2 q}{s}, \quad d < q < 1 \qquad \text{A-5.22}$$

$$\text{As} \quad q \to 0+, \; V(q,s) \to 0 \qquad \text{A-5.23}$$

$$\text{As} \quad q \to 1-, \; V(q,s) \to 0 \qquad \text{A-5.24}$$

$$\lim_{q \to d-} V(q,s) = \lim_{q \to d+} V(q,s) \qquad \text{A-5.25}$$

$$\lim_{q \to d-} \left(k_3 \frac{\delta V}{\delta q} \right) + \frac{(k_3 - k_2)\gamma}{s^2} = \lim_{q \to d+} \left(k_2 \frac{\delta V}{\delta q} \right) \qquad \text{A-5.26}$$

Equations A-5.21 and A-5.22 are elementary and have the respective general solutions:

$$V(q,s) = -\frac{\gamma q}{s^2} + A(s) \sinh(H_3 q \sqrt{s}) + B(s) \cosh(H_3 q \sqrt{s}), \quad 0 < q < d \qquad \text{A-5.27}$$

$$V(q,s) = -\frac{\gamma q}{s^2} + C(s) \sinh(H_2 q \sqrt{s}) + D(s) \cosh(H_2 q \sqrt{s}) \quad d < q < 1 \qquad \text{A-5.28}$$

Using Equations A-5.23 to A-5.26 in A-5.27 and A-5.28 there results a set of four simultaneous equations for A(s), B(s), C(s) and

D(s). Solving these for A(s), B(s), C(s) and D(s), substituting these results in to Equations A-5.27 and A-5.28 and simplifying, the following expressions for the Laplace transform, V(q, s), of v(q, t) result:

$$V(q, s) = -\frac{\gamma q}{s^2} + \frac{\gamma c}{s^2} \frac{\sinh (H_3 q \sqrt{s})}{[\cosh (H_3 d \sqrt{s}) \sinh (H_2 (1-d) \sqrt{s}) + c \sinh (H_3 d \sqrt{s}) \cosh (H_2 (1-d) \sqrt{s})]}$$

valid in $0 < q < d$ A-5.29

$$V(q, s) = -\frac{\gamma q}{s^2} + \frac{\gamma}{s^2} \frac{[\cosh (H_3 d \sqrt{s}) \sinh (H_2 (q-d) \sqrt{s}) + c \sinh (H_3 d \sqrt{s}) \cosh (H_2 (q-d) \sqrt{s})]}{[\cosh (H_3 d \sqrt{s}) \sinh (H_2 (1-d) \sqrt{s}) + c \sinh (H_3 d \sqrt{s}) \cosh (H_2 (1-d) \sqrt{s})]}$$

valid in $d < q < 1$ A-5.30

where

$$c = \frac{k_2 H_2}{k_3 H_3} \qquad \text{A-5.31}$$

These transform functions may be inverted and will give the solution for the boundary value problem. The inverse transform is given by the inversion integral:*

$$v(q, t) = \lim_{\beta \to \infty} \int_{M-i\beta}^{M+i\beta} V(q, s)\, e^{st}\, ds \qquad \text{A-5.32}$$

---

* Cf. Churchill (18) p. 176 ff. In particular all the conditions of theorem 5, p. 178, are satisfied.

which satisfies the condition $v(q,t) = 0$ for $t < 0$. Here M is a real number so large that all the singularities of the complex function $V(q, s)$ of the complex variable s lie in the left half plane $Re(s) < M$.

By expanding the hyperbolic functions, appearing in $V(q, s)$, in Maclaurin series in the complex s plane, it is easy to see that $V(q, s)$ has no branch cuts in the s-plane. Hence we may evaluate the integral A-5.32 by closing the contour in the left half plane $Re(s) < M$, as in Figure A-V-1. The curve BB'CA'A is an arc of a parabola with focus at the origin and so chosen that it passes through no singularities of $V(q, s)$. By Cauchy's theorem, it then follows that

$$\frac{1}{2\pi i} \oint_{\mathcal{C}} V(q, s)\, e^{st}\, ds = \text{sum of the residues of } V(q, s) \text{ inside } \mathcal{C} \qquad \text{A-5.33}$$

where $\mathcal{C}$ is the contour ABB'CA'A of Figure A-V-1. By arguments similar to those in Churchill (18) p. 204 ff, it is easily seen that the integral of $V(q, s)\, e^{st}$ over the arc of the parabola BB'CA'A vanishes as $\beta \to \infty$. Hence it follows that the inverse transform $v(q, t)$ of $V(q, s)$ is given by:

$$v(q, t) = \text{sum of the residues of } V(q, s)e^{st} \text{ in the left half plane } Re(s) < M \qquad \text{A-5.34}$$

The function $V(q, s)$ defined by Equations A-5.27 and A-5.28 has a double pole at $s = 0$ and it also has singularities at the roots of the transcendental equation:

$$\cosh H_3 d\sqrt{s}\ \sinh H_2(1-d)\sqrt{s} + c \sinh H_3 d\sqrt{s} \cosh H_2(1-d)\sqrt{s} = 0 \qquad \text{A-5.35}$$

which may be written as

$$\sin H_2(1-d)\beta \cos H_3 d\beta + c \cos H_2(1-d)\beta \sin H_3 d\beta = 0 \qquad \text{A-5.36}$$

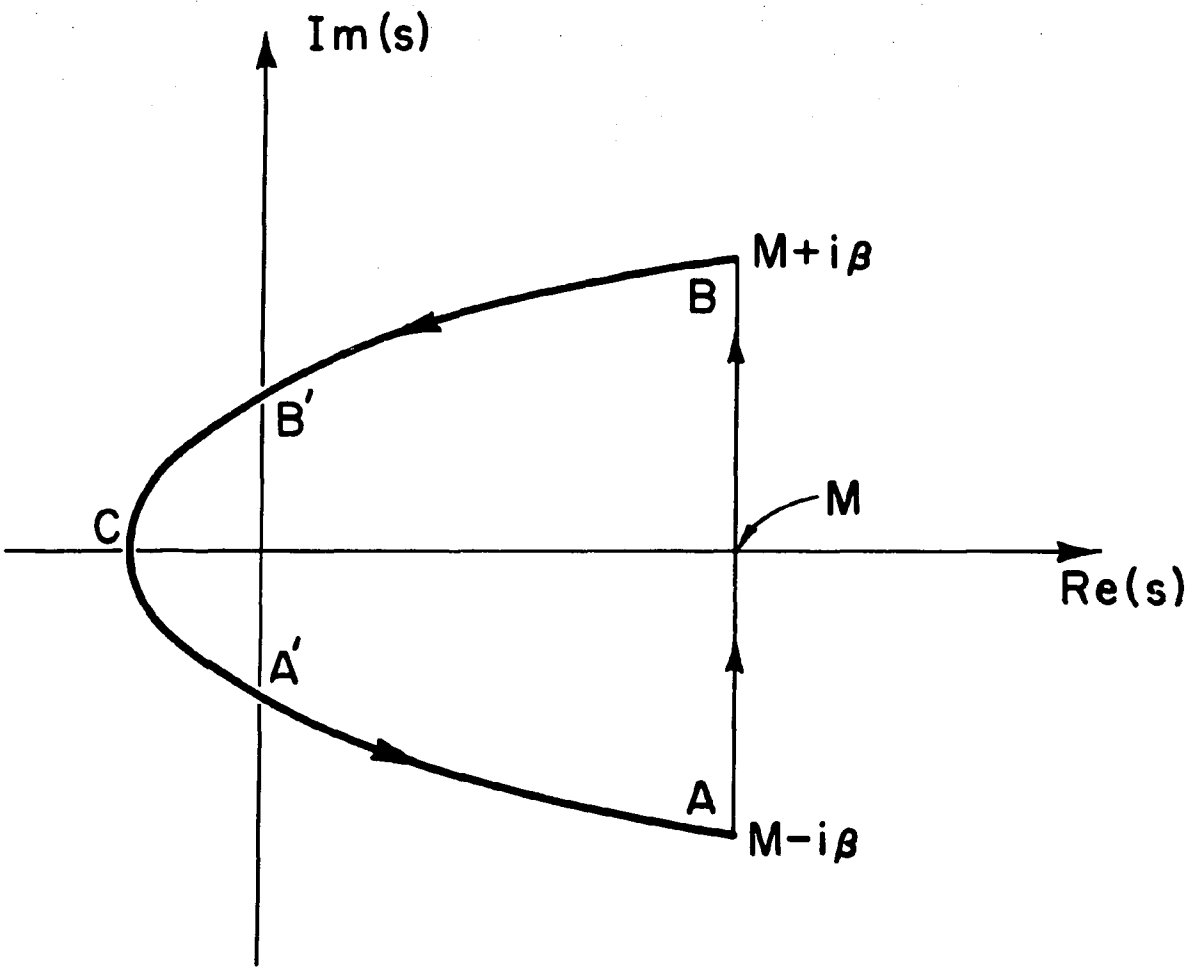


Figure A-V-1. Contour in the Complex Plane for Inversion of the Laplace Transforms, Equations A-5.29 and A-5.30.

with

$$\beta = i\sqrt{s} \qquad \text{A-5.37}$$

It has been shown* that all the roots, β_n of Equation A-5.36 are real and simple, so that it follows that $V(q, s)e^{st}$ has only simple poles at the non-zero roots of A-5.35.

The residue $\rho_o(t)$ at the double pole $s = 0$ is:

$$\rho_o(t) = A_1 + A_2 t \qquad \text{A-5.38}$$

where

$$A_1 = \gamma c \left[\frac{H_3^3 q^3}{6\{H_2(1-d) + c H_3 d\}} - \frac{H_3 q}{\{H_2(1-d) + c H_3 d\}^2} \right.$$

$$\left. - \frac{H_3^2 d^2 H_2(1-d)}{2} + \frac{H_2^3(1-d)^3}{6} + \frac{c}{6} H_3^3 d^3 + \frac{c H_3 H_2 d(1-d)^2}{2} \right]$$

valid for $0 < q < d$ A-5.39

$$A_2 = \gamma c \left[\frac{H_3 q}{H_2(1-d) + c H_3 d} \right] - \gamma q$$

valid for $0 < q < d$ A-5.40

$$A_1 = \gamma \left[\frac{H_3^2 H_2 d(q-d) + \frac{H_2^3}{6}(q-d)^3 + \frac{c H_3^3 d^3}{6} + \frac{c}{2} H_3 H_2^2 (q-d)^2}{H_2(1-d) + c H_3 d} \right.$$

$$\left. - \frac{H_2(q-d) - c H_3 d}{\{H_2(1-d) + c H_3 d\}^2} \left\{ \frac{H_3^2 H_2 d^2(1-d)}{2} + \frac{H_2^3(1-d)^3}{6} + \frac{c H_3^3 d^3}{6} + \frac{c H_3 H_2^2 d(1-d)^2}{2} \right\} \right]$$

valid in $d < q < 1$ A-5.41

* Cf. Carslaw and Jaeger (17), p. 324 ff.

$$A_2 = \gamma \frac{H_2(q-d) - c H_3 d}{H_2(1-d) + c H_3 d} - \gamma q \qquad \text{valid in } d < q < 1$$

A-5.42

The non-vanishing roots of Equation A-5.35 are designated β_n, $n = 1, 2, 3, \ldots$ and ordered so that $\beta_1 < \beta_2 < \ldots < \beta_n < \ldots$ Putting

$$\beta_n = i\sqrt{s_n} \qquad \text{A-5.43a}$$

one sees that the non-vanishing roots of Equation A-5.35 in the complex s-plane are all negative:

$$s_n = -\beta_n^2 \qquad \text{A-5.43b}$$

so that we need only take β_n to be the positive roots of A-5.36. The residue $\rho_n(t)$ of $V(q, s)\, e^{st}$ at β_n is:

$$\rho_n(t) = -2\gamma \frac{1}{\beta_n^3} \frac{B_n(q) \exp(-\beta_n^2 t)}{C_n} \qquad \text{A-5.44}$$

where

$$B_n(q) = c \sin H_3 \beta_n q \qquad 0 < q < d$$

and

$$B_n(q) = \cos(H_3 d\beta_n)\sin(H_2(q-d)\beta_n) + c \sin(H_3 d\beta_n)\cos(H_2(q-d)\beta_n)$$

$$\text{for } d < q < 1 \qquad \text{A-5.45}$$

and

$$C_n = \left[\left\{H_2(1-d) + c H_3 d\right\} \cos(H_3 d\beta_n)\cos(H_2(1-d)\beta_n)\right.$$

$$\left. + -\left\{c H_2(1-d) + H_3 d\right\} \sin(H_3 d\beta_n) \sin(H_2(1-d)\beta_n)\right]$$

$$0 < q < 1 \qquad \text{A-5.46}$$

So it follows that

$$v(q,t) = A_1 + A_2 t - 2\gamma \sum_{n=1}^{\infty} \frac{B_n(q)}{\beta_n^3 C_n} \exp(-\beta_n^2 t)$$

$$0 < q < 1 \qquad \text{A-5.47}$$

where β_n are the positive roots of Equation A-5.36, and A_1, A_2, $B_n(q)$ and C_n are defined above. It is now easily verified that Equation A-5.47 satisfies all the boundary conditions A-5.15 to A-5.18 and the differential equations A-5.12 and A-5.13 of the boundary value problem for $v(q,t)$. It has already been shown in Equation A-5.32 that $v(q,t)$ satisfies the initial condition A-5.14. Hence Equation A-5.47 is completely established as the solution of the boundary value problem defined by the expressions A-5.12 to A-5.18.

It then follows, via Equation A-5.11, that the solution of the boundary value problem defined by the expressions A-5.2 to A-5.8 is given by:

$$T(x,t) = v(q,t) + \gamma q t \qquad \text{A-5.48}$$

where q, d are defined by Equation A-5.10.

It is of interest to know the behavior of Equation A-5.48 as $H_2 \to 0$. This represents the situation of the gas film corresponding to a negligibly small heat sink. If one takes the limit of Equation A-5.47 as $H_2 \to 0$, one finds after a slightly tedious (but straightforward) calculation:

$$\lim_{H_2 \to 0} T(q,t) = \frac{\gamma q t}{\left[d + \frac{k_3}{k_2}(1-d)\right]} + \frac{\gamma H_3^2 q^3}{6\left[d + \frac{k_3}{k_2}(1-d)\right]} +$$

$$- \frac{\gamma H_3^2 d^2 q}{6\left[d + \frac{k_3}{k_2}(1-d)\right]} - \frac{\gamma k_3 H_3^2 d^2 (1-d)}{3k_2\left[d + \frac{k_3}{k_2}(1-d)\right]^2} +$$

$$-2\gamma H_3^2 d^2 \sum_{n=1}^{\infty} \frac{\sin\left[\frac{\alpha_n q}{d}\right] \exp -\left(\frac{\alpha_n}{H_3 d}\right)^2 t}{\alpha_n^3 \left\{\frac{k_3}{k_2}\frac{(1-d)}{d}\cos\alpha_n + \cos\alpha_n + \frac{k_3(1-d)}{k_2 d} + \alpha_n \sin\alpha_n\right\}}$$

valid in $0 < q < d$ A-5.49

where $\alpha_n = H_3 d \beta_n$.

and also

$$\lim_{H_2 \to 0} T(q,t) = \frac{\gamma k_3 H_3^2 d^3 (q-1)}{3k_2\left[d + \frac{k_3}{k_2}(1-d)\right]^2} + \frac{\gamma t\left[d + \frac{k_3}{k_2}(q-d)\right]}{\left[d + \frac{k_3}{k_2}(1-d)\right]} +$$

$$-2\gamma d^2 H_3^2 \sum_{n=1}^{\infty} \frac{1}{\alpha_n^3} \frac{\left[\sin\alpha_n + \frac{k_3}{k_2}\frac{(q-d)}{d}\alpha_n \cos\alpha_n\right] \exp -\left(\frac{\alpha_n}{H_3 d}\right)^2 t}{\left[\frac{k_3}{k_2}\frac{(1-d)}{d}\cos\alpha_n + \cos\alpha_n - \frac{k_3}{k_2}\frac{(1-d)}{d}\alpha_n \sin\alpha_n\right]}$$

valid in $d < q < 1$ A-5.50

where α_n are the positive roots of

$$\alpha \cot \alpha + \frac{k_2}{k_3} \frac{d}{(1-d)} = 0 \qquad \text{A-5.51}$$

The parameters and variables ζ', ζ'', η', η'', ϕ', τ' of Chapter II are related to the variables above as follows:

$$(\zeta' - 1) = \frac{q(X_1 - X_3)}{X_3} \qquad \text{A-5.52}$$

$$\eta' = X_2/X_3 \qquad \text{A-5.53}$$

$$(\zeta'' - 1) = \frac{q(X_1 - X_3) - (X_2 - X_1)}{X_2} \qquad \text{A-5.54}$$

$$\eta'' = X_1/X_2 \qquad \text{A-5.55}$$

$$\phi' = k_3/k_4 \qquad \text{A-5.56}$$

$$\tau' = X_3^2/h_3^2 \qquad \text{A-5.57}$$

The region $0 < q < d$ corresponds to the region $1 < \zeta' < \eta'$ and the region $d < q < 1$ corresponds to the region $1 < \zeta'' < \eta''$. If one designates $\lim_{H_2 \to O} T(q, t)$ as $y(\zeta', t)$ in $0 < q < d$ and $\lim_{H_2 \to O} T(q, t)$ as $z(\zeta'', t)$ in $d < q < 1$, then Equations A-5.49 and A-5.50 become identically Equations 2.39 and 2.40.

Thus Equations 2.39 and 2.40 result if the approximation can be made that

$$\sin H_2 (1-d) \beta = \sin \frac{H_2}{H_3} \frac{1-d}{d} \alpha \cong \frac{H_2}{H_3} \frac{1-d}{d} \alpha$$

A-5.58

In our problem typical values of the parameters are $X_1 - X_3 = 0.175$ cm, $X_2 - X_3 = 0.150$ cm, $H_2 = 0.127\ \text{sec}^{1/2}$ and $H_3 = 1.81\ \text{sec}^{1/2}$ so that $H_2(1-d)/H_3 d = 0.0117$. Therefore the approximation A-5.58 is valid for

$$\alpha < \frac{0.1}{0.01} = 10 \text{ radians}$$

Now the roots of Equation A-5.51 are tabulated by Carslaw and Jaeger (17). In particular, for $k_3/k_2 = 35.7$ the roots of

$$\alpha \cot \alpha + 0.168 = 0$$

are

$$\alpha_1 = 1.65$$
$$\alpha_2 = 4.75$$
$$\alpha_3 = 7.87$$
$$\alpha_4 = 11.0$$

so that it may be concluded that the approximate solution given in Chapter II is sufficiently precise.

Finally it is of interest to investigate the value for the time constant for damping out of the transient portion of the solution. It is clear from Equations A-5.49 and A-5.50 that this time constant may be written as follows:

$$\tau_1 = H_3^2 d^2/\alpha_1^2 \qquad \text{A-5.59}$$

whence

$$\tau_1 = \frac{1.81^2 \times 0.857^2}{1.65^2} = 0.89 \text{ sec.}$$

For the cylindrical problem* it is expected that this time constant would be given by

$$\tau_1 = \tau'/\beta_1^2 \qquad \text{A-5.60}$$

---

* Cf. Chapter II, Equations 2.30.

where β_1 is the first positive root of

$$J_o(\beta)\,Y_o(\eta'\beta) - Y_o(\beta)\,J_o(\eta'\beta) - \eta'\phi'\beta \ln \eta'' \; J_o(\beta)\,Y_1(\eta'\beta) - Y_o(\beta)J_1(\eta'\beta) = 0$$

A-5.61

For the typical values of the parameters given on page 16, which correspond to the values used above, it may be found that the values of β_n computed from Equation A-5.61 are:

$$\beta_1 = 5.34$$
$$\beta_2 = 15.74$$
$$\beta_3 = 26.20$$

etc., whence

$$\tau_1 = \tau'/\beta_1^2 = 26.6/(5.34)^2 = 0.94 \text{ sec.}$$

Thus the agreement between Equations A-5.59 and A-5.60 is excellent. It is thus concluded that as melting of the DTA sample is initiated the thermal conductance will increase from its value prior to melting to the steady state value within one or two seconds as shown schematically in Figure 2.2.

APPENDIX VI

COMPUTER PROGRAMS AND EXPERIMENTAL DATA

In this appendix the computer programs used in evaluating the experimental data are described, and the numerical values of the necessary parameters are reported.

Program Number DTA-19 for Direct Calculation of the Thermal Conductance

This calculation consists in finding the gas film thickness by a trial and error comparison of the theoretical and experimental time constants for exponential decay of the DTA curve until agreement within a specified error (one percent) is achieved. The conductance and latent heat are then found in a straightforward manner via Equations 3.2 through 3.5 and Equation 1.7 respectively. The variables used are defined below, and the MAD* listing of the program together with the data processed follow.

MAD Variable	Variable in Text	Explanation
AREA	$\int \lvert \theta - \theta_{ss} \rvert \, dt$	Area under DTA curve, $^{\circ}C$ min
A		Lower value of β in interval to be scanned
B		Upper value of β in interval to be scanned
CYCLE		Cycle of DTA run
D3	$2R_3$	Outside diameter of silica tube, cm
D4	$2R_4$	Outside diameter of sample, cm
D5	$2R_5$	Outside diameter of thermo-couple well, cm

* Michigan Algorithm Decoder, University of Michigan Computing Center, Ann Arbor, Michigan.

Variable Listing for Program DTA-19 (Cont'd)

MAD Variable	Variable in Text	Explanation
DELTA		Increment function for changing η''
DELX		Increment for changing β in scanning the interval, A to B
DP	D_p	Cf. Equation 2.58
EPS	ϵ	Cf. Equation 2.56
ERROR		Percent disagreement between TAUX and TAUC
ETAPP1		Initial estimate of η''
ETAPP	η''	R_1/R_2
ETAP	η'	R_2/R_3
ETA		R_3/R_4
G3	G_3	Thermal Conductance of the silica tube, cal/cm min ^oK
G4	G_4	Thermal Conductance of sample
GS2	G_2^*	Thermal Conductance of gas film
GS	G^*	Overall Thermal Conductance
I		Subscript of DELTA
JOX, etc.	$J_o(\beta)$, etc.	Bessel function of first kind
K3	k_3	Thermal conductivity of silica tube, cal/cm min ^oK
K4	k_4	Thermal conductivity of sample
KS2	k_2^*	Thermal conductivity of gas film
LF	L_f, L_t	Latent heat, cal/g
L	L	Sample height, cm
M	m	Sample mass, g
NUMBER		DTA sample number
NU	ν	Cf. Equation 2.48
PHIP	ϕ'	k_3/k_2
PHI	ϕ	k_4/k_3

Variable Listing for Program DTA-19 (Cont'd)

MAD Variable	Variable in Text	Explanation
R1		Maximum value of R
RHOCP3	$(\rho c_p)_3$	Specific heat of silica, cal/cc ^{o}K
RHOCP4	$(\rho c_p)_4$	Specific heat of sample, cal/cc ^{o}K
R		Running index
RUN		DTA run number
SAMPLE		DTA sample composition
T1	t_5	Cf. Equation 2.7
TAUC		Calculated value of τ_{exp}, min
TAUX	τ_{exp}	
TAUP	τ'	Cf. Equation 2.4
TAU	τ	Cf. Equation 2.3
TF	T	Absolute temperature, $^{o}K \times 10^{3}$
U	$\eta\beta$	
V	$\epsilon\beta$	
W	$\epsilon\eta'\beta$	
X	β	Cf. Equation 2.28
YOX, etc.	$Y_o(\beta)$, etc.	Bessel function of the second kind

```
          MAD LISTING FOR COMPUTER PROGRAM NUMBER DTA-19
$COMPILE MAD, EXECUTE, DUMP, PRINT OBJECT, PUNCH OBJECT          DTA19
            INTEGER N, J, I, K
            DIMENSION L(20) , DELTA(10)
            READ DATA
START       READ FORMAT INPUT, NUMBER, SAMPLE, RUN, CYCLE, D3, D4,
           1  D5, L, K4, RHOCP4, M, TF, TAUX, AREA
            PRINT COMMENT $1$
            PRINT FORMAT LABEL, NUMBER, SAMPLE, RUN, CYCLE
            KS2 = 0.00060 + 0.01085*TF - 0.00180*TF*TF
            K3 = 0.155 + 0.19*TF
            RHOCP3 = 0.58 + 0.13*TF
            PRINT COMMENT $0DATA$
            PRINT RESULTS D3, D4, D5, L, KS2, K3, K4, RHOCP3,
           1  RHOCP4, M, TF
            ETA = D4/D5
            ETAP = D3/D4
            PHI = K4/K3
            PHIP = K3/KS2
            TAU = D5*D5*RHOCP4/(4.*K4)
            TAUP = D4*D4*RHOCP3/(4.*K3)
            EPS = (TAUP/TAU).P.0.5
            T1 = RHOCP3*(D5*D5 - 0.16)/(8.*K4)
            NU = TAU/T1
            PRINT RESULTS ETA, ETAP, PHI, PHIP, TAU, TAUP, T1, NU
            C1 = EPS/(ETA*ETAP*PHI*PHIP)
            C4 = 1./(ETAP*PHIP)
            I = 1
            R = 1.
            ERROR = 2.*EPS3
```

PROGRAM DTA-19 (CONT.)

```
          THROUGH END,FOR ETAPP=ETAPP1,DELTA(I),.ABS.ERROR.LE.EPS3
          WHENEVER ETAPP .GE. 1.200
          PRINT COMMENT $0ETAPP HAS BECOME GREATER THAN 1.200$
          TRANSFER TO START
          END OF CONDITIONAL
          EXECUTE UITR2.(A,DELX,B,EPS1,EPS2,N,X)
OPEN      U = X*ETA
          V = X*EPS
          W = X*EPS*ETAP
          C2 = (EPS*EPS*ELOG.(ETAPP))/(ETA*PHI)
          C3 = EPS*ELOG.(ETAPP)
          L(1)=BSL1.(X,1,0,J0X,K)
          L(2)=BSL1.(X,1,1,J1X,K)
          DEL1 = X*J0X - NU*J1X
          L(3)=BSL1.(X,4,0,Y0X,K)
          L(4)=BSL1.(X,4,1,Y1X,K)
          DEL2 = X*Y0X - NU*Y1X
          L(5)=BSL1.(U,1,0,J0U,K)
          L(6)=BSL1.(U,1,1,J1U,K)
          L(7)=BSL1.(U,4,0,Y0U,K)
          L(8)=BSL1.(U,4,1,Y1U,K)
          L(9)=BSL1.(V,1,0,J0V,K)
          L(10)=BSL1.(V,1,1,J1V,K)
          L(11)=BSL1.(V,4,0,Y0V,K)
          L(12)=BSL1.(V,4,1,Y1V,K)
          L(13)=BSL1.(W,1,0,J0W,K)
          L(14)=BSL1.(W,1,1,J1W,K)
          L(15)=BSL1.(W,4,0,Y0W,K)
          L(16)=BSL1.(W,4,1,Y1W,K)
```

```
PROGRAM DTA-19 (CONT.)
 SUM = 0.
 THROUGH ALPHA, FOR J = 1, 1, J .G. 16
ALPHA  SUM = SUM + L(J)
 WHENEVER SUM .G. 16.5
 PRINT COMMENT $0LSUM IS GREATER THAN 16$
 PRINT RESULTS L(1)...L(16)
 TRANSFER TO START
 END OF CONDITIONAL
 DP1 = DEL1*Y0U - DEL2*J0U
 DP2 = DEL1*Y1U - DEL2*J1U
 DP3 = J1V*Y0W - Y1V*J0W
 DP4 = J1V*Y1W - Y1V*J1W
 DP5 = J0V*Y1W - Y0V*J1W
 DP6 = J0V*Y0W - Y0V*J0W
 DP = DP1*(C1*DP3 - X*C2*DP4) + DP2*(X*C3*DP5 - C4*DP6)
 I1 = UITR2A.(DP)
 WHENEVER I1 .L. 1.5, TRANSFER TO OPEN
 WHENEVER I1 .L. 2.5
 PRINT COMMENT $0THERE ARE NO ROOTS IN THIS INTERVAL$
 PRINT RESULTS A, B, I1
 TRANSFER TO END
 END OF CONDITIONAL
 TAUC = TAU/(X*X)
 ERROR = (TAUX - TAUC)/TAUX
 WHENEVER R/5. .G. R1
 PRINT COMMENT $0INTERMEDIATE VALUES$
 PRINT FORMAT OUTPUT, ETAPP, DELTA(I), DP, X, TAUC, ERROR
 R = 0.
 END OF CONDITIONAL
```

```
PROGRAM DTA-19 (CONT.)
      R = R + 1.
      WHENEVER ERROR .GE. 100.*EPS4
      I = 1
      TRANSFER TO END
      END OF CONDITIONAL
      WHENEVER ERROR .GE. 10.*EPS4
      I = 2
      TRANSFER TO END
      END OF CONDITIONAL
      WHENEVER ERROR .GE. EPS4
      I = 3
      TRANSFER TO END
      END OF CONDITIONAL
      I = 4
      WHENEVER ERROR .L. 0., I = 5
END   CONTINUE
      GS2 = 6.2832*KS2/ELOG.(ETAPP)
      G3 = 6.2832*K3/ELOG.(ETAP)
      G4 = 6.2832*K4/(1.-(ELOG.(ETA)/(ETAP - 1.)))
      GS = 1./((1./GS2) + (1./G3) + (1./G4))
      LF = GS*L*AREA/M
      PRINT COMMENT $0RESULTS$
      PRINT RESULTS X, I1
      PRINT RESULTS ETAPP, DELTA(I)
      PRINT RESULTS GS, LF
      TRANSFER TO START
      VECTOR VALUES INPUT = $I3,C6,C4,C6,10F6.3*$
      VECTOR VALUES LABEL = $S5,I3,S5,C6,S5,C4,S5,C6*$
```

```
          PROGRAM DTA-19 (CONT.)
           VECTOR VALUES OUTPUT = $S10, 9H ETAPP = F7.5,S10,
          1    9H DELTA = F7.5/S10, 6H DP = E10.5, S10, 5H X = F11.5/
          2    S10, 8H TAUC = F8.5, S10, 9H ERROR = F7.4*$
           END OF PROGRAM
$DATA
K=6, N=100, A=0.01, B=1.00, EPS1=1.E-5, EPS2=1.E-6, EPS3=0.01, EPS4=0.02,
   DELX = 0.10, ETAPP1 = 1.010, R1 = 0.9,
   DELTA(1) = 0.04, 0.02, 0.004, 0.002, -0.001    *
```

DATA CARD FORMAT FOR PROGRAM DTA-19

CODE	VARIABLE	COLUMNS ALLOTTED
I	NUMBER	1-3
II	SAMPLE	4-9
III	RUN	10-13
IV	CYCLE	14-19
V	D3	20-25
VI	D4	26-31
VII	D5	32-37
VIII	L	38-43
IX	K4	44-49
X	RHOCP4	50-55
XI	M	56-61
XII	TF	62-67
XIII	TAUX	68-73
XIV	AREA	74-80

DATA CARDS FOR MAD PROGRAM NO. DTA-19

STANDARDS AT THE MELTING POINT

I	II	III	IV	V	VI	VII	VIII	IX	X	XI	XII	XIII	XIV
93	AG	C-4	1C-N2	1.244	0.968	0.593	6.0	39.	0.58	28.80	1.226	0.690	93.9
93	AG	C-4	2H-N2	1.244	0.968	0.593	6.0	39.	0.63	28.80	1.247	0.620	93.0
97	AG	C-5	1C-N2	1.227	0.965	0.606	6.3	39.	0.58	28.80	1.229	0.679	96.6
97	AG	C-5	2H-N2	1.227	0.965	0.606	6.3	39.	0.63	28.80	1.237	0.631	93.5
115	AG	C-132	H-N2	1.303	0.992	0.605	5.9	39.	0.63	28.80	1.244	0.491	65.9
99	IN	C-123	H-N2	1.310	0.992	0.602	6.1	6.0	0.46	21.30	0.439	1.045	38.7
99	IN	C-122	C-N2	1.310	0.992	0.602	6.1	3.18	0.44	21.30	0.429	1.140	39.3
152	IN	C-32	1H-N2	1.290	0.980	0.590	6.6	6.0	0.46	21.3	0.432	1.40	58.848
152	IN	C-32	1C-N2	1.290	0.980	0.590	6.6	3.2	0.44	21.3	0.428	1.58	57.024
94	PB	C-3	1C-N2	1.252	0.978	0.585	6.15	4.2	0.36	32.40	0.592	1.170	51.8
94	PB	C-3	2H-N2	1.252	0.978	0.585	6.15	2.4	0.39	32.40	0.632	1.025	52.6
94	PB	C-3	4H-N2	1.252	0.978	0.585	6.15	2.4	0.39	32.40	0.607	1.075	49.8
91	SB	C-2	2C-N2	1.250	0.988	0.585	6.0	3.12	0.38	19.50	0.860	0.693	122.
91	SB	C-2	3H-N2	1.250	0.988	0.585	6.0	3.12	0.38	19.50	0.919	0.645	116.
92	TE	C-1	2H-N2	1.250	0.980	0.593	6.7	2.0	0.31	18.60	0.740	0.890	148.3
92	TE	C-1	2C-N2	1.250	0.980	0.593	6.7	0.54	0.31	18.60	0.672	1.050	160.7

COMPOUNDS AT THE MELTING POINT

148	AG	IN	SEC-273	H-N2	1.314	1.000	0.592	6.5	1.0	0.42	18.50	1.095	0.673	61.6
148	AG	IN	SEC-273	C-N2	1.314	1.000	0.592	6.5	1.0	0.42	18.50	1.075	0.893	66.6
149	AG	IN	SEC-291	C-N2	1.286	0.984	0.572	6.9	1.0	0.42	18.50	1.072	1.00	69.7
149	AG	IN	SEC-292	C-N2	1.286	0.984	0.572	6.9	1.0	0.42	18.50	1.072	0.714	55.2
149	AG	IN	SEC-293	H-N2	1.286	0.984	0.572	6.9	1.0	0.42	18.50	1.095	0.791	63.2
149	AG	IN	SEC-293	C-N2	1.286	0.984	0.572	6.9	1.0	0.42	18.50	1.072	1.14	66.9

COMPOUNDS DTA-19 (CONT.)

I	II	III	IV	V	VI	VII	VIII	IX	X	XI	XII	XIII	XIV
149	AGINSE	C-294	C-N2	1.286	0.984	0.572	6.9	1.0	0.42	18.50	1.072	1.008	61.3
113	AG2SE	C-111	C-N2	1.318	1.039	0.597	6.1	1.0	0.55	24.00	1.160	0.483	18.6
136	AG2SE	C-243	H-N2	1.306	1.020	0.610	6.4	1.0	0.55	24.00	1.173	0.473	16.7
136	AG2SE	C-243	C-N2	1.306	1.020	0.610	6.4	1.0	0.55	24.00	1.159	0.522	17.1
112	AG2TE	C-102	C-N2	1.290	0.998	0.578	6.5	1.0	0.46	25.50	1.225	0.302	13.2
135	AG2TE	C-283	C-N2	1.310	1.000	0.570	6.3	1.0	0.46	25.50	1.223	0.614	19.63
111	BI2SE3	C-9 3	C-N2	1.310	1.016	0.586	6.4	0.5	0.32	20.40	0.968	0.635	98.0
131	BI2SE3	C-221	C-N2	1.300	1.019	0.602	5.9	0.5	0.32	20.35	0.958	0.710	125.
131	BI2SE3	C-222	H-N2	1.300	1.019	0.602	5.9	0.5	0.32	20.35	0.991	0.740	109.
110	BI2TE3	C-9 2	C-N2	1.310	1.016	0.610	6.6	0.5	0.29	23.10	0.855	0.792	112.
130	BI2TE3	C-222	H-N2	1.303	0.993	0.616	6.1	0.5	0.29	23.10	0.868	0.580	106.6
130	BI2TE3	C-222	C-N2	1.303	0.993	0.616	6.1	0.5	0.29	23.10	0.852	0.730	110.
145	CDSE	C-251	C-N2	1.280	0.994	0.600	7.1	1.0	0.37	17.50	1.511	0.421	60.7
145	CDSE	C-252	H-N2	1.280	0.994	0.600	7.1	1.0	0.37	17.50	1.535	0.315	58.8
104	CDTE	C-102	H-N2	1.315	1.010	0.585	6.7	1.0	0.32	18.60	1.378	0.318	62.1
129	GAAS	C-191	C-N2	1.294	1.010	0.598	6.1	1.08	0.46	16.50	1.503	0.295	164.
102	GASB	C-6 2	H-N2	1.282	1.013	0.606	6.4	0.78	0.41	17.40	1.001	0.625	194.5
102	GASB	C-6 2	C-N2	1.282	1.013	0.606	6.4	0.78	0.41	17.40	0.977	0.576	186.
128	GASB	C-192	C-N2	1.309	0.990	0.597	6.2	0.78	0.41	17.40	0.976	0.602	187.5
101	INAS	C-7 2	H-N2	1.302	1.033	0.606	6.4	1.20	0.37	17.70	1.225	0.396	145.6
127	INAS	C-181	C-N2	1.280	0.983	0.597	7.0	1.20	0.37	17.70	1.198	0.435	124.0
127	INAS	C-182	H-N2	1.280	0.983	0.597	7.0	1.20	0.37	17.70	1.223	0.455	151.0
100	INSB	C-6 2	C-N2	1.255	0.985	0.606	6.4	1.08	0.30	18.30	0.786	0.852	184.
126	INSB	C-182	C-N2	1.314	0.989	0.595	6.2	1.08	0.30	18.30	0.786	0.717	149.2
119	IN2SE3	C-143	H-N2	1.318	0.990	0.593	6.8	0.5	0.39	17.10	1.167	0.639	57.6
119	IN2SE3	C-143	C-N2	1.318	0.990	0.593	6.8	0.5	0.39	17.10	1.148	0.694	61.1

COMPOUNDS DTA-19 (CONT.)

I	II	III	IV	V	VI	VII	VIII	IX	X	XI	XII	XIII	XIV
142	INTE	C-172	H-N2	1.275	1.022	0.615	6.7	0.50	0.32	18.90	0.977	0.600	69.0
118	IN2TE	3C-212	C-N2	1.303	0.991	0.615	6.5	0.50	0.29	17.40	0.930	1.220	72.2
118	IN2TE	3C-213	H-N2	1.303	0.991	0.615	6.5	0.50	0.29	17.40	0.955	0.762	70.7
139	IN2TE	3C-261	C-N2	1.289	1.013	0.607	6.6	0.50	0.29	17.40	0.930	1.175	80.6
106	PBSE	C-8 1	C-N2	1.285	1.013	0.606	6.6	0.40	0.33	24.30	1.353	0.352	54.7
106	PBSE	C-8 2	H-N2	1.285	1.013	0.606	6.6	0.40	0.33	24.30	1.363	0.338	54.1
133	PBSE	C-232	C-N2	1.275	0.997	0.597	6.8	0.40	0.33	24.30	1.347	0.447	56.5
105	PBTE	C-8 3	H-N2	1.278	1.005	0.606	6.5	0.40	0.39	24.60	1.213	0.440	65.6
132	PBTE	C-231	C-N2	1.312	1.010	0.612	6.8	0.40	0.39	24.60	1.189	0.575	59.4
132	PBTE	C-232	H-N2	1.312	1.010	0.612	6.8	0.40	0.39	24.60	1.204	0.409	58.5
117	SB2SE	3C-153	H-N2	1.289	1.021	0.602	6.5	0.5	0.41	19.20	0.897	0.823	106.3
117	SB2SE	3C-153	C-N2	1.289	1.021	0.602	6.5	0.5	0.41	19.20	0.861	0.714	98.5
138	SB2SE	3C-241	C-N2	1.291	1.026	0.600	7.1	0.5	0.41	19.20	0.833	0.851	88.6
138	SB2SE	3C-242	H-N2	1.291	1.026	0.600	7.1	0.5	0.41	19.20	0.903	0.936	97.7
116	SB2TE	3C-141	C-N2	1.300	1.016	0.600	6.6	0.5	0.32	19.80	0.884	0.82	115.2
137	SB2TE	3C-171	C-N2	1.276	1.044	0.602	6.6	0.5	0.32	19.80	0.881	0.741	126.0
137	SB2TE	3C-172	H-N2	1.276	1.044	0.602	6.6	0.5	0.32	19.80	0.903	0.740	114.5
103	SNTE	C-7 3	H-N2	1.292	1.025	0.607	6.0	1.0	0.29	19.50	1.100	0.527	76.0
141	SNTE	C-162	H-N2	1.276	0.983	0.591	6.7	1.0	0.29	19.50	1.083	0.514	72.0

COMPOUNDS AT THE TRANSITION POINT

148	AGINSE	C-27T3	H-N2	1.314	1.000	0.592	6.5	0.40	0.42	18.50	1.025	0.624	10.2
148	AGINSE	C-27T3	C-N2	1.314	1.000	0.592	6.5	0.40	0.42	18.50	1.010	1.42	9.08
149	AGINSE	C-29T1	C-N2	1.286	0.984	0.572	6.9	0.40	0.42	18.50	1.010	2.85	11.85
149	AGINSE	C-29T2	C-N2	1.286	0.984	0.572	6.9	0.40	0.42	18.50	1.010	1.474	7.77

TRANSITIONS DTA-19 (CONT.)

I	II	III	IV	V	VI	VII	VIII	IX	X	XI	XII	XIII	XIV
149AGINSEC-29T3H-N21.286				0.984	0.572	6.9		0.40	0.42	18.50	1.025	0.736	14.06
149AGINSEC-29T3C-N21.286				0.984	0.572	6.9		0.40	0.42	18.50	1.010	1.404	9.77
149AGINSEC-29T4C-N21.286				0.984	0.572	6.9		0.40	0.42	18.50	1.010	1.663	6.57
113AG2SE C-11T1C-N21.318				1.039	0.597	6.1		0.20	0.55	24.00	0.396	1.85	72.6
113AG2SE C-11T2H-N21.318				1.039	0.597	6.1		0.20	0.55	24.00	0.427	1.85	72.3
136AG2SE C-24T2H-N21.306				1.020	0.610	6.4		0.20	0.55	24.00	0.436	1.825	56.3
112AG2TE C-10T2C-N21.290				0.998	0.578	6.5		0.20	0.46	25.50	0.410	3.00	50.0
135AG2TE C-28T4H-N21.310				1.000	0.570	6.3		0.20	0.46	25.50	0.447	1.43	60.6
135AG2TE C-28T4C-N21.310				1.000	0.570	6.3		0.20	0.46	25.50	0.407	2.80	59.6
112AG2TE C-10T1C-N21.290				0.998	0.578	6.5		0.40	0.46	25.50	1.605	0.485	1.66
112AG2TE C-10T2H-N21.290				0.998	0.578	6.5		0.40	0.46	25.50	1.075	0.543	1.58
135AG2TE C-28T2H-N21.310				1.000	0.570	6.3		0.40	0.46	25.50	1.081	0.547	2.14
135AG2TE C-28T2C-N21.310				1.000	0.570	6.3		0.40	0.46	25.50	1.065	0.529	2.12
119IN2SE3C-14T3H-N21.318				0.990	0.593	6.8		0.20	0.57	17.10	0.483	1.42	10.1

Program Number DTA-16 for Direct Calculation of the Thermal Conductance

In this method a double trial and error calculation is required because a value of G is needed in order to compute the gas film thickness from two measurements of the area under the DTA curve obtained when two gases of widely different thermal conductivity alternately fill the system. The definitions of the variables which are different from those used for Program DTA-19 are tabulated below, and the MAD listing of the computer program follows.

MAD Variable	Variable in Text	Explanation
A	a	Cf. Equation 2.61
ALPHA	α	Cf. Equation 3.9
B	b	Cf. Equation 2.61
BETA	β	Cf. Equation 3.8
CHECK		Function for choosing C to insure convergence
C		Function for incrementing LF
D1	$2R_1$	Units are cm
DELTAD	$2(R_1-R_2)$	Units are cm
E1	ϵ_1	Emissivity of nickel oxide
E3	ϵ_3	Equivalent emissivity of silica
E4	ϵ_4	Emissivity of sample
EPSLN		Desired limiting value of ERROR
ERROR		Percent difference between calculated and assumed values of LF
F5, F6	F_5, F_6	Shape factors, Equations 2.62, 2.63
F, FS		Multiplicative factors for correcting k_2 and k_2^*
G, GS	G, G^*	Overall conductances with helium and nitrogen, cal/cm min ^oK

Variable Listing for Program DTA-16 (Cont'd)

MAD Variable	Variable in Text	Explanation
I, IS		Area under DTA curve with helium and nitrogen, ^{o}C min
JMAX		Maximum value of J
J		Variable subscript of F and FS
K		Variable subscript of C
K2, KS2	k_2, k_2^*	Thermal conductivity of helium and nitrogen, cal/cm min ^{o}K
LF0		Initial estimate of LF
NMAX		Maximum value of N
N		Variable subscript of XI
SMAX		Maximum value of S
S		Running index, subscript of LF
XI		Arbitrary parameter, normally unity
ZETA2	$1/\ln \eta''$	

MAD LISTING FOR COMPUTER PROGRAM NUMBER DTA-16

```
$COMPILE MAD, EXECUTE, DUMP, PRINT OBJECT, PUNCH OBJECT          DTA-16
         INTEGER  S, J, JMAX, N, NMAX, NUMBER, SAMPLE, RUN, CYCLE
         INTEGER SMAX, K
         DIMENSION XI(20), F(10), FS(10), LF(750), C(10), ERROR(750)
         READ DATA
START    READ DATA
         PRINT COMMENT $1$
         PRINT FORMAT LABEL, NUMBER, SAMPLE, RUN, CYCLE
         PRINT COMMENT $0$
         K2 = 0.01163 + 0.03625*TF - 0.00278*TF*TF
         KS2 = 0.00060 + 0.01085*TF - 0.00180*TF*TF
         K3 = 0.155 + 0.19*TF
         E1 = 0.143 + 0.48*TF
         WHENEVER TF .LE. 0.39/0.93
         E3 = 1.
         OTHERWISE
         E3 = EXP.(-(TF.P.0.5)*((0.93*TF) - 0.39))
         END OF CONDITIONAL
         PRINT COMMENT $0DATA$
         PRINT RESULTS D3,D4,D5,K2,KS2,K3,K4,E1,E3,E4,TF,I,IS,M,LF0,L
         G3 = 6.2832*K3/ELOG.(D3/D4)
         G4 = 6.2832*K4/(1.-(ELOG.(D4/D5)/((D4/D5) - 1.)))
         A=D3/D1
         B=D4/D1
         F5 = E3*(A-B*E4)/(1.0+A*E3*((1.0/E1)-1.0))
         F6 = B*E4/(1.0+(A*E3+B*E4)*((1.0/E1)-1.0))
         G5 = 1.021*D1*(TF.P.3)*F5
         G6 = 1.021*D1*(TF.P.3)*F6
```

```
PROGRAM DTA-16 (CONT.)
 ALPHA=(G5+G6+G5*G6/G3)/(1.0+(G5/G3)+((G5+G6)/G4)+(G5*G6/(G3
1 *G4)))
 BETA=1.0/((1.0+(G5/G3)+((G5+G6)/G4)+(G5*G6/(G3*G4))))
 THROUGH ENDJ, FOR J= 1, 1, J .G. JMAX
 PRINT COMMENT $0$
 PRINT COMMENT $0$
 PRINT COMMENT $0    THE VALUES OF F ARE$
 PRINT RESULTS F(J), FS(J)
 PRINT COMMENT $0$
 THROUGH ENDN, FOR N = 1, 1, N .G. NMAX
 PRINT COMMENT $0$
 PRINT COMMENT $0      THE VALUE OF XI IS$
 PRINT RESULTS XI(N)
 PRINT COMMENT $0        RESULTS$
 K = 1
 R = 1.
 S = 1
 LF(S) = LF0
IN
 G = M*LF(S)/(I*L)
 GS = M*LF(S)/(IS*L)
 G = G/XI(N)
 GS = GS/XI(N)
 ZETA2=(1./(6.2832*(BETA.P.2 )))*
1 ((1./(FS(J)*KS2)) - (1./(F(J)*K2)))*
2((G-ALPHA)*(GS-ALPHA)/(G-GS))
 WHENEVER ZETA2 .LE. 1.442
 PRINT COMMENT $0        ETA2 IS LARGER THAN 2.000$
 PRINT RESULTS ZETA2, LF(S)
```

```
PROGRAM DTA-16 (CONT.)
 TRANSFER TO ENDN
 END OF CONDITIONAL
 WHENEVER ZETA2 .GE. 200.
 PRINT COMMENT $0        ETA2 IS SMALLER THAN 1.005$
 PRINT RESULTS ZETA2, LF(S)
 TRANSFER TO ENDN
 END OF CONDITIONAL
 ETA2 = EXP.(1./ZETA2)
 DELTAD = D3*(ETA2 - 1.)
 D2=D3+DELTAD
 G2 = F(J)*6.2832*K2/ELOG.(D2/D3)
 GS2 = FS(J)*6.2832*KS2/ELOG.(D2/D3)
 G=(G6+(G2+G5)*(1.0+G6/G3))/(1.0+(G2+G5)*((1.0/G4)+(1.0/G3)+
1(G6/(G3*G4))))
 GS=(G6+(GS2+G5)*(1.0+G6/G3))/(1.0+(GS2+G5)*((1.0/G4)+
1(1./G3)+(G6/(G3*G4))))
 G = G*XI(N)
 GS = GS*XI(N)
 ERROR(S) = 1.0 - G*L*I/(M*LF(S))
 WHENEVER S .GE. 10
 CHECK = .ABS. ERROR(10)- .ABS. ERROR(5)
 OTHERWISE
 CHECK = - 0.5
 END OF CONDITIONAL
 WHENEVER R .G. R1
 PRINT COMMENT $0          INTERMEDIATE VALUES$
 PRINT RESULTS LF(S), C(K), DELTAD, ERROR(S)
 R = 0.
 END OF CONDITIONAL
```

PROGRAM DTA-16 (CONT.)

```
          R = R + 1.
          WHENEVER .ABS. ERROR(S) .L. EPSLN/100.
          PRINT COMMENT $0          FINAL VALUES$
          PRINT RESULTS F5, F6
          PRINT RESULTS G, GS
          PRINT RESULTS DELTAD, LF(S)
          TRANSFER TO ENDN
          OTHERWISE
          WHENEVER S .G. SMAX - 1
          PRINT COMMENT $0        SMAX HAS BEEN EXCEEDED$
          PRINT RESULTS LF(S), C(K), DELTAD, ERROR(S)
          TRANSFER TO ENDN
          END OF CONDITIONAL
          WHENEVER ERROR(S) .L. 0., TRANSFER TO OPEN
          WHENEVER ERROR(S) .GE. EPSLN
          K = 1
          OTHERWISE
          WHENEVER ERROR(S) .GE. EPSLN/10.
          K = 2
          OTHERWISE
          WHENEVER ERROR(S) .GE. EPSLN/100., K=3
          END OF CONDITIONAL
          END OF CONDITIONAL
          WHENEVER CHECK .G. 0., TRANSFER TO ENTR2
ENTR1     S = S + 1
          LF(S) = (1. - C(K))*LF(S-1)
          TRANSFER TO IN
OPEN      WHENEVER ERROR(S) .LE. -EPSLN
```

```
          PROGRAM DTA-16 (CONT.)

           K = 1
           OTHERWISE
           WHENEVER ERROR(S) .LE. -EPSLN/10.
           K = 2
           OTHERWISE
           WHENEVER ERROR(S) .LE. -EPSLN/100., K=3
           END OF CONDITIONAL
           END OF CONDITIONAL
           WHENEVER CHECK .G. 0., TRANSFER TO ENTR1
ENTR2      S = S + 1
           LF(S) = (1. + C(K))*LF(S-1)
           TRANSFER TO IN
           END OF CONDITIONAL
ENDN       CONTINUE
ENDJ       CONTINUE
           TRANSFER TO START
           VECTOR VALUES LABEL = $S5,I3,S5,C6,S5,C4,S5,C6*$
           END OF PROGRAM
$DATA
D1 = 1.37, JMAX = 1, NMAX = 1, F(1) = .8, FS(1) = 1., C(1)=.08,.02,.005,
   XI(1) = 1.,     SMAX = 750, R1 =19., EPSLN = 1.    *
D3 = 1.290, D4 = 0.980, D5 = 0.590, K4 = 6.0, E4 = 0.10, TF = 0.432,
   I = 18.048, IS = 58.848, M = 21.3, LF0 = 6.8, L = 6.6,
   RUN = $C-32$, NUMBER = 152, CYCLE = $HEATNG$, SAMPLE = $IN$    *
```

Program Number DTA-17 for Analysis of DTA Data

This short program was devised in order to facilitate the processing of the experimental data according to the method whereby the conductance is estimated from the experimental time constant plus the estimated thermal capacity. It was designed so that either the data on standards could be used for computing the correlation factor Z, or the latent heat could be computed from the data on compounds using a specified value of Z. The definitions of the MAD variables are listed below, and the computer programs plus the experimental data follow.

MAD Variable	Variable in Text	Explanation
AREA	$\int \lvert \theta - \theta_{ss} \rvert \, dt$	Area under DTA curve, $^{\circ}C$ min
C	C	"Correct" thermal capacity, cal/$^{\circ}C$
CEST	C'	Estimated thermal capacity, cal/$^{\circ}C$
CP	$c_{p,4}$	Specific heat of sample, cal/g $^{\circ}C$
CPQ	$c_{p,3}$	Specific heat of silica, cal/g $^{\circ}C$
INDEX		Variable subscript; INDEX = 1 refers to data on compounds for series B; 2- compounds, series C; 4- standards, series B; 5- standards, series C
MQCONT		Mass of silica in contact with the sample, g
TAU	τ_{exp}	Units are min
TF	T	Temperature, $^{\circ}K \times 10^{3}$
VQCONT		Volume of silica in contact with the sample, cc
Z		Correlation factor, C/C'

The remaining symbols used in this program have already been defined.

```
            MAD LISTING FOR COMPUTER PROGRAM NUMBER DTA-17
$COMPILE MAD, EXECUTE, DUMP, PRINT OBJECT, PUNCH OBJECT          DTA17
            INTEGER INDEX, NUMBER
            DIMENSION Z(10), L(10)
            PRINT COMMENT $1$
            READ DATA
START       READ FORMAT INPUT,  INDEX, NUMBER, SAMPLE, RUN, CYCLE,
           1  D3, D4, D5, L, M, CP, LF, TF, TAU, AREA
            PRINT COMMENT$4$
            PRINT FORMAT LABEL, NUMBER, SAMPLE, RUN, CYCLE
            CPQ = 0.223 + 0.0613*TF - 0.00575/(TF*TF)
            PRINT COMMENT $0DATA$
            PRINT RESULTS D3, D4, D5, L, M, CP, CPQ, TF
            PRINT RESULTS TAU, AREA
            VQCONT = 0.785*(L*(D3*D3 - D4*D4) + L(INDEX)*(D5*D5 - 0.10))
           1   + 0.03
            MQCONT = 2.20*VQCONT
            CEST = MQCONT*CPQ + M*CP
            WHENEVER INDEX .L. 3, TRANSFER TO OVER
            C = M*LF*TAU/AREA
            Z(INDEX) = C/CEST
            PRINT COMMENT $0RESULTS$
            PRINT RESULTS LF, MQCONT, Z(INDEX)
            TRANSFER TO START
```

PROGRAM DTA-17 (CONT.)

```
OVER    C = CEST*Z(INDEX)
        LF = C*AREA/(M*TAU)
        PRINT COMMENT $0RESULTS$
        PRINT RESULTS Z(INDEX), MQCONT, LF
        TRANSFER TO START
        VECTOR VALUES INPUT = $I1,I3,C6,C4,C5,4,5,3,6F6.4*$
        VECTOR VALUES LABEL = $S5,I3,S5,C6,S5,C4,S5,C6*$
        END OF PROGRAM
$DATA
      Z(1) = 1.300, 1.115, L(1) = 2.54, 6.0, L(4) = 2.54, 6.0  *
```

DATA CARD FORMAT FOR PROGRAM DTA-17

CODE	VARIABLE	COLUMNS ALLOTTED
I	INDEX	1
II	NUMBER	2-4
III	SAMPLE	5-10
IV	RUN	11-14
V	CYCLE	15-20
VI	D3	21-25
VII	D4	26-30
VIII	D5	31-35
IX	I	36-40
X	M	41-46
XI	CP	47-52
XII	LF	53-58
XIII	TF	59-64
XIV	TAU	65-70
XV	AREA	71-76

DATA CARDS FOR PROGRAM DTA-17
STANDARDS AT THE MELTING POINT

I	II	III	IV	V	VI	VII	VIII	IX	X	XI	XII	XIII	XIV	XV
4	40	AG	B-141C-HE	1.35	1.18	0.59	3.6	31.53	0.0707	25.0	1.229	0.269	51.7	
4	40	AG	B-142H-HE	1.35	1.18	0.59	3.6	31.53	0.0677	25.0	1.236	0.260	50.6	
4	40	AG	B-142C-N2	1.35	1.18	0.59	3.6	31.53	0.0707	25.0	1.227	0.544	96.1	
4	46	AG	B-181C-HE	1.356	1.193	0.59	3.7	31.50	0.0707	25.0	1.226	0.345	61.0	
4	46	AG	B-182H-HE	1.356	1.193	0.59	3.7	31.50	0.0677	25.0	1.234	0.344	62.7	
4	46	AG	B-182C-N2	1.356	1.193	0.59	3.7	31.50	0.0707	25.0	1.216	0.725	122.0	
5	93	AG	C-4 1C-N2	1.244	0.968	0.593	6.0	28.80	0.0707	25.0	1.226	0.690	93.9	
5	93	AG	C-4 2H-N2	1.244	0.968	0.593	6.0	28.80	0.0677	25.0	1.247	0.620	93.0	
5	93	AG	C-4 2C-HE	1.244	0.968	0.593	6.0	28.80	0.0707	25.0	1.225	0.363	51.4	
5	93	AG	C-4 3H-HE	1.244	0.968	0.593	6.0	28.80	0.0677	25.0	1.253	0.364	49.7	
5	97	AG	C-5 1C-N2	1.227	0.965	0.606	6.3	28.80	0.0707	25.0	1.229	0.679	96.6	
5	97	AG	C-5 2H-N2	1.227	0.965	0.606	6.3	28.80	0.0677	25.0	1.237	0.631	93.5	
5	97	AG	C-5 3C-HE	1.227	0.965	0.606	6.3	28.80	0.0707	25.0	1.229	0.372	50.9	
5	97	AG	C-5 3H-HE	1.227	0.965	0.606	6.3	28.80	0.0677	25.0	1.237	0.366	53.5	
5	115	AG	C-132H-N2	1.303	0.992	0.605	5.9	28.80	0.0677	25.0	1.244	0.491	65.9	
5	115	AG	C-133H-HE	1.303	0.992	0.605	5.9	28.80	0.0677	25.0	1.238	0.310	42.7	
4	9	CU	B-1 1C-HE	1.34	1.18	0.59	3.9	26.88	0.115	48.7	1.351	0.322	76.5	
4	9	CU	B-1 2H-HE	1.34	1.18	0.59	3.9	26.88	0.118	48.7	1.359	0.309	84.0	
4	9	CU	B-1 2C-HE	1.34	1.18	0.59	3.9	26.88	0.115	48.7	1.350	0.349	80.0	
4	26	CU	B-141C-N2	1.35	1.18	0.59	4.0	26.88	0.115	48.7	1.346	0.640	138.	
4	26	CU	B-142H-HE	1.35	1.18	0.59	4.0	26.88	0.118	48.7	1.362	0.345	81.5	
4	26	CU	B-142C-HE	1.35	1.18	0.59	4.0	26.88	0.115	48.7	1.348	0.336	75.0	
4	45	CU	B-181C-N2	1.352	1.173	0.59	3.8	26.88	0.115	48.7	1.346	0.691	134.	
4	45	CU	B-182H-HE	1.352	1.173	0.59	3.8	26.88	0.118	48.7	1.359	0.382	86.6	

STANDARDS DTA-17 (CONT.)

I	II	III	IV	V	VI	VII	VIII	IX	X	XI	XII	XIII	XIV	XV
4	45	CU	B-182C-N2	1.352	1.173	0.59	3.8	26.88	0.115	48.7	1.348	0.368	82.9
4	61	CU	B-241C-N2	1.35	1.175	0.59	3.75	26.88	0.115	48.7	1.345	0.752	160.
4	61	CU	B-242H-N2	1.35	1.175	0.59	3.75	26.88	0.118	48.7	1.363	0.736	163.
4	61	CU	B-242C-HE	1.35	1.175	0.59	3.75	26.88	0.115	48.7	1.333	0.411	88.7
4	61	CU	B-243H-HE	1.35	1.175	0.59	3.75	26.88	0.118	48.7	1.365	0.400	90.5
4	61	CU	B-243C-HE	1.35	1.175	0.59	3.75	26.88	0.115	48.7	1.332	0.415	89.6
4	6	IN	B-1 1H-HE	1.34	1.17	0.59	3.5	21.93	0.0677	6.8	0.437	0.28	16.6
4	6	IN	B-1 1C-HE	1.34	1.17	0.59	3.5	21.93	0.0599	6.8	0.428	0.265	15.3
4	6	IN	B-1 2H-HE	1.34	1.17	0.59	3.5	21.93	0.0677	6.8	0.434	0.28	16.1
4	30	IN	B-9 2H-HE	1.32	1.14	0.59	3.7	21.93	0.0677	6.8	0.436	0.345	20.6
4	30	IN	B-9 2C-HE	1.32	1.14	0.59	3.7	21.93	0.0599	6.8	0.429	0.355	19.9
4	30	IN	B-9 3H-HE	1.32	1.14	0.59	3.7	21.93	0.0677	6.8	0.436	0.345	19.6
4	30	IN	B-9 4H-HE	1.32	1.14	0.59	3.7	21.93	0.0677	6.8	0.446	0.321	18.0
4	30	IN	B-9 4C-HE	1.32	1.14	0.59	3.7	21.93	0.0599	6.8	0.429	0.341	18.0
4	30	IN	B-9 5H-HE	1.32	1.14	0.59	3.7	21.93	0.0677	6.8	0.433	0.311	18.1
4	30	IN	B-9 6H-A	1.32	1.14	0.59	3.7	21.93	0.0677	6.8	0.441	0.942	48.9
4	30	IN	B-9 6C-A	1.32	1.14	0.59	3.7	21.93	0.0599	6.8	0.428	0.992	49.7
4	30	IN	B-101H-A	1.32	1.14	0.59	3.7	21.93	0.0677	6.8	0.437	0.635	31.0
4	30	IN	B-101C-A	1.32	1.14	0.59	3.7	21.93	0.0599	6.8	0.428	0.700	31.8
4	30	IN	B-102H-HE	1.32	1.14	0.59	3.7	21.93	0.0677	6.8	0.433	0.265	13.5
4	30	IN	B-103H-HE	1.32	1.14	0.59	3.7	21.93	0.0677	6.8	0.433	0.246	12.9
4	30	IN	B-9 1C-HE	1.32	1.14	0.59	3.7	21.93	0.0599	6.8	0.429	0.362	19.5
4	41	IN	B-191C-N2	1.36	1.18	0.59	3.7	21.93	0.0599	6.8	0.429	0.831	37.9
4	41	IN	B-192H-N2	1.36	1.18	0.59	3.7	21.93	0.0677	6.8	0.434	0.819	36.9
4	41	IN	B-192C-N2	1.36	1.18	0.59	3.7	21.93	0.0599	6.8	0.430	0.287	14.6
4	41	IN	B-193H-N2	1.36	1.18	0.59	3.7	21.93	0.0677	6.8	0.439	0.255	13.7

STANDARDS DTA-17 (CONT.)

I	II	III	IV	V	VI	VII	VIII	IX	X	XI	XII	XIII	XIV	XV
5	99	IN	C-121C-HE	1.3100.	9920.	6026.	1		21.30	0.0599	6.8	0.427	0.560	20.4
5	99	IN	C-122H-HE	1.3100.	9920.	6026.	1		21.30	0.0677	6.8	0.434	0.517	19.6
5	99	IN	C-122C-N2	1.3100.	9920.	6026.	1		21.30	0.0599	6.8	0.429	1.140	39.3
5	99	IN	C-123H-N2	1.3100.	9920.	6026.	1		21.30	0.0677	6.8	0.439	1.045	38.7
4	22	PB	B-101C-HE	1.3181.	14	0.59	3.7		34.02	0.03405	.89	0.596	0.219	14.7
4	22	PB	B-102H-HE	1.3181.	14	0.59	3.7		34.02	0.0365	5.89	0.602	0.208	14.2
4	22	PB	B-102C-HE	1.3181.	14	0.59	3.7		34.02	0.0340	5.89	0.595	0.225	14.4
4	53	PB	B-231C-N2	1.3261.	1750.	59	3.7		34.02	0.0340	5.89	0.597	0.845	49.0
4	53	PB	B-232H-N2	1.3261.	1750.	59	3.7		34.02	0.0365	5.89	0.607	0.836	49.2
4	53	PB	B-233H-HE	1.3261.	1750.	59	3.7		34.02	0.0365	5.89	0.605	0.290	21.2
4	53	PB	B-233C-HE	1.3261.	1750.	59	3.7		34.02	0.0340	5.89	0.597	0.300	21.9
4	53	PB	B-234H-HE	1.3261.	1750.	59	3.7		34.02	0.0365	5.89	0.608	0.288	22.5
5	94	PB	C-3 1C-N2	1.2520.	9780.	5856.	15		32.40	0.0340	5.89	0.592	1.17	51.8
5	94	PB	C-3 2H-N2	1.2520.	9780.	5856.	15		32.40	0.0365	5.89	0.632	1.025	52.6
5	94	PB	C-3 2C-HE	1.2520.	9780.	5856.	15		32.40	0.0340	5.89	0.595	0.46	21.0
5	94	PB	C-3 3H-HE	1.2520.	9780.	5856.	15		32.40	0.0365	5.89	0.608	0.423	21.4
5	94	PB	C-3 4H-N2	1.2520.	9780.	5856.	15		32.40	0.0365	5.89	0.607	1.075	49.8
4	23	SB	B-8 2H-HE	1.35	1.18	0.59	3.5		19.04	0.0616	39.0	0.908	0.230	61.5
4	23	SB	B-8 3H-HE	1.35	1.18	0.59	3.5		19.04	0.0616	39.0	0.908	0.232	62.5
4	29	SB	B-112H-N2	1.3451.	17	0.59	3.5		19.04	0.0616	39.0	0.911	0.404	111.
4	37	SB	B-151C-N2	1.3501.	16	0.59	3.5		19.04	0.0586	39.0	0.861	0.594	140.
4	37	SB	B-152H-HE	1.3501.	16	0.59	3.5		19.04	0.0616	39.0	0.910	0.244	68.1
4	37	SB	B-152C-HE	1.3501.	16	0.59	3.5		19.04	0.0586	39.0	0.864	0.262	65.5
5	91	SB	C-2 1C-HE	1.2500.	9880.	5856.	0		19.50	0.0586	39.0	0.854	0.382	69.4
5	91	SB	C-2 2H-HE	1.2500.	9880.	5856.	0		19.50	0.0616	39.0	0.909	0.395	66.0
5	91	SB	C-2 2C-N2	1.2500.	9880.	5856.	0		19.50	0.0586	39.0	0.860	0.693	122.

STANDARDS DTA-17 (CONT.)

I	II	III	IV	V	VI	VII	VIII	IX	X	XI	XII	XIII	XIV	XV
5	91	SB	C-2	3H-N2	1.2500	.9880	.5856	.0	19.50	0.0616	39.0	0.919	0.645	116.
4	13	TE	B-3	2H-HE	1.33	1.17	0.59	3.7	18.72	0.0705	32.7	0.727	0.252	62.2
4	13	TE	B-3	3H-HE	1.33	1.17	0.59	3.7	18.72	0.0705	32.7	0.727	0.251	61.7
4	25	TE	B-11	2H-N2	1.32	1.14	0.59	3.9	18.72	0.0705	32.7	0.732	0.574	103.
4	25	TE	B-11	3H-HE	1.32	1.14	0.59	3.9	18.72	0.0705	32.7	0.726	0.245	57.1
4	25	TE	B-11	4H-HE	1.32	1.14	0.59	3.9	18.72	0.0705	32.7	0.731	0.254	56.0
4	48	TE	B-19	1C-N2	1.3441	.1740	.59	4.1	18.72	0.0658	32.7	0.659	0.897	185.5
4	48	TE	B-19	2H-N2	1.3441	.1740	.59	4.1	18.72	0.0705	32.7	0.736	0.850	167.
4	48	TE	B-19	2C-HE	1.3441	.1740	.59	4.1	18.72	0.0658	32.7	0.664	0.459	92.2
4	48	TE	B-19	3H-HE	1.3441	.1740	.59	4.1	18.72	0.0705	32.7	0.731	0.356	79.5
5	92	TE	C-1	2H-N2	1.2500	.9800	.593	6.7	18.60	0.0705	32.7	0.740	0.890	148.3
5	92	TE	C-1	2C-N2	1.2500	.9800	.593	6.7	18.60	0.0658	32.7	0.672	1.050	160.7
5	92	TE	C-1	3H-HE	1.2500	.9800	.593	6.7	18.60	0.0705	32.7	0.731	0.464	77.7
5	92	TE	C-1	3C-HE	1.2500	.9800	.593	6.7	18.60	0.0658	32.7	0.752	0.503	82.0

COMPOUNDS AT THE MELTING POINT

2148AGINSEC-271C-HE	1.3141	.0000	.592	6.5	18.50	0.0596	1.	1.069	0.695	55.7
2148AGINSEC-272H-HE	1.3141	.0000	.592	6.5	18.50	0.0596	1.	1.095	0.603	49.8
2148AGINSEC-272C-HE	1.3141	.0000	.592	6.5	18.50	0.0596	1.	1.071	0.660	55.5
2148AGINSEC-273H-N2	1.3141	.0000	.592	6.5	18.50	0.0596	1.	1.095	0.673	61.6
2148AGINSEC-273C-N2	1.3141	.0000	.592	6.5	18.50	0.0596	1.	1.075	0.893	66.6
2149AGINSEC-291C-N2	1.2860	.9840	.572	6.9	18.50	0.0596	1.	1.072	1.00	69.7
2149AGINSEC-292H-HE	1.2860	.9840	.572	6.9	18.50	0.0596	1.	1.095	0.714	64.8
2149AGINSEC-292C-N2	1.2860	.9840	.572	6.9	18.50	0.0596	1.	1.072	0.714	55.2

COMPOUNDS DTA-17 (CONT.)

I	II	III	IV	V	VI	VII	VIII	IX	X	XI	XII	XIII	XIV	XV
2149AGINSEC-293H-N2					1.286	0.984	0.572	6.9	18.50	0.0596	1.	1.095	0.791	63.2
2149AGINSEC-293C-N2					1.286	0.984	0.572	6.9	18.50	0.0596	1.	1.072	1.14	66.9
2149AGINSEC-294H-HE					1.286	0.984	0.572	6.9	18.50	0.0596	1.	1.095	0.781	51.1
2149AGINSEC-294C-N2					1.286	0.984	0.572	6.9	18.50	0.0596	1.	1.072	1.008	61.3
1	62	AG2SEB-291C-N2			1.347	1.720	0.59	3.6	24.00	0.0738	1.	1.154	0.632	30.2
1	62	AG2SEB-292H-N2			1.347	1.720	0.59	3.6	24.00	0.0738	1.	1.173	0.621	29.2
1	62	AG2SEB-292C-HE			1.347	1.720	0.59	3.6	24.00	0.0738	1.	1.153	0.443	19.0
1	62	AG2SEB-293H-HE			1.347	1.720	0.59	3.6	24.00	0.0738	1.	1.176	0.431	18.7
2113AG2SE		C-111C-N2			1.318	1.039	0.597	6.1	24.00	0.0738	1.	1.160	0.483	18.6
2113AG2SE		C-112H-HE			1.318	1.039	0.597	6.1	24.00	0.0738	1.	1.173	0.331	13.6
2113AG2SE		C-112C-HE			1.318	1.039	0.597	6.1	24.00	0.0738	1.	1.158	0.291	13.3
2136AG2SE		C-241C-HE			1.306	1.020	0.610	6.4	24.00	0.0738	1.	1.157	0.345	13.0
2136AG2SE		C-242H-HE			1.306	1.020	0.610	6.4	24.00	0.0738	1.	1.170	0.351	12.8
2136AG2SE		C-242C-HE			1.306	1.020	0.610	6.4	24.00	0.0738	1.	1.158	0.336	12.6
2136AG2SE		C-243H-N2			1.306	1.020	0.610	6.4	24.00	0.0738	1.	1.173	0.473	16.7
2136AG2SE		C-243C-N2			1.306	1.020	0.610	6.4	24.00	0.0738	1.	1.159	0.522	17.1
1	63AG2TE	B-281C-N2			1.345	1.700	0.59	4.0	25.50	0.0633	1.	1.225	0.650	26.0
1	63AG2TE	B-282H-N2			1.345	1.700	0.59	4.0	25.50	0.0633	1.	1.246	0.579	26.7
1	63AG2TE	B-282C-HE			1.345	1.700	0.59	4.0	25.50	0.0633	1.	1.223	0.548	19.8
1	63AG2TE	B-283H-HE			1.345	1.700	0.59	4.0	25.50	0.0633	1.	1.243	0.401	19.1
1	63AG2TE	B-283C-HE			1.345	1.700	0.59	4.0	25.50	0.0633	1.	1.224	0.532	20.0
2112AG2TE		C-101C-HE			1.290	0.998	0.578	6.5	25.50	0.0633	1.	1.224	0.658	13.3
2112AG2TE		C-102H-HE			1.290	0.998	0.578	6.5	25.50	0.0633	1.	1.240	0.895	16.4
2112AG2TE		C-102C-N2			1.290	0.998	0.578	6.5	25.50	0.0633	1.	1.225	0.302	13.2
2135AG2TE		C-282H-HE			1.310	1.000	0.570	6.3	25.50	0.0633	1.	1.241	0.406	15.1
2135AG2TE		C-282C-HE			1.310	1.000	0.570	6.3	25.50	0.0633	1.	1.222	0.421	15.62

COMPOUNDS DTA-17 (CONT.)

I	II	III	IV	V	VI	VII	VIII	IX	X	XI	XII	XIII	XIV	XV
2135AG2TE	C-283H-HE	1.3101	.0000	.570	6.3	25.50	0.0633	1.	1.240	0.307	14.5			
2135AG2TE	C-283C-N2	1.3101	.0000	.570	6.3	25.50	0.0633	1.	1.223	0.614	19.63			
1 55BI2SE3B	-272C-N2	1.33	1.17	0.59	3.5	20.46	0.0553	1.	0.963	0.750	193.			
1 55BI2SE3B	-273H-N2	1.33	1.17	0.59	3.5	20.46	0.0553	1.	0.983	0.800	160.			
1 55BI2SE3B	-273C-HE	1.33	1.17	0.59	3.5	20.46	0.0553	1.	0.963	0.454	109.			
1 55BI2SE3B	-274H-HE	1.33	1.17	0.59	3.5	20.46	0.0553	1.	0.983	0.344	93.			
2111BI2SE3C	-9 2C-HE	1.3101	.0160	.586	6.4	20.40	0.0553	1.	0.966	0.407	59.1			
2111BI2SE3C	-9 3H-HE	1.3101	.0160	.586	6.4	20.40	0.0553	1.	0.981	0.426	56.0			
2111BI2SE3C	-9 3C-N2	1.3101	.0160	.586	6.4	20.40	0.0553	1.	0.968	0.635	98.0			
2131BI2SE3C	-221C-N2	1.3001	.0190	.602	5.9	20.35	0.0553	1.	0.958	0.710	125.			
2131BI2SE3C	-222H-N2	1.3001	.0190	.602	5.9	20.35	0.0553	1.	0.991	0.740	109.			
2131BI2SE3C	-222C-HE	1.3001	.0190	.602	5.9	20.35	0.0553	1.	0.964	0.425	71.9			
2131BI2SE3C	-223H-HE	1.3001	.0190	.602	5.9	20.35	0.0553	1.	0.983	0.473	70.4			
1 54BI2TE3B	-272H-N2	1.33	1.18	0.59	3.65	22.10	0.0473	1.	0.877	0.728	213.			
1 54BI2TE3B	-272C-N2	1.33	1.18	0.59	3.65	22.10	0.0473	1.	0.856	0.751	195.			
1 54BI2TE3B	-273H-N2	1.33	1.18	0.59	3.65	22.10	0.0473	1.	0.874	0.728	192.			
1 54BI2TE3B	-273C-HE	1.33	1.18	0.59	3.65	22.10	0.0473	1.	0.859	0.352	105.			
1 54BI2TE3B	-274H-HE	1.33	1.18	0.59	3.65	22.10	0.0473	1.	0.868	0.385	97.3			
2110BI2TE3C	-9 1C-HE	1.3101	.0160	.610	6.6	23.10	0.0473	1.	0.854	0.376	59.0			
2110BI2TE3C	-9 2H-HE	1.3101	.0160	.610	6.6	23.10	0.0473	1.	0.863	0.378	58.5			
2110BI2TE3C	-9 2C-N2	1.3101	.0160	.610	6.6	23.10	0.0473	1.	0.855	0.792	112.			
2130BI2TE3C	-222H-N2	1.3030	.9930	.616	6.1	23.10	0.0473	1.	0.868	0.580	106.6			
2130BI2TE3C	-222C-N2	1.3030	.9930	.616	6.1	23.10	0.0473	1.	0.852	0.730	110.			
2130BI2TE3C	-223H-HE	1.3030	.9930	.616	6.1	23.10	0.0473	1.	0.865	0.344	60.8			
2130BI2TE3C	-223C-HE	1.3030	.9930	.616	6.1	23.10	0.0473	1.	0.853	0.356	64.0			
1 19 CDSE	B-7 2H-HE	1.34	1.17	0.59	3.7	17.43	0.0757	1.	1.535	0.382	107.			

COMPOUNDS DTA-17 (CONT.)

I	II	III	IV	V	VI	VII	VIII	IX	X	XI	XII	XIII	XIV	XV
1	49	CDSE	B-242H-N2	1.	3171.	15	0.59	3.85	17.43	0.0757	1.	1.536	0.326	145.
1	49	CDSE	B-243H-HE	1.	3171.	15	0.59	3.85	17.43	0.0757	1.	1.524	0.294	91.0
2123		CDSE	C-162H-HE	1.	3170.	9900.	594	6.9	17.50	0.0757	1.	1.535	0.238	54.
2145		CDSE	C-251C-N2	1.	2800.	9940.	600	7.1	17.50	0.0757	1.	1.511	0.421	60.7
2145		CDSE	C-252H-N2	1.	2800.	9940.	600	7.1	17.50	0.0757	1.	1.535	0.315	58.8
2145		CDSE	C-252C-HE	1.	2800.	9940.	600	7.1	17.50	0.0757	1.	1.510	0.351	47.3
2145		CDSE	C-253H-HE	1.	2800.	9940.	600	7.1	17.50	0.0757	1.	1.528	0.244	42.6
2145		CDSE	C-253C-HE	1.	2800.	9940.	600	7.1	17.50	0.0757	1.	1.508	0.328	41.9
1	14	CDTE	B-4 2H-HE	1.	34	1.	16	0.59	3.9	18.60	0.0604	1.	1.383	0.398	104.
1	27	CDTE	B-9 2H-HE	1.	34	1.	17	0.59	3.8	18.60	0.0604	1.	1.375	0.330	94.7
1	33	CDTE	B-122H-HE	1.	35	1.	17	0.59	3.8	18.60	0.0604	1.	1.368	0.387	94.5
1	47	CDTE	B-222H-HE	1.	32	1.	1730.	59	4.2	18.60	0.0604	1.	1.373	0.338	86.1
2104		CDTE	C-102H-N2	1.	3151.	0100.	585	6.7	18.60	0.0604	1.	1.378	0.318	62.1
2121		CDTE	C-152H-HE	1.	2741.	0090.	575	6.5	18.60	0.0604	1.	1.368	0.255	58.9
1	18	GAAS	B-6 2H-HE	1.	33	1.	16	0.59	3.2	15.93	0.100	1.	1.513	0.182	165.0
1	39	GAAS	B-172H-HE	1.	38	1.	18	0.59	3.3	15.93	0.100	1.	1.517	0.207	160.0
2107		GAAS	C-122H-HE	1.	3211.	0210.	602	6.9	16.50	0.100	1.	1.514	0.243	147.0
2129		GAAS	C-191C-HE	1.	2941.	0100.	598	6.1	16.50	0.100	1.	1.500	0.198	145.0
2129		GAAS	C-191C-N2	1.	2941.	0100.	598	6.1	16.50	0.100	1.	1.503	0.295	164.0
1	21	GASB	B-7 1H-HE	1.	34	1.	17	0.59	3.6	16.86	0.0757	1.	0.991	0.263	131.
1	52	GASB	B-262H-A	1.	3411.	1750.	59	3.7	16.86	0.0757	1.	1.005	0.545	168.
1	52	GASB	B-263H-A	1.	3411.	1750.	59	3.7	16.86	0.0757	1.	1.010	0.535	168.
1	52	GASB	B-264H-HE	1.	3411.	1750.	59	3.7	16.86	0.0757	1.	1.002	0.252	82.1
2102		GASB	C-6 2H-N2	1.	2821.	0130.	606	6.4	17.40	0.0757	1.	1.001	0.625	194.5
2102		GASB	C-6 2C-N2	1.	2821.	0130.	606	6.4	17.40	0.0757	1.	0.977	0.576	186.
2102		GASB	C-6 3H-HE	1.	2821.	0130.	606	6.4	17.40	0.0757	1.	0.993	0.304	96.7

COMPOUNDS DTA-17 (CONT.)

I	II	III	IV	V	VI	VII	VIII	IX	X	XI	XII	XIII	XIV	XV
2102		GASB	C-6	3C-HE	1.2821	.0130	.606	6.4	17.40	0.0757	1.	0.980	0.424	102.
2128		GASB	C-191C-HE		1.3090	.9900	.597	6.2	17.40	0.0757	1.	0.971	0.297	96.5
2128		GASB	C-192H-HE		1.3090	.9900	.597	6.2	17.40	0.0757	1.	0.994	0.29	100.7
2128		GASB	C-192C-N2		1.3090	.9900	.597	6.2	17.40	0.0757	1.	0.976	0.602	187.5
1	17	INAS	B-5	2H-HE	1.32	1.14	0.59	3.8	17.10	0.0764	1.	1.223	0.282	134.7
1	38	INAS	B-162H-HE		1.36	1.18	0.59	3.6	17.10	0.0764	1.	1.225	0.236	125.7
1	69	INAS	B-332H-N2		1.3471	.1710	.59	3.8	17.10	0.0764	1.	1.227	0.515	231.
1	69	INAS	B-333H-HE		1.3471	.1710	.59	3.8	17.10	0.0764	1.	1.222	0.284	141.3
2101		INAS	C-7	2H-N2	1.3021	.0330	.606	6.4	17.70	0.0764	1.	1.225	0.396	145.6
2101		INAS	C-7	3H-HE	1.3021	.0330	.606	6.4	17.70	0.0764	1.	1.219	0.231	99.2
2127		INAS	C-181C-N2		1.2800	.9830	.597	7.0	17.70	0.0764	1.	1.198	0.435	124.0
2127		INAS	C-182H-N2		1.2800	.9830	.597	7.0	17.70	0.0764	1.	1.223	0.455	151.0
2127		INAS	C-182C-HE		1.2800	.9830	.597	7.0	17.70	0.0764	1.	1.200	0.27	94.0
1	16	INSB	B-5	2H-HE	1.33	1.17	0.59	3.5	17.37	0.0626	1.	0.805	0.241	79.1
1	42	INSB	B-152H-HE		1.3451	.18	0.59	3.6	17.37	0.0626	1.	0.805	0.239	96.8
1	68	INSB	B-331C-N2		1.3601	.1830	.59	3.9	17.37	0.0555	1.	0.764	0.770	239.0
1	68	INSB	B-332H-N2		1.3601	.1830	.59	3.9	17.37	0.0626	1.	0.814	0.715	231.
1	68	INSB	B-333H-HE		1.3601	.1830	.59	3.9	17.37	0.0626	1.	0.806	0.307	108.3
2100		INSB	C-6	1C-HE	1.2550	.9850	.606	6.4	18.30	0.0555	1.	0.778	0.470	98.8
2100		INSB	C-6	2C-N2	1.2550	.9850	.606	6.4	18.30	0.0555	1.	0.786	0.852	184.
2126		INSB	C-181C-HE		1.3140	.9890	.595	6.2	18.30	0.0555	1.	0.776	0.337	79.8
2126		INSB	C-182C-N2		1.3140	.9890	.595	6.2	18.30	0.0555	1.	0.786	0.717	149.2
1	59	IN2SE	3B-251C-N2		1.3601	.1750	.59	4.0	17.70	0.12	1.	1.145	1.02	138.
1	59	IN2SE	3B-252H-N2		1.3601	.1750	.59	4.0	17.70	0.12	1.	1.175	0.817	151.
1	59	IN2SE	3B-252C-HE		1.3601	.1750	.59	4.0	17.70	0.12	1.	1.144	0.939	110.
1	59	IN2SE	3B-253H-HE		1.3601	.1750	.59	4.0	17.70	0.12	1.	1.173	0.703	133.

COMPOUNDS DTA-17 (CONT.)

I	II	III	IV	V	VI	VII	VIII	IX	X	XI	XII	XIII	XIV	XV
1	59	IN2SE3B-253C-N2			1.3601	.1750	.59	4.0	17.70	0.12	1.	1.148	1.18	129.
2119		IN2SE3C-142H-HE			1.3180	.9900	.593	6.8	17.10	0.12	1.	1.168	0.556	56.6
2119		IN2SE3C-142C-HE			1.3180	.9900	.593	6.8	17.10	0.12	1.	1.148	0.518	47.2
2119		IN2SE3C-143H-N2			1.3180	.9900	.593	6.8	17.10	0.12	1.	1.167	0.639	57.6
2119		IN2SE3C-143C-N2			1.3180	.9900	.593	6.8	17.10	0.12	1.	1.148	0.694	61.1
1	59	IN2SE3B-251C-N2			1.3601	.1750	.59	4.0	17.70	0.0775	1.	1.145	1.02	138.
1	59	IN2SE3B-252H-N2			1.3601	.1750	.59	4.0	17.70	0.0775	1.	1.175	0.817	151.
1	59	IN2SE3B-252C-HE			1.3601	.1750	.59	4.0	17.70	0.0775	1.	1.144	0.939	110.
1	59	IN2SE3B-253H-HE			1.3601	.1750	.59	4.0	17.70	0.0775	1.	1.173	0.703	133.
1	59	IN2SE3B-253C-N2			1.3601	.1750	.59	4.0	17.70	0.0775	1.	1.148	1.18	129.
2119		IN2SE3C-142H-HE			1.3180	.9900	.593	6.8	17.10	0.0775	1.	1.168	0.556	56.6
2119		IN2SE3C-142C-HE			1.3180	.9900	.593	6.8	17.10	0.0775	1.	1.148	0.518	47.2
2119		IN2SE3C-143H-N2			1.3180	.9900	.593	6.8	17.10	0.0775	1.	1.167	0.639	57.6
2119		IN2SE3C-143C-N2			1.3180	.9900	.593	6.8	17.10	0.0775	1.	1.148	0.694	61.1
2142		INTE C-171C-N2			1.2751	.0220	.615	6.7	18.90	0.0599	1.	0.952	1.05	77.0
2142		INTE C-172H-N2			1.2751	.0220	.615	6.7	18.90	0.0599	1.	0.977	0.600	69.0
2142		INTE C-172C-HE			1.2751	.0220	.615	6.7	18.90	0.0599	1.	0.941	0.512	56.0
2120		INTE C-201C-N2			1.3401	.0350	.597	6.3	18.90	0.0599	1.	0.943	0.930	82.9
2120		INTE C-202C-HE			1.3401	.0350	.597	6.3	18.90	0.0599	1.	0.940	0.426	51.6
2120		INTE C-203H-HE			1.3401	.0350	.597	6.3	18.90	0.0599	1.	0.972	0.376	37.1
2120		INTE C-203C-HE			1.3401	.0350	.597	6.3	18.90	0.0599	1.	0.933	0.534	54.0
1	58	IN2TE3B-251C-N2			1.3461	.1750	.59	3.6	17.37	0.0592	1.	0.928	1.170	136.
1	58	IN2TE3B-252H-N2			1.3461	.1750	.59	3.6	17.37	0.0592	1.	0.955	1.145	120.
1	58	IN2TE3B-253H-HE			1.3461	.1750	.59	3.6	17.37	0.0592	1.	0.957	0.862	85.3
2118		IN2TE3C-211C-HE			1.3030	.9910	.615	6.5	17.40	0.0592	1.	0.930	0.883	52.3
2118		IN2TE3C-212C-N2			1.3030	.9910	.615	6.5	17.40	0.0592	1.	0.930	1.220	72.2

COMPOUNDS DTA-17 (CONT.)

I	II	III	IV	V	VI	VII	VIII	IX	X	XI	XII	XIII	XIV	XV
2118	IN2TE3C-212H-HE				1.303	0.991	0.615	6.5	17.40	0.0592	1.	0.955	0.491	49.6
2118	IN2TE3C-213H-N2				1.303	0.991	0.615	6.5	17.40	0.0592	1.	0.955	0.762	70.7
2139	IN2TE3C-261C-N2				1.289	1.013	0.607	6.6	17.40	0.0592	1.	0.930	1.175	80.6
2139	IN2TE3C-262H-N2				1.289	1.013	0.607	6.6	17.40	0.0592	1.	0.955	0.302	74.2
2139	IN2TE3C-262C-HE				1.289	1.013	0.607	6.6	17.40	0.0592	1.	0.930	0.917	56.0
2139	IN2TE3C-263H-HE				1.289	1.013	0.607	6.6	17.40	0.0592	1.	0.955	0.493	49.8
2139	IN2TE3C-263C-HE				1.289	1.013	0.607	6.6	17.40	0.0592	1.	0.930	0.956	61.8
1	64	PBSE	B-301C-N2		1.347	1.172	0.59	3.8	24.30	0.0506	1.	1.349	0.426	111.1
1	64	PBSE	B-302H-N2		1.347	1.172	0.59	3.8	24.30	0.0506	1.	1.364	0.479	109.0
1	64	PBSE	B-302C-HE		1.347	1.172	0.59	3.8	24.30	0.0506	1.	1.345	0.218	76.0
1	64	PBSE	B-303H-HE		1.347	1.172	0.59	3.8	24.30	0.0506	1.	1.360	0.309	71.3
1	64	PBSE	B-303C-HE		1.347	1.172	0.59	3.8	24.30	0.0506	1.	1.347	0.242	77.9
2106	PBSE	C-8	1C-N2		1.285	1.013	0.606	6.6	24.30	0.0506	1.	1.353	0.352	54.7
2106	PBSE	C-8	2H-N2		1.285	1.013	0.606	6.6	24.30	0.0506	1.	1.363	0.338	54.1
2106	PBSE	C-8	2C-HE		1.285	1.013	0.606	6.6	24.30	0.0506	1.	1.350	0.251	41.7
2106	PBSE	C-8	3H-HE		1.285	1.013	0.606	6.6	24.30	0.0506	1.	1.366	0.240	41.0
2106	PBSE	C-8	3C-HE		1.285	1.013	0.606	6.6	24.30	0.0506	1.	1.350	0.287	42.7
2133	PBSE	C-231C-HE			1.275	0.997	0.597	6.8	24.30	0.0506	1.	1.344	0.330	43.9
2133	PBSE	C-232H-HE			1.275	0.997	0.597	6.8	24.30	0.0506	1.	1.363	0.240	40.9
2133	PBSE	C-232C-N2			1.275	0.997	0.597	6.8	24.30	0.0506	1.	1.347	0.447	56.5
2133	PBSE	C-233H-HE			1.275	0.997	0.597	6.8	24.30	0.0506	1.	1.358	0.398	53.8
1	65	PBTE	B-301C-N2		1.344	1.174	0.59	3.5	24.48	0.0433	1.	1.179	0.532	120.8
1	65	PBTE	B-302H-N2		1.344	1.174	0.59	3.5	24.48	0.0433	1.	1.220	0.520	116.2
1	65	PBTE	B-302C-HE		1.344	1.174	0.59	3.5	24.48	0.0433	1.	1.186	0.313	77.3
1	65	PBTE	B-303H-HE		1.344	1.174	0.59	3.5	24.48	0.0433	1.	1.211	0.309	69.9
2105	PBTE	C-8	1C-HE		1.278	1.005	0.606	6.5	24.60	0.0433	1.	1.205	0.300	47.6

COMPOUNDS DTA-17 (CONT.)

I	II	III	IV	V	VI	VII	VIII	IX	X	XI	XII	XIII	XIV	XV
2105	PBTE	C-8	3H-N2	1.278	1.005	0.606	6.5	24.60	0.0433	1.	1.213	0.440	65.6
2132	PBTE	C-231	C-N2	1.312	1.010	0.612	6.8	24.60	0.0433	1.	1.189	0.575	59.4
2132	PBTE	C-232	H-N2	1.312	1.010	0.612	6.8	24.60	0.0433	1.	1.204	0.409	58.5
2132	PBTE	C-232	C-HE	1.312	1.010	0.612	6.8	24.60	0.0433	1.	1.188	0.368	36.0
2132	PBTE	C-233	H-HE	1.312	1.010	0.612	6.8	24.60	0.0433	1.	1.201	0.300	37.8
2132	PBTE	C-233	C-HE	1.312	1.010	0.612	6.8	24.60	0.0433	1.	1.189	0.392	43.6
1	57SB2SE3B	-292	H-N2	1.347	1.720	0.59	4.3	19.20	0.0755	1.	0.898	0.976	209.5
1	57SB2SE3B	-292	C-N2	1.347	1.720	0.59	4.3	19.20	0.0755	1.	0.849	0.822	158.0
1	57SB2SE3B	-293	H-HE	1.347	1.720	0.59	4.3	19.20	0.0755	1.	0.898	0.806	148.1
1	57SB2SE3B	-293	C-HE	1.347	1.720	0.59	4.3	19.20	0.0755	1.	0.858	0.495	101.0
2117	SB2SE3C	-152	H-HE	1.289	1.021	0.602	6.5	19.20	0.0755	1.	0.899	0.633	82.7
2117	SB2SE3C	-152	C-HE	1.289	1.021	0.602	6.5	19.20	0.0755	1.	0.865	0.396	65.8
2117	SB2SE3C	-153	H-N2	1.289	1.021	0.602	6.5	19.20	0.0755	1.	0.897	0.823	106.3
2117	SB2SE3C	-153	C-N2	1.289	1.021	0.602	6.5	19.20	0.0755	1.	0.861	0.714	98.5
2138	SB2SE3C	-241	C-N2	1.291	1.026	0.600	7.1	19.20	0.0755	1.	0.833	0.851	88.6
2138	SB2SE3C	-242	H-N2	1.291	1.026	0.600	7.1	19.20	0.0755	1.	0.903	0.936	97.7
2138	SB2SE3C	-242	C-HE	1.291	1.026	0.600	7.1	19.20	0.0755	1.	0.841	0.510	61.0
2138	SB2SE3C	-243	H-HE	1.291	1.026	0.600	7.1	19.20	0.0755	1.	0.895	0.688	72.1
1	56SB2TE3B	-281	C-N2	1.345	1.700	0.59	4.0	19.80	0.0579	1.	0.876	0.671	147.3
1	56SB2TE3B	-282	H-N2	1.345	1.700	0.59	4.0	19.80	0.0579	1.	0.913	0.715	143.2
1	56SB2TE3B	-282	C-HE	1.345	1.700	0.59	4.0	19.80	0.0579	1.	0.878	0.425	83.0
1	56SB2TE3B	-283	H-HE	1.345	1.700	0.59	4.0	19.80	0.0579	1.	0.900	0.278	72.9
2116	SB2TE3C	-141	C-N2	1.300	1.016	0.600	6.6	19.80	0.0579	1.	0.884	0.82	115.2
2116	SB2TE3C	-142	H-HE	1.300	1.016	0.600	6.6	19.80	0.0579	1.	0.900	0.348	65.0
2116	SB2TE3C	-142	C-HE	1.300	1.016	0.600	6.6	19.80	0.0579	1.	0.884	0.445	70.5
2137	SB2TE3C	-171	C-N2	1.276	1.044	0.602	6.6	19.80	0.0579	1.	0.881	0.741	126.0

COMPOUNDS DTA-17 (CONT.)

I	II	III	IV	V	VI	VII	VIII	IX	X	XI	XII	XIII	XIV	XV
2137	SB2	TE3	C-172	H-N2	1.2761	.0440	.602	6.6	19.80	0.0579	1.	0.903	0.740	114.5
2137	SB2	TE3	C-172	C-HE	1.2761	.0440	.602	6.6	19.80	0.0579	1.	0.876	0.470	71.7
2103	SNTE		C-7	1C-HE	1.2921	.0250	.607	6.0	19.50	0.0590	1.	1.063	0.653	52.5
2103	SNTE		C-7	2H-HE	1.2921	.0250	.607	6.0	19.50	0.0590	1.	1.081	0.311	48.3
2103	SNTE		C-7	2C-N2	1.2921	.0250	.607	6.0	19.50	0.0590	1.	1.067	1.03	81.4
2103	SNTE		C-7	3H-N2	1.2921	.0250	.607	6.0	19.50	0.0590	1.	1.100	0.527	76.0
2141	SNTE		C-161	C-N2	1.2760	.9830	.591	6.7	19.50	0.0590	1.	1.065	0.982	85.2
2141	SNTE		C-162	H-N2	1.2760	.9830	.591	6.7	19.50	0.0590	1.	1.083	0.514	72.0
2141	SNTE		C-162	C-HE	1.2760	.9830	.591	6.7	19.50	0.0590	1.	1.065	0.635	57.5
2141	SNTE		C-163	H-HE	1.2760	.9830	.591	6.7	19.50	0.0590	1.	1.083	0.353	53.3
1	20	ZNTE	B-6	2H-HE	1.33	1.16	0.59	3.8	16.62	0.0752	1.	1.573	0.277	132.
1	35	ZNTE	B-202	H-HE	1.3521	.1550	.59	3.8	16.62	0.0752	1.	1.569	0.295	131.
1	73	ZNTE	B-352	H-N2	1.3451	.13	0.59	3.8	16.62	0.0752	1.	1.564	0.234	96.5
1	73	ZNTE	B-353	H-HE	1.3451	.13	0.59	3.8	16.62	0.0752	1.	1.568	0.322	96.0
2146	ZNTE		C-281	C-HE	1.2890	.9830	.597	6.6	16.60	0.0752	1.	1.555	0.292	74.4
2146	ZNTE		C-282	H-HE	1.2890	.9830	.597	6.6	16.60	0.0752	1.	1.571	0.260	66.1
2146	ZNTE		C-282	C-HE	1.2890	.9830	.597	6.6	16.60	0.0752	1.	1.552	0.332	76.3

COMPOUNDS AT THE TRANSITION TEMPERATURE

2148	AGINSE		C-27T1	C-HE	1.3141	.0000	.592	6.5	18.50	0.0596	1.	1.010	0.675	5.85
2148	AGINSE		C-27T2	C-HE	1.3141	.0000	.592	6.5	18.50	0.0596	1.	1.010	1.245	10.2
2148	AGINSE		C-27T3	H-N2	1.3141	.0000	.592	6.5	18.50	0.0596	1.	1.025	0.624	10.2
2148	AGINSE		C-27T3	C-N2	1.3141	.0000	.592	6.5	18.50	0.0596	1.	1.010	1.42	9.08
2149	AGINSE		C-29T1	C-N2	1.2860	.9840	.572	6.9	18.50	0.0596	1.	1.010	2.85	11.85

TRANSITIONS DTA-17 (CONT.)

I	II	III	IV	V	VI	VII	VIII	IX	X	XI	XII	XIII	XIV	XV
2149AGINSEC-29T2H-HE1					.2860	.9840	.572	6.9	18.50	0.0596	1.	1.025	0.582	6.52
2149AGINSEC-29T2C-N21					.2860	.9840	.572	6.9	18.50	0.0596	1.	1.010	1.474	7.77
2149AGINSEC-29T3H-N21					.2860	.9840	.572	6.9	18.50	0.0596	1.	1.025	0.736	14.06
2149AGINSEC-29T3C-N21					.2860	.9840	.572	6.9	18.50	0.0596	1.	1.010	1.404	9.77
2149AGINSEC-29T4H-HE1					.2860	.9840	.572	6.9	18.50	0.0596	1.	1.025	0.466	9.18
2149AGINSEC-29T4C-N21					.2860	.9840	.572	6.9	18.50	0.0596	1.	1.010	1.663	6.57
1	62AG2SE	B-29T4C-HE1			.3471	.1720	.59	3.6	24.00	0.0736	1.	0.396	1.000	46.1
1	62AG2SE	B-29T5H-HE1			.3471	.1720	.59	3.6	24.00	0.0691	1.	0.420	0.597	48.8
1	62AG2SE	B-29T5C-N21			.3471	.1720	.59	3.6	24.00	0.0736	1.	0.396	1.67	80.1
1	62AG2SE	B-29T6H-N21			.3471	.1720	.59	3.6	24.00	0.0691	1.	0.420	1.44	72.6
2113AG2SE		C-11T1C-N21			.3181	.0390	.597	6.1	24.00	0.0736	1.	0.396	1.85	72.6
2113AG2SE		C-11T2H-N21			.3181	.0390	.597	6.1	24.00	0.0691	1.	0.427	1.85	72.3
2113AG2SE		C-11T2C-HE1			.3181	.0390	.597	6.1	24.00	0.0736	1.	0.397	0.935	34.7
2113AG2SE		C-11T3H-HE1			.3181	.0390	.597	6.1	24.00	0.0691	1.	0.416	0.833	31.8
2136AG2SE		C-24T2H-N21			.3061	.0200	.610	6.4	24.00	0.0691	1.	0.436	1.825	56.3
2136AG2SE		C-24T2C-HE1			.3061	.0200	.610	6.4	24.00	0.0736	1.	0.392	0.873	28.6
2136AG2SE		C-24T3H-HE1			.3061	.0200	.610	6.4	24.00	0.0691	1.	0.418	0.763	28.4
1	63AG2TE	B-28T4H-HE1			.3451	.1700	.59	4.0	25.50	0.0645	1.	0.440	0.600	29.8
1	63AG2TE	B-28T4C-HE1			.3451	.1700	.59	4.0	25.50	0.0674	1.	0.410	1.33	30.4
1	63AG2TE	B-28T5H-N21			.3451	.1700	.59	4.0	25.50	0.0645	1.	0.440	1.39	76.0
1	63AG2TE	B-28T5C-N21			.3451	.1700	.59	4.0	25.50	0.0674	1.	0.410	2.63	84.3
2112AG2TE		C-10T1C-HE1			.2900	.9980	.578	6.5	25.50	0.0674	1.	0.410	1.88	27.2
2112AG2TE		C-10T2H-HE1			.2900	.9980	.578	6.5	25.50	0.0645	1.	0.440	0.675	24.9
2112AG2TE		C-10T2C-N21			.2900	.9980	.578	6.5	25.50	0.0674	1.	0.410	3.00	50.0
2135AG2TE		C-28T3H-HE1			.3101	.0000	.570	6.3	25.50	0.0645	1.	0.436	0.645	28.4
2135AG2TE		C-28T3C-HE1			.3101	.0000	.570	6.3	25.50	0.0674	1.	0.413	1.66	26.7

TRANSITIONS DTA-17 (CONT.)

I	II	III	IV	V	VI	VII	VIII	IX	X	XI	XII	XIII	XIV	XV
2135	AG2	TE	C-28	T4H-N21.	3101.	0000.	570	6.3	25.50	0.0645	1.	0.447	1.43	60.6
2135	AG2	TE	C-28	T4C-N21.	3101.	0000.	570	6.3	25.50	0.0674	1.	0.407	2.80	59.6
2112	AG2	TE	C-10	T1C-N21.	2900.	9980.	578	6.5	25.50	0.0633	1.	1.065	0.485	1.66
2112	AG2	TE	C-10	T2H-N21.	2900.	9980.	578	6.5	25.50	0.0633	1.	1.075	0.543	1.58
2112	AG2	TE	C-10	T2C-HE1.	2900.	9980.	578	6.5	25.50	0.0633	1.	1.065	0.341	1.23
2135	AG2	TE	C-28	T2H-N21.	3101.	0000.	570	6.3	25.50	0.0633	1.	1.081	0.547	2.14
2135	AG2	TE	C-28	T2C-N21.	3101.	0000.	570	6.3	25.50	0.0633	1.	1.065	0.529	2.12
2135	AG2	TE	C-28	T3H-HE1.	3101.	0000.	570	6.3	25.50	0.0633	1.	1.075	0.357	1.54
2135	AG2	TE	C-28	T3C-HE1.	3101.	0000.	570	6.3	25.50	0.0633	1.	1.064	0.325	1.53
1	59	IN2	SE	3B-25	T4C-N21.	3601.	1750.	59	4.0	17.70	0.10	1.	0.374	1.63	11.1
1	59	IN2	SE	3B-25	T5H-N21.	3601.	1750.	59	4.0	17.70	0.11	1.	0.483	1.34	14.8
1	59	IN2	SE	3B-25	T6H-HE1.	3601.	1750.	59	4.0	17.70	0.11	1.	0.483	0.762	8.63
1	59	IN2	SE	3B-25	T6C-HE1.	3601.	1750.	59	4.0	17.70	0.10	1.	0.374	1.33	7.28
2119	IN2	SE	3C	-14	T2H-HE1.	3180.	9900.	593	6.8	17.10	0.11	1.	0.483	0.662	5.03
2119	IN2	SE	3C	-14	T3H-N21.	3180.	9900.	593	6.8	17.10	0.11	1.	0.483	1.42	10.1
1	58	IN2	TE	3B-25	T4H-N21.	3461.	1750.	59	3.6	17.37	0.0592	1.	0.900	0.545	3.68
1	58	IN2	TE	3B-25	T5H-HE1.	3461.	1750.	59	3.6	17.37	0.0592	1.	0.900	0.620	3.04
2118	IN2	TE	3C	-21	T2C-N21.	3030.	9910.	615	6.5	17.40	0.0592	1.	0.800	1.95	1.935

APPENDIX VII

NOMENCLATURE

A = Area, cm^2

A = Coefficient in solution of differential equation

B = Coefficient in solution of differential equation

B_n = Function defined by Equation A-5.45

C = Heat capacity, cal/^oK

C = Coefficient in solution of differential equation

C_n = Function defined by Equation A-5.46

D = Determinant

D = Coefficient in solution of differential equation

D = Diameter, cm

E = Energy, cal

F = Free energy

F = Shape factor (Cf. Eqs. 2.62 and 2.65)

F = Various functions of β (Cf. Eq. 2.58)

G = Thermal conductance per unit height, cal/cm sec ^oK

H = Square root of time constant (Cf. Eq. A-5.19)

H = Enthalpy

I_1 = Integrand of excess free energy function (Cf. Eq. 5.1 ff.)

J_n = Bessel function of the first kind of order n

K = Thermal conductance, cal/sec ^oK

K = Time constant (Appendix II only)

L = Sample height, cm

L = Lorentz number

L_f or L_t = Heat of fusion or transition, cal/g

M = A positive, real number (Cf. Eq. A-5.32)

M = Molecular Weight

N = Atom fraction

N = Number of items in computing an average

P = Coefficient in the solution of a differential equation

Q = Rate of heat flow, cal/sec

Q = Coefficient in the solution of a differential equation

R = A specific value of r (or x), cm

R = Gas constant, 1.987 cal/g atom $^{\circ}K$

S = Entropy

T = Temperature, $^{\circ}K$

T_f or T_t = Melting point or transition temperature

U = Overall heat transfer coefficient, cal/cm^2 sec $^{\circ}K$

V = Volume

V = Laplace transform of v (Appendix V)

X = A specific value of x, cm

X = The group of variables $\sigma A T^4$ (Chapter II)

Y = Autotransformer setting, % of scale (Appendix II)

Y_n = Bessel function of the second kind of order n

Z = Correlation factor defined in Chapter III

a = Radius ratio R_2/R_1 (Cf. Eq. 2.60)

a = Function defined in Chapter II (Cf. Eq. 2.39 ff.)

b = Radius ratio R_3/R_1 (Cf. Eq. 2.60)

b_n = Function of α_n (Cf. Eqs. 2.39 and 2.40 ff.)

c = Function defined in Chapter II (Cf. Eq. 2.39 ff.)

c = Constant defined by Equation A-5.31

c_p = Specific heat, cal/g ^{o}K

d = Constant defined by Equation A-5.10b

e = 2.71828...

f = Fraction of total radiation emitted by one surface which is seen by other

h = Square root of thermal diffusivity (Cf. Eq. A-5.9)

i = $\sqrt{-1}$

k = Thermal conductivity, cal/cm sec ^{o}K

m = Mass, g

m = Heating rate, ^{o}K/min (Appendix II only)

n = Average number of atoms in cluster

n = Index of refraction

q = Dimensionless variable defined by Equation A-5.10a.

r = Radius, cm

s = Laplace transform variable

t = Time, sec or min; with subscript, a time constant

v = Temperature variable (Cf. Eq. 2.3)

v = Temperature variable (Cf. Eq. A-5.11)

x = Distance variable, cm

x = Mole fraction of compound in solution

y = Temperature function (Cf. Eq. 2.4)

z = Temperature function (Cf. Eq. 2.5)

α = A defined function of s; with subscript, an eigenvalue

α = A function of the equivalent conductances for radiation (Cf. Eq. 3.9)

α = Temperature coefficient of electrical resistance

α = Absorptivity

β = A defined function of s; with subscript, an eigenvalue

β = A function of the equivalent conductances for radiation (Cf. Eq. 3.8)

β = Real number in Equation A-5.32

γ = Heating rate, $^{o}K/min$

γ = Activity coefficient

ϵ = Dimensionless parameter (Cf. Eq. 2.56 ff.)

ϵ = Emissivity

ζ = Dimensionless space variable, r/R or x/R

η = Dimensionless parameter, R_{i-1}/R_i

θ = Differential temperature, $T - T_R$, ^{o}K

ν = Dimensionless parameter, τ/t_5 (Cf. Eq. 2.58 ff.)

π = 3.14159...

ρ = Density, g/cm^3

ρ = Reflectivity

ρ = Residue

σ = Stefan-Boltzmann constant

σ = Standard deviation

σ = Entropy factor (Cf. Eq. 4.2)

σ = Electrical conductivity

τ = Time constant, sec or min

τ = Transmissivity

ϕ = Dimensionless parameter (Cf. Eq. 1.3)

ϕ = Thermal conductivity ratio (Cf. Eq. 2.10 ff.)

ϕ = Function defined by Equation 5.3

BIBLIOGRAPHY

1. B. ABELES, J. PHYS. CHEM. SOL., 8 (340) 1959.
2. KH. I. AMIRKHANOV, G. B. BAGDUEV, AND M. A. KAZHALEV, DOKLADY, AN SSSR, 117 (953) 1957.
3. ASTM STANDARDS, 3, E14-51T, 1961.
4. R. BARRIE, F. A. CUNNELL, J. T. EDMOND, AND I. M. ROSS, PHYSICA , XX (1087) 1954.
5. D. S. BEERS, G. D. CODY, AND B. ABELES, INT. CONF. SEMICOND. PHYS., EXETER, JULY 16-20, 1962.
6. L. G. BERG AND V. YA. ANOSOV, ZH. OBSHCH. KHIM., 12 (31) 1942.
7. S. L. BOERSMA, J. AM. CER. SOC., 38 (281) 1955.
8. G. F. BOLLING, J. CHEM. PHYS., 33 (305) 1960.
9. G. F. BOLLING, J. CHEM. PHYS., 36 (1085) 1962.
10. E. BONNIER AND P. DESRE, COMPT. REND., (PARIS), 252 (3448) 1961.
11. E. BONNIER AND P. DESRE, COMPT. REND. (PARIS), 253 (867) 1961.
12. H. J. BORCHARDT AND F. DANIELS, J. AM. CHEM. SOC., 79 (41) 1957.
13. R. BOWERS, R. W. URE, J. BAURLE, AND A. CORNISH, J. APP. PHYS., 30 (930) 1959.
14. R. BOWERS, J. E. BAURLE, AND A. J. CORNISH, J. APP. PHYS., 30 (1050) 1959.
15. G. BUSCH AND M. SCHNEIDER, PHYSICA, XX, (1084) 1954.
16. M. CARDONA, PROC. INT. CONF. SEMICOND. PHYS., PRAGUE, 1961.
17. H. S. CARSLAW AND J. C. JAEGER, CONDUCTION OF HEAT IN SOLIDS, SECOND EDITION, OXFORD UNIVERSITY PRESS, 1959.
18. R. V. CHURCHILL, OPERATIONAL MATHEMATICS, SECOND EDITION, MC-GRAW HILL BOOK COMPANY, INC., NEW YORK, 1958.
19. D. H. DAMON, BULL. AM. PHYS. SOC., II-8, 23 JAN. 1963.
20. E. D. DEVYATKOVA, B. YA. MOIZHES, AND I. A. SMIRNOV, FIZ. TV. TELA, 1 (555) 1959.
21. A. S. DWORKIN AND M. A. BREDIG, J. PHYS. CHEM., 64 (269) 1960.
22. E. R. G. ECKERT AND R. M. DRAKE, HEAT AND MASS TRANSFER, MC-GRAW HILL BOOK COMPANY, INC., NEW YORK, 1959.
23. C. EYRAUD, COMPT. REND., 238 (1511) 1954.
24. H. P. R. FREDERIKSE AND R. F. BLUNT, PROC. I.R.E., 43 (1828) 1955.
25. K. FURUKAWA, REPTS. ON PROG. IN PHYS., XXV (395) 1962.
26. A. GOLDMAN AND G. I. POST, W.A.D.C. TECHNICAL NOTE 58-254, A.S.T.I.A. DOCUMENT NO. AD155887, AUGUST 1958.
27. A. GOLDSMITH, T. E. WATERMAN, AND H. J. HIRSCHHORN, HANDBOOK OF THERMO-PHYSICAL PROPERTIES OF SOLID MATERIALS, REVISED EDITION, MACMILLAN COMPANY, NEW YORK, 1961.
28. E. S. GREINER AND P. BREIDT, J. METALS, 4 (1044) 1952.
29. E. G. GROCHOWSKI AND D. R. MASON, ELECTROCHEMICAL SOCIETY, ELECTRONICS DIVISION ABSTRACTS, 10 (100) 1961.
30. HANDBOOK OF CHEMISTRY AND PHYSICS, 41ST EDITION, CHEMICAL RUBBER PUBLISHING COMPANY, CLEVELAND, 1959.
31. M. HANSEN, CONSTITUTION OF BINARY ALLOYS, SECOND EDITION, MC-GRAW HILL BOOK COMPANY, INC., NEW YORK, 1960.
32. R. J. HODGKINSON, J. ELECTRONICS, 1 (612), MAY 1956.
33. N. L. HOZAK, J. S. COOK, AND D. R. MASON, J. ELECTROCHEM. SOC., 108 (105) 1961.
34. H. J. HROSTOWSKI, SEMICONDUCTORS, EDITED BY N. B. HANNAY, REINHOLD PUBLISHING CORP., NEW YORK, 1959.
35. INTERNATIONAL CRITICAL TABLES, MC-GRAW HILL BOOK COMPANY, INC., NEW YORK, 1929.
36. A. F. JOFFE, CAN. J. PHYS., 34 (1342) 1956.
37. A. F. JOFFE AND A. R. REGEL, PROG. IN SEMICOND., 4, HEYWOOD AND CO., LTD., LONDON, 1960. P. 239FF.
38. L. B. JOHNSON, IND. ENG. CHEM., 52 (241) 1960.
39. P. JUNOD, HELV. PHYS. ACTA, 32 (567) 1959.
40. Y. KANAI AND R. NII, J. PHYS. CHEM. SOL., 8 (338) 1959.
41. J. J. KEAVNEY AND E. C. EBERLIN, J. APP. POLY. SCIENCE, 3 (47) 1960.
42. M. KOBAYASHI, Z. ANORG. CHEM., 69 (1) 1911.
43. M. KOBAYASHI, INTERN. Z. METALLOG., 2 (65) 1912.
44. I. V. KORNEEVA, A. V. BELYAEV, AND A. V. NOVOSELOVA, J. INORG. CHEM. (RUSSIAN), 5 (1) 1960.
45. I. I. KORNILOV AND N. M. MATVEEVA, ZH. NEORG. KHIM., 5 (671) 1960.
46. R. KROENIG AND R. SNOODIJK, J. APPL. SCI. RESEARCH, A3 (27) 1951.
47. O. KUBASCHEWSKI AND E. EVANS, METALLURGICAL THERMOCHEMISTRY, THIRD EDITION, PERGAMON PRESS, LTD., NEW YORK, 1958.

BIBLIOGRAPHY (CONT.)

48. N. A. LANGE, HANDBOOK OF CHEMISTRY, EIGHTH EDITION, HANDBOOK PUBLISHERS, INC., SANDUSKY, OHIO, 1952.
49. W. P. LAWSON, S. NIELSEN, E. H. PUTLEY, AND A. S. YOUNG, J. PHYS. CHEM. SOL., 9 (325) 1959.
50. H. LE CHATELIER, Z. PHYSIK. CHEM., 1 (396) 1887.
51. H. LE CHATALIER, BULL. SOC. FR. MIN., 10 (204) 1887.
52. G. N. LEWIS AND M. RANDALL, THERMODYNAMICS, REVISED BY K. S. PITZER AND L. BREWER, SECOND EDITION, MCGRAW-HILL BOOK COMPANY, NEW YORK, 1961.
53. C. E. LOCKE AND H. F. RASE, IND. ENG. CHEM., 52 (515) 1960.
54. M. R. LORENZ, J. PHYS. CHEM. SOL., 23 (939) 1962.
55. C. H. LUECK, L. F. BESTE, AND H. K. HALL, J. PHYS. CHEM., 67 (972) 1963.
56. M. M. MARKOWITZ AND D. A. BORYTA, J. PHYS. CHEM., 66 (1477) 1962.
57. D. R. MASON AND B. M. KULWICKI, ELECTROCHEMICAL SOCIETY, ELECTRONICS DIVISION, ABSTR. 9, NO. 1, (192) 1960.
58. D. R. MASON AND D. F. O KANE, PROC. INT. CONF. SEMICOND. PHYS., PRAGUE, 1960.
59. H. S. MICKLEY, T. K. SHERWOOD, AND C. E. REED, APPLIED MATHEMATICS IN CHEMICAL ENGINEERING, SECOND EDITION, MCGRAW-HILL BOOK COMPANY, INC., NEW YORK, 1957.
60. S. MIYATANI, J. PHYS. SOC. JAP., 13 (341) 1958.
61. H. MIYAZAWA AND S. SUGAIKE, J. PHYS. SOC. JAP., 12 (312) 1957.
62. N. NACHTRIEB AND N. CLEMENT, J. PHYS. CHEM., 61 (1424) 1958.
63. D. DE NOBEL, THESIS, UNIVERSITY OF LEIDEN, MAY 1958, PHILIPS RESEARCH REPORTS, 14 (361) 1959.
64. F. H. NORTON, J. AM. CER. SOC., 22 (54) 1939.
65. G. OFFERGELD AND J. VAN CAKENBERGHE, NATURE, 184 (185) 1959.
66. D. F. O KANE, PH.D. THESIS, UNIVERSITY OF MICHIGAN, 1962.
67. M. OLETTE, PHYS. CHEM. STEELMAKING, PROC., DEDHAM, MASS., 1956.
68. O. H. OLSON AND J. C. MORRIS, W.A.D.C. TR 56-222, PT. III, CONTRACT NO. AF33(616)-3002, PROJECT NO. 7360, 1959.
69. W. PLATO, Z. PHYS. CHEM., 55 (721) 1906.
70. R. C. REID AND T. K. SHERWOOD, THE PROPERTIES OF GASES AND LIQUIDS, MCGRAW-HILL BOOK COMPANY, INC., NEW YORK, 1958.
71. N. DE ROCHE, Z. METALL., 48 (59) 1957.
72. A. SCHNEIDER AND R. BLACHNIK, DIE NATURWISSENSCHAFTEN, 49 (465) 1962.
73. W. F. SCHOTTKY AND M. B. BEVER, ACTA MET., 6 (320) 1958.
74. S. A. SEMILETOV, SOV. PHYS. SOL. STATE, 3 (544) 1961.
75. G. A. SLACK AND C. GLASSBRENNER, PHYS. REV., 120 (782) 1960.
76. C. S. SMITH, TRANS. A.I.M.E., 137 (236) 1940.
77. C. J. SMITHELLS, METALS REFERENCE BOOK, THIRD EDITION, BUTTERWORTHS SCIENTIFIC PUBLICATIONS, LONDON, 1962.
78. W. J. SMOTHERS AND Y. CHIANG, DIFFERENTIAL THERMAL ANALYSIS, CHEMICAL PUBLISHING COMPANY, NEW YORK, 1958.
79. S. SPEIL, REPT. INV. NO. 3765, U.S. BUREAU OF MINES, 1944.
80. L. E. STEINER AND J. JOHNSTON, J. PHYS. CHEM., 32 (912) 1928.
81. A. D. STUCKES, PHYS. REV., 107 (427) 1957.
82. E. STURM, J. PHYS. CHEM., 65 (1935) 1961.
83. C. D. THURMOND AND M. KOWALCHIK, BELL SYSTEM TECH. JOUR., 39 (169) 1960.
84. E. T. TURKDOGAN AND J. PEARSON, J. APPL. CHEM., 3 (495) 1953.
85. J. UMEDA, M. JEONG, AND T. OKADA, JAP. J. APPL. PHYS., 1 (277) 1962.
86. R. W. URE, PRIVATE COMMUNICATION.
87. M. J. VOLD, J. ANAL. CHEM., 21 (683) 1949.
88. C. WAGNER, ACTA MET., 6 (309) 1958.
89. P. N. WALSH, E. W. ART, AND D. WHITE, J. PHYS. CHEM., 66 (1546) 1962.
90. W. D. WEATHERFORD, JR., J. C. TYLER, AND P. M. KU, W.A.D.D. TECH. REPT. 61-96, AERONAUTICAL SYSTEMS DIVISION, WRIGHT PATTERSON AIR FORCE BASE, OHIO, 1961.
91. F. E. WITTIG, Z. ELEKTROCHEM., 54 (288) 1950.
92. W. J. WOESTEN, J. PHYS. CHEM., 65 (1949) 1961.
93. W. J. WOESTEN AND M. G. GEERS, J. PHYS. CHEM., 66 (1252) 1962.
94. T. YOSHIOKA, TOHOKU UNIV. SCI. REPTS., 44 (99) 1960.
95. A. I. ZASLAVSKII AND V. M. SERGEYEVA, FIZ. TV. TELA, 2 (2872) 1960.